UNIVERSITÀ DELLA CALABRIA
DOTTORATO DI RICERCA
IN
INGEGNERIA DEI MATERIALI E DELLE STRUTTURE
XXI° CICLO

MODELLING THE LATERAL PEDESTRIAN FORCE ON RIGID AND MOVING FLOORS BY A SELF-SUSTAINED OSCILLATOR

Tesi presentata per il conseguimento del titolo
di Dottore di Ricerca in Ingegneria dei Materiali e delle Strutture
da

Andrea TROVATO

Coordinatore del Corso di Dottorato
Prof. Renato S. Olivito

Tutori del candidato
Prof. Domenico Bruno
Prof. Pierre Argoul

Università della Calabria
Dipartimento di Strutture
Novembre 2009

A Dio per avermi donato la forza e la salute
per raggiungere questo obiettivo.

Alla mia famiglia per l'amore sincero e
silenzioso con cui mi ha sostenuto.

A Giusy l'amore della mia vita.

DEPARTMENT OF STRUCTURES
UNIVERSITY OF CALABRIA

Thesis for the Degree of Doctor of Engineering

Modelling the lateral pedestrian force on rigid and moving floors by a self-sustained oscillator

by

Andrea TROVATO

ABSTRACT

For the serviceability analysis of civil engineering structures under human induced vibrations, a correct modelling of the pedestrian-structure interaction is needed. The proposed approach consists in thinking the human body as a Single Degree of Freedom oscillator: the force transmitted to the floor is the restoring force of this oscillator [1, 2]. In *rigid floor* conditions, such an oscillator must be able to reproduce two experimentally observed phenomena: (i) the time-history of lateral force can be approximated by a periodic signal with a "natural" frequency related with the single pedestrian characteristics; (ii) the motion of a pedestrian is *self-sustained*, in the sense that the pedestrian produces by itself the energy needed to walk.

Accounting for these aspects, a *modified Van der Pol* (MVdP) oscillator is proposed here to represent the lateral pedestrian force. The suitable form of its nonlinear restoring force is inferred from experimental data concerning a sample of twelve pedestrians. The experimental and model lateral forces show an excellent agreement.

For a *laterally moving floor*, the MVdP oscillator representing a pedestrian becomes non-autonomous. It is well-known that self-sustained oscillators in the non-autonomous regime are characterized by the so-called *entrainment phenomenon*. It means that under certain conditions, the vibration

frequency switches from the ”natural” value to that of the external force: the response frequency is entrained by the excitation frequency. According to the physical interpretation considered here, the entrainment corresponds to the situation where the pedestrian changes its natural walking frequency and synchronizes with the floor oscillation frequency. The steady response of the MVdP oscillator subjected to a harmonic excitation is discussed in terms of non-dimensional amplitude response curves, obtained using the harmonic balance method truncated at the first harmonic. The model predictions are compared with some experimental results concerning pedestrians available in the literature and a good agreement is obtained. These topics are detailed in this thesis and also in the companion papers [3, 4] and in the report [5].

Keywords: *pedestrian lateral force*, *self-sustained oscillator*, *modified Van der Pol oscillator*, *frequency entrainment*.

Index

List of Symbols and Abbreviations

B_H	Hopf Bifurcation
B_N	Node-Spiral Bifurcation
B_S	Saddle-Node Bifurcation
HB	Harmonic Balance
FFT	Fast Fourier Transform
SDoF	Single Degree of Freedom
MVdP	Modified Van der Pol

$\mathbf{a}=[a_1, a_2, a_3, a_4, a_5]^T$	vector of the parameters used for the identification
f_1 [Hz]	fundamental frequency of the lateral pedestrian force
$h(u_y, \dot{u}_y; \omega_0, \beta, \gamma, \delta)$	nonlinear damping term
m [kg]	mass of a single degree of freedom oscillator
$\mathbf{p}=[\omega_0, \mu, \beta, \gamma, \delta]^T$	vector of the parameters of the modified Van der Pol model
$\mathbf{r}$	non-dimensional response amplitude
$\ddot{\mathbf{u}}^{abs}$ [m/s^2]	absolute acceleration of m
$\mathbf{u}(t)=[u_x(t),u_y(t),u_z(t)]^T$	vector of the displacement of m
$u_{y,per}(t)$ [m]	periodic approximation of the lateral pedestrian displacement
v_x [km/h]	walking speed

A_{acc} [m/s^2]	floor acceleration amplitude
A_d [m]	floor vibration amplitude
C_k [N]	amplitude of the Fourier components of the lateral pedestrian force

$C_{1,dyn}$ [N]	amplitude of the periodic lateral force applied on the floor by a walker assuming entrained conditions
F=[F_x, F_y, F_z] [N]	*restoring force* of a three degrees-of-freedom dynamic system
$F_{y,per}$ (t) [N]	periodic approximation of the lateral pedestrian force
T [s]	period of the oscillator
S	set of the admissible values for the parameters vector **a**
α	normalized form of the parameter γ
λ	non-dimensional external acceleration amplitude
ν	non-dimensional difference (detuning) between the floor frequency ω and the frequency ω_0 of the underlying linear system associated with the MVdP oscillator
ϕ_k [rad]	phase of the k-th Fourier component
ω [rad/s]	frequency of the floor
ω_0 [rad/s]	circular frequency of the underlying linear system associated with the MVdP oscillator
ω_1 [rad/s]	natural frequency of the autonomous MVdP oscillator
$\Delta\phi_{1,k} := \phi_k - k\,\phi_1$ [rad]	phase difference of the k-th Fourier component
$\Delta\Pi$ [J]	variation of Π on a period T
Π [J]	total mechanical energy

List of Figures

List of Tables

Chapter 1

Introduction

The increased use of large span floors within buildings and of light and streamlined footbridges around the world as well as the increasing number of full-crowded stadium during concerts or matches have emphasized the incidence of human induced vibration problems in the design of civil engineering structures. Famous examples of such phenomena can be found in newspapers and in scientific literature. One was during the 1985 Bruce Springsteen concert in the Ullevi Stadium of Göteborg (Sweden), where the rhythmic movement (vertical jumping) of tens of thousands of people was close to causing a structural collapse. Another was during the opening day of the Millennium Footbridge in London, where due to people crossing, the south span had been moving laterally through an amplitude of about 50 *mm* at 0.8 *Hz* and the center span about 75 *mm* at 1 *Hz* approximately. In both cases, the stadium and the footbridge were closed to public for two years in order to remedy these vibration problems.

Other situations, similar to the Millennium Footbridge with unexpected large lateral vibrations, occurred in 1999 on the Solférino footbridge in Paris [6] and, more recently, the same behavior has been detected on the "Pedro and Ines footbridge" in Coimbra, Portugal, during the tests carried out before the opening of the structure [7].

Most of problems are caused by feet impacts which generate a nearly periodic force with a frequency close to the natural frequency of the floor or the structure in contact with feet: a resonance phenomenon is activated. In the case of footbridges, when the first mode of *lateral* vibration falls in the same frequency range of the pedestrians' walking frequency (this was the case for the Millennium Footbridge in London and the Solférino Footbridge in Paris), the amplitude of the structural oscillations increases and pedestrians are forced to change their way of walking when the oscillation amplitude is large

enough. A certain percentage of pedestrians changes the walking frequency, synchronizing the rhythm of the walk with that of the bridge deck oscillation. This phenomenon of structure-pedestrian synchronization has been often experimentally detected and has been analyzed in several studies [6, 8-14]. Recently, [15] proposed a model for the evaluation of the crowd lateral force accounting for the "saturation" phenomenon, i.e. the fact that the synchronization cannot occur when the footbridge oscillation amplitude becomes too large, since pedestrians stop walking; see also [13].

In order to correctly model the pedestrian-structure interaction, a good understanding of the pedestrian walking phenomenon is needed. The first phase of analysis should concern the basic case of a pedestrian walking on a *rigid floor*: an extensive review of the scientific literature concerning this situation is reported in [16]. The main information that can be extracted from the literature is that the walking force on a rigid floor is nearly periodic [17-19]. Hence, the lateral (and vertical and longitudinal) component of the force exerted by a pedestrian on the floor can be represented by their Fourier series [16, 20]. In this thesis, it is often pointed out that the *amplitude* of the first superharmonics is not negligible in comparison with that of the fundamental component. The experimental analysis discussed here confirms this experimental finding. Moreover, a suitable definition of *phase difference* between the fundamental harmonic and each superharmonic is given, in order to clarify the experimental data interpretation. It is also proposed a "physical" interpretation for the first of the these phase differences, between the fundamental harmonic and the third superharmonics.

The human body is a complex dynamic system. Several more or less complicated approaches can be used to model such a system for rigid floor conditions; see for instance [21, 22]. Since our objective is the modelling of the lateral walking force component, a simpler approach is discussed here: the human body is thought as a Single Degree of Freedom (SDoF) dynamic system fulfilling some fundamental requirements observed from experimental results: (i) its mass is equal to the pedestrian mass; (ii) the time-history of lateral force is an approximately periodic signal with a fundamental frequency close to 0.8-1 *Hz*; (iii) the amplitude of the first five odd superharmonics is not negligible. The presence of superharmonics indicates that the SDoF oscillator must be nonlinear; (iv) the motion of pedestrians is "self-sustained", i.e. he produces the energy needed to sustain its walk.

A *modified* Van der Pol (MVdP) model fulfils all previous requirements: like the standard Van der Pol (VdP) model, it is nonlinear and self-sustained, i.e. it possesses a stable limit cycle [23]. The suitable form of the model, i.e. the number and maximum power of the polynomial terms constituting the restoring force, is discussed in [1] and presented here. Moreover, the model parameters are identified from experimental data concerning a sample of twelve pedestrians walking on a *rigid floor*. Numerical and experimental results are discussed and compared.

According to this approach, the *motion of the floor* introduces an external excitation on the self-sustained oscillator representing the walker, that becomes *non-autonomous*. The last part of this thesis concerns the analysis of this situation. One of the most important properties of non-autonomous self-sustained oscillators is that they may have an *entrained* response [24], i.e. a response characterized by the same frequency as that of the excitation. The *entrained* response of the MVdP model has never been analyzed, even if analogous results are well-known for the standard Van der Pol model and for the Rayleigh model [23, 25]. Actually, an entrained response represents a pedestrian *synchronized* with the moving floor, even if its natural frequency is different. This interpretation explains the practical interest of the research of an *approximated analytical solution of the MVdP oscillator in the non-autonomous regime*. The particular case of a harmonic excitation is considered, because a floor lateral motion at constant frequency and amplitude is a simple experimental condition, easy to obtain using a shake table where pedestrians are asked to walk. This experimental situation is studied e.g. in [26]. A similar situation is obtained when pedestrians walk on a treadmill placed on a shake table [27, 28]. In addition, an harmonic excitation is the natural assumption required to apply the *harmonic balance method*.

After the Introduction, in Chapter II the general equation of motion of a SDoF oscillator schematically representing a pedestrian is given. Then, the main results of the experimental analysis performed on a set of twelve pedestrians on a *rigid floor* are presented. These outcomes are used to define the suitable restoring force of a self-sustained SDoF model able to reproduce the experiments. The parameters of this model are then identified and model predictions are finally compared with experimental results. Chapter III deals with the analysis of the *moving floor* case. The response amplitude equation for the MVdP oscillator is derived using the harmonic balance method. Then, the response curves at constant excitation frequency are compared with some

experimental results concerning pedestrians walking on a shake table. Chapter IV recall the main relationships defining the amplitude of its stationary entrained response to a harmonic excitation. The main theoretical goal of this Chapter is the stability analysis of these responses. Then, the pedestrian-floor *synchronization* is discussed. Finally the last Chapter presents the conclusions.

Chapter 2

Modelling the lateral pedestrian force on a rigid floor by a self-sustained oscillator

For the serviceability analysis of civil engineering structures under human induced vibrations, a correct modelling of the pedestrian-structure interaction is needed. The first phase of this modelling must concern the force applied by a pedestrian walking on a rigid floor: the present Chapter deals with the *lateral* component of this force. The approach proposed here consists in thinking the human body as a Single Degree of Freedom oscillator: the force transmitted to the floor is the restoring force of this oscillator. Such an oscillator must be able to reproduce two experimentally observed phenomena: (i) the time-history of lateral force can be approximated by a periodic signal and the amplitude of the first five odd superharmonics is not negligible; (ii) the motion of a pedestrian is self-sustained, in the sense that the pedestrian produces by itself the energy needed to walk. Taking into account these aspects, a modified Van der Pol (self-sustained) oscillator is proposed here to represent the lateral pedestrian force. A suitable form of its nonlinear restoring force is inferred from experimental data concerning a sample of twelve pedestrians. The experimental and model lateral forces show a good agreement.

2.1. Introduction

Several recently built footbridges have shown to be sensitive to the human induced vibration, e.g. the Millennium Footbridge in London, the Solférino Footbridge and the Simone de Beauvoir Footbridge in Paris. The causes of this phenomenon may be described as follows: the crowd walking on a footbridge imposes to the structure a dynamic *lateral* excitation at a frequency close to 1 *Hz*. When the first mode of lateral vibration of the footbridge falls in the same frequency range, a resonance phenomenon is activated. Hence, the oscillation amplitude increases and, provided that the oscillation amplitude becomes large enough, pedestrians change their way of walking, synchronizing their frequency with that of the bridge deck. This *synchronization* phenomenon has been often experimentally detected and has been analyzed in several studies, e.g. [6, 8 - 16].

In order to correctly model the pedestrian-structure interaction, a good understanding of the pedestrian walking mechanisms is needed. The first phase of this analysis must concern the basic case of a pedestrian walking on a rigid floor. The main information that can be extracted from the literature is that the walking force on a rigid floor is nearly periodic [17- 19]. Hence, the vertical, lateral and longitudinal components of the force exerted by a pedestrian on the floor can be represented by their Fourier series [16, 20]. In this thesis, it is often pointed out that the *amplitude* of the first harmonics is not negligible in front of that of the fundamental component. However, most of these experimental studies underestimate the importance of the *phase* information. This aspect will be discussed in this Chapter.

The human body is a complex dynamic system, but the modelling of the *lateral* force exchanged by the feet with the floor could be based, as a first trial, on the use of a single degree of freedom (SDoF) oscillator. Such an oscillator should be able to reproduce two experimentally observed phenomena: (i) the lateral force is quasi-periodic, with fundamental frequency close to one Hertz and where the first 4-5 odd super-harmonics are not negligible. This implies that the SDoF oscillator must be *nonlinear*; (ii) the motion of a pedestrian is "self-sustained", in the sense that the pedestrian behaves like a system producing by itself the energy needed to walk. In order to represent these properties of the pedestrian lateral force, we propose here the use of a modified Van der Pol (VdP) model: like the standard VdP model, it is

nonlinear and self-sustained, i.e. it possesses a stable limit cycle in the phase plane [23].

After the Introduction, the general equation of motion of a SDoF oscillator schematically representing a pedestrian is given. Then, in Section 2.3, the main results of the experimental analysis performed on a set of twelve pedestrians are presented. These outcomes are used in Section 2.4 to define the suitable restoring force of a self-sustained SDoF model able to reproduce the experiments. The parameters of this model are identified according to a procedure discussed in Subsection 2.5.1 and results are presented in Subsection 2.5.2.

2.2. The pedestrian as a single mass oscillator

A pedestrian is a complex system composed of several interacting parts. To precisely model its behaviour under different "working" conditions, i.e. walking, running, bouncing, horizontal body swaying, etc., is a challenging task. As already said in the introduction, an interesting approach is based on the multi-body dynamics [21, 22], where each main part of the human body is represented by a rigid body connected with the other parts. In view of the stability analysis of a footbridge under the crowd load, simpler approaches have been used in several past studies [29-31]. In most of them, the single pedestrian is modeled as a discrete mass m subjected to the inertial forces and to the force of interaction with the bridge floor. The same approach based on a SDoF system representing a pedestrian is used here; see Fig. 2.1.

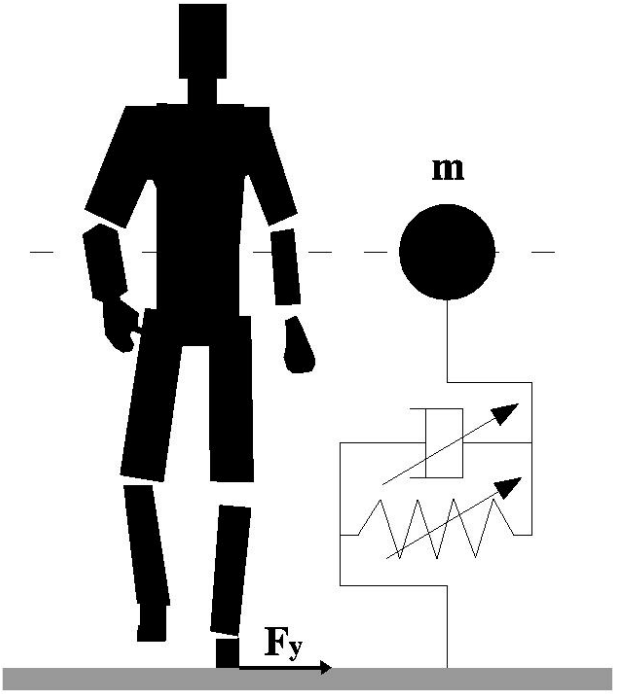

Figure 2.1: Scheme of the SDoF system representing the lateral motion of a pedestrian.

The equilibrium in an inertial reference of all the forces acting on m reads

$$m\ddot{\mathbf{u}}^{abs}(t)+\mathbf{F}(t)=m\mathbf{g} \tag{2.1}$$

where the superposed dot indicates the (partial) time-differentiation; m is the pedestrian mass; $\mathbf{F}=[F_x, F_y, F_z]$ is the contact force between the pedestrian and the bridge deck; $\mathbf{g}$ is the gravity acceleration vector; $\ddot{\mathbf{u}}^{abs}(t)$ is the absolute acceleration of the mass m, accounting for both the motion of the floor and the relative acceleration $\ddot{\mathbf{u}}(t)$ between m and the floor. The expression of $\ddot{\mathbf{u}}^{abs}(t)$ in the general case is complex, since it depends on both the deck movement $\mathbf{U}(\mathbf{x},t)$, with $\mathbf{x}=[x, y, z]^T$ the generic Lagrangian co-ordinate of a deck point, and the pedestrian motion, composed by its trajectory on the bridge floor and by the oscillations $\mathbf{u}(t)=[u_x(t), u_y(t), u_z(t)]^T$ relative to the floor. However, we consider here the case of a rigid horizontal floor and constant walking speed on a straight trajectory. Under these assumptions, one has $\ddot{\mathbf{u}}^{abs}(t)=\ddot{\mathbf{u}}(t)$. Moreover, only the *lateral* oscillations of m are analyzed in this thesis: supposing that the x-axis is parallel to the straight trajectory, the lateral direction is parallel to the y-axis. Projecting (2.1) in this direction, one has

$$m\ddot{u}_y(t) + F_y(t) = 0 \tag{2.2}$$

This relationship shows that when $F_y(t)$ is known from measurements, the motion $u_y(t)$ of the mass m can be derived. The next Section will concern this analysis of experimental data collected from tests on a sample of twelve pedestrians walking on a rigid floor. A *model* for the force **F** can be defined as follows:

$$\mathbf{F} = \mathbf{F}(\mathbf{u}, \dot{\mathbf{u}}) \tag{2.3}$$

i.e. **F** is thought as the *restoring force* of a three degrees-of-freedom dynamic system, and it depends on the displacements and velocities *relative* to the floor. Projecting (2.3) in the y-direction under the same simplifying assumptions discussed above, one has

$$F_y = F_y\left(u_x, u_y, u_z, \dot{u}_x, \dot{u}_y, \dot{u}_z\right) \tag{2.4}$$

where F_y depends on all the x, y, and z components of the displacements and velocities around the mean trajectory. Hence, this general expression accounts for a coupling between the different components. However, it is supposed here that this coupling is negligible, i.e.

$$F_y = F_y\left(u_y, \dot{u}_y\right)$$

This leads to a single degree-of-freedom oscillator defined by the following dynamics equation (see also Fig. 2.1):

$$m\ddot{u}_y(t) + F_y\left(u_y(t), \dot{u}_y(t)\right) = 0 \tag{2.5}$$

In order to have a self-sustained oscillator, F_y must have some special characteristics, i.e. the solution $u_y(t)$ of the autonomous system (2.5) must have a stable periodic orbit in the phase plane [23]. A classical example of this kind of behaviour is given by the Van der Pol oscillator

$$\frac{F_y\left(u_y,\dot{u}_y;\omega_0,\mu,\beta\right)}{m}=-2\mu\omega_0\dot{u}_y\left(1-\beta u_y^2\right)+\omega_0^2 u_y \tag{2.6}$$

where ω_0 is the circular frequency of the underlying linear system, μ>0 and β>0 are associated with the nonlinear damping term. The data analysis of Section 2.3 will show that the classical VdP model (2.6) is not general enough for well representing the walker lateral behaviour. For this reason a different self-sustained model is proposed in Section 2.4 and its parameters are identified in Section 2.5.

2.3. The lateral force of a single pedestrian on rigid floor: experimental results

This Section is dedicated to the analysis of the experimental data provided by the Research Center of Decathlon in Villeneuve d'Ascq (France) concerning twelve pedestrians. The mass of pedestrians varies from 64 kg to 96 kg; see Table 2.1. They are numbered according to the increasing mass order. The lateral force of each walker has been measured at four different walking speeds: v_x=3.75 km/h, v_x=4.5 km/h, v_x=5.25 km/h, v_x=6.0 km/h. All walking conditions were realized on a treadmill dynamometer equipped with four force transducers, allowing to determine the ground reaction forces exerted under each foot [32].

Pedestrian	1	2	3	4	5	6	7	8	9	10	11	12
m (kg)	64	66	68	68	71	71	71	73	74	74	78	96
H (cm)	175	174	163	177	189	178	186	185	186	183	180	179

Table 2.1 – Mass and height of the twelve pedestrians involved in the tests performed at the Decathlon Research Center.

The nominal walking speed v_x associated with each measure is the velocity of the treadmill during the test. The sampling time step is Δt=0.005 *s*, while the number of recorded force values is N=6000, corresponding to a signal length

$t_N=(N-1)\Delta t=29.995$ *s*. The sets of the discrete instants and frequencies are then defined as $\{\mathbf{t}\}_n=t_n=(n-1)\Delta t$ and $\{\mathbf{f}\}_m=f_m=(m-1)\Delta f$, respectively. The frequency increment is $\Delta f=1/(N\,\Delta t)=0.0333$ Hz. The recorded signals for pedestrian "8" at four different walking speeds are reported in Fig. 2.2. Hereafter, the main results will be illustrated with reference to the pedestrian "8". For all the other pedestrians, only a summary of the main results is given. For the complete data analysis, the reader is referred to [33].

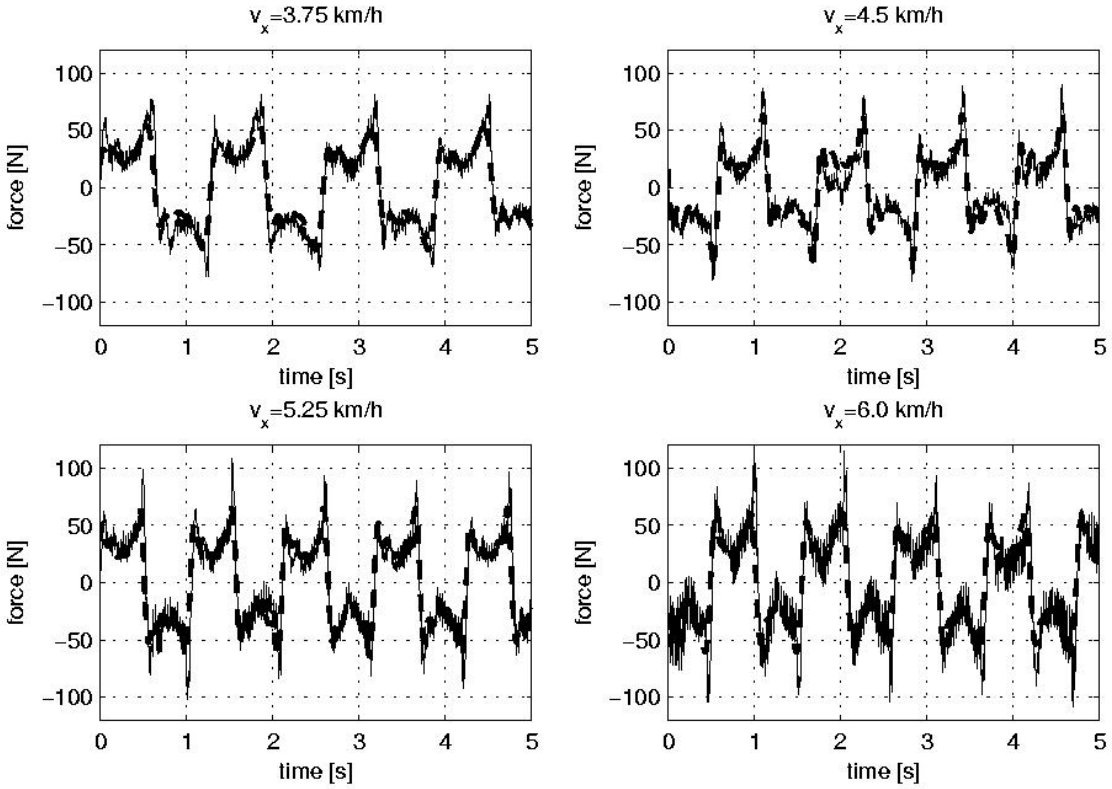

Figure 2.2: Pedestrian "8": time-history of the lateral force for four different walking speeds. Experiment (continuous line) vs. Fourier Series (dashed line) according to Eq.(2.10).

When a pedestrian walks on a rigid floor, along a straight trajectory and with constant speed, the force $F_y(t)$ exerted on the floor is approximately periodic. This statement has been discussed by several investigators, e.g. [17-18]. Under this assumption, the measured force signal $F_y(t)$ can be approximated by its Fourier series (see the Appendix A):

$$F_y(t) \simeq F_{y,per}(t) = \frac{C_0}{2} + \sum_{k=1}^{\infty} C_k \cos\left(2\pi k f_1 t - \phi_k\right) \tag{2.7}$$

where f_1 is the pacing or fundamental walking lateral frequency; $C_k>0$ and $\phi_k \in (-\pi,\pi]$ are the harmonic amplitudes and phases, respectively. Note that for a given periodic signal, the phases ϕ_k depend on the initial time. Hence, their values are not physically significant. However, it is always possible to define a suitable translation of the time scale such that $\tilde{t}=t-t_0$ with $2\pi f_1 t_0-\phi_1=0$. In this situation, one can write

$$\tilde{F}_{y,per}(\tilde{t}) := \tilde{F}_{y,per}(\tilde{t}+t_0) = \frac{C_0}{2} + \sum_{k=1}^{\infty} C_k \cos\left(2\pi k f_1 \tilde{t} - \Delta\phi_{1,k}\right) \tag{2.8}$$

with the phase "differences" defined as follows

$$\Delta\phi_{1,k} := \phi_k - k\,\phi_1, \qquad \text{for} \quad k \geq 1$$

These quantities are an intrinsic property of a periodic signal. Hereafter, the tilde associated with the translated time-scale will be omitted for the sake of simplicity.

The recorded signals have been first analyzed by the Fast Fourier Transform (FFT), in order to find the fundamental frequency and to have an estimation of the relative amplitude between the different harmonics. The definition used here for the FFT reads

$$\hat{F}_y(m) = \frac{2}{\bar{N}} \sum_{n=1}^{\bar{N}} F_y(n)\, e^{-i\frac{2\pi}{N}(m-1)(n-1)} \qquad \text{for } m=1,\ldots,\bar{N} \tag{2.9}$$

where $\bar{N}\Delta t$ is the length of the largest time-interval of the recorded signal containing an integer number of periods. According to (2.9), $\hat{F}_y(f_m) := \hat{F}_y(m-1)$. The factor $2/\bar{N}$ introduced in (2.9) leads to define a complex quantity $\hat{F}_y$, measured in Newtons, whose modulus is directly comparable to the Fourier series coefficients C_k. The plots of the modulus of $\hat{F}_y$ for the lateral walking force of pedestrian "8" at several walking speeds are given in Fig. 2.3. The Nyquist frequency is equal to $f_{Ny}=1/(2\Delta t)=100$ Hz, but, for the sake of clarity, the plot is represented up to $f=20$ *Hz*. As a matter of fact,

this analysis shows that the first odd harmonics up to that of order 9 are non negligible for all walking speeds. This confirms analogous findings of other authors, e.g. [20]. More in detail, for the pedestrian "8", the peaks having amplitude greater than 3-4 *N* are those of the harmonics of order 1, 3, 5, 7, 9. The harmonics 11 and 13 and the even harmonics always have smaller amplitude. The mean value of the walking force F_y, estimated from $\hat{F}_y(m=1)/2$ is also small in general. Similar results have been found for the other eleven pedestrians.

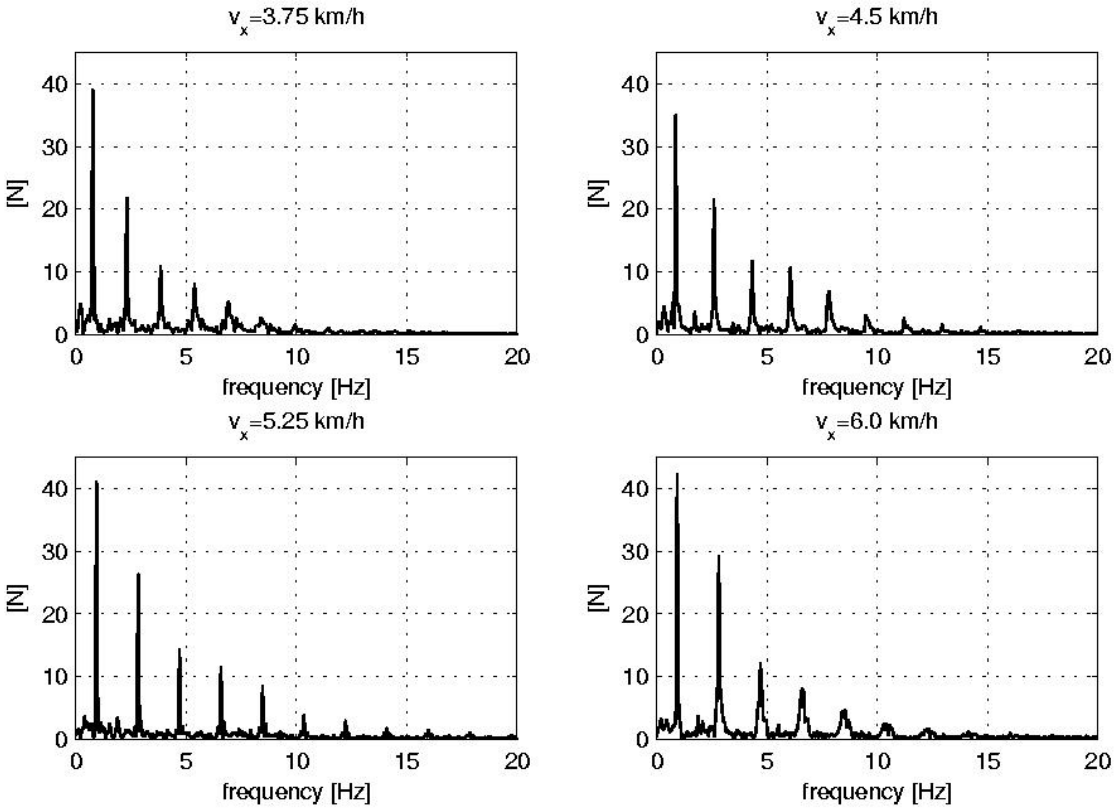

Figure 2.3: FFT modulus of the lateral walking force of pedestrian "8".

In summary of this study, it is assumed that the lateral force can be approximated as a periodic signal with zero mean limited to its odd harmonics from the order 1 to 9:

$$F_{y,per}(t) \simeq \sum_{k=1}^{k_{\max}} C_{2k-1} \cos\left(2\pi(2k-1) f_1 t - \Delta\phi_{1,2k-1}\right) \tag{2.10}$$

with k_{max}=5. Assuming that Eq. (2.2) holds, one has an estimation of the experimental acceleration of *m* by the following expression

$$\ddot{u}_{y,per}(t) = -\frac{F_{y,per}(t)}{m} = -\frac{1}{m}\sum_{k=1}^{k_{max}} C_{2k-1}\cos\left(2\pi(2k-1)f_1 t - \Delta\phi_{1,2k-1}\right) \tag{2.11}$$

from which the analytical expressions of the lateral velocity and displacement can be easily found:

$$\begin{aligned}\dot{u}_{y,per}(t) &= -\frac{1}{m}\sum_{k=1}^{k_{max}} \frac{C_{2k-1}}{2\pi(2k-1)f_1}\sin\left(2\pi(2k-1)f_1 t - \Delta\phi_{1,2k-1}\right)\\ u_{y,per}(t) &= \frac{1}{m}\sum_{k=1}^{k_{max}} \frac{C_{2k-1}}{\left(2\pi(2k-1)f_1\right)^2}\cos\left(2\pi(2k-1)f_1 t - \Delta\phi_{1,2k-1}\right)\end{aligned} \tag{2.12}$$

The frequencies and amplitudes of the first odd harmonics computed using (2.9) are collected in Table 2.2. The fundamental frequency estimation obtained from the FFT is retained, while the amplitudes C_{2k-1} and phase differences $\Delta\phi_{1,2k-1}$ are computed by a Fourier series analysis. The results of Table 2.3 are obtained. The frequencies and amplitudes are similar to those computed by the FFT. The measured force and the periodic approximation are compared in Fig. 2.2.

	3.75 km/h	4.5 km/h	5.25 km/h	6.0 km/h
$f_1\,[Hz]$	0.77	0.87	0.941	0.943
$f_3\,[Hz]$	2.31	2.61	2.82	2.83
$f_5\,[Hz]$	3.85	4.34	4.70	4.72
$f_7\,[Hz]$	5.39	6.08	6.59	6.60
$f_9\,[Hz]$	6.93	7.82	8.47	8.56
$\left\|\hat{F}_y\left(f_1\right)\right\|[N]$	38.96	34.88	41.01	42.26
$\left\|\hat{F}_y\left(f_3\right)\right\|[N]$	21.75	21.45	26.26	29.17
$\left\|\hat{F}_y\left(f_5\right)\right\|[N]$	10.74	11.7	14.28	11.99
$\left\|\hat{F}_y\left(f_7\right)\right\|[N]$	8.00	10.54	11.47	7.97
$\left\|\hat{F}_y\left(f_9\right)\right\|[N]$	5.25	6.85	8.40	4.55

Table 2.2 – FFT of the lateral force of pedestrian "8". Frequencies and amplitudes of the odd harmonics from order 1 to 9.

	3.75 km/h	4.5 km/h	5.25 km/h	6.0 km/h
$f_1\,[Hz]$	0.77	0.87	0.941	0.943
$C_1\,[N]$	39.10	34.91	41.08	42.28
$C_3\,[N]$	21.16	21.59	26.19	29.37
$C_5\,[N]$	9.25	11.73	13.70	12.26
$C_7\,[N]$	5.76	10.79	10.69	8.32
$C_9\,[N]$	3.04	7.38	7.17	3.68
$\Delta\phi_{1,3}\,[rad]$	2.47	2.42	2.92	2.66
$\Delta\phi_{1,5}\,[rad]$	-1.48	-1.56	-0.52	-0.66
$\Delta\phi_{1,7}\,[rad]$	1.12	0.92	2.28	2.19
$\Delta\phi_{1,9}\,[rad]$	-1.87	-2.71	-0.98	-0.97

Table 2.3 – Pedestrian "8", Fourier series analysis: amplitudes and phase differences of the odd harmonics from order 1 to 9, at different walking speeds. The fundamental frequencies are estimated by the FFT.

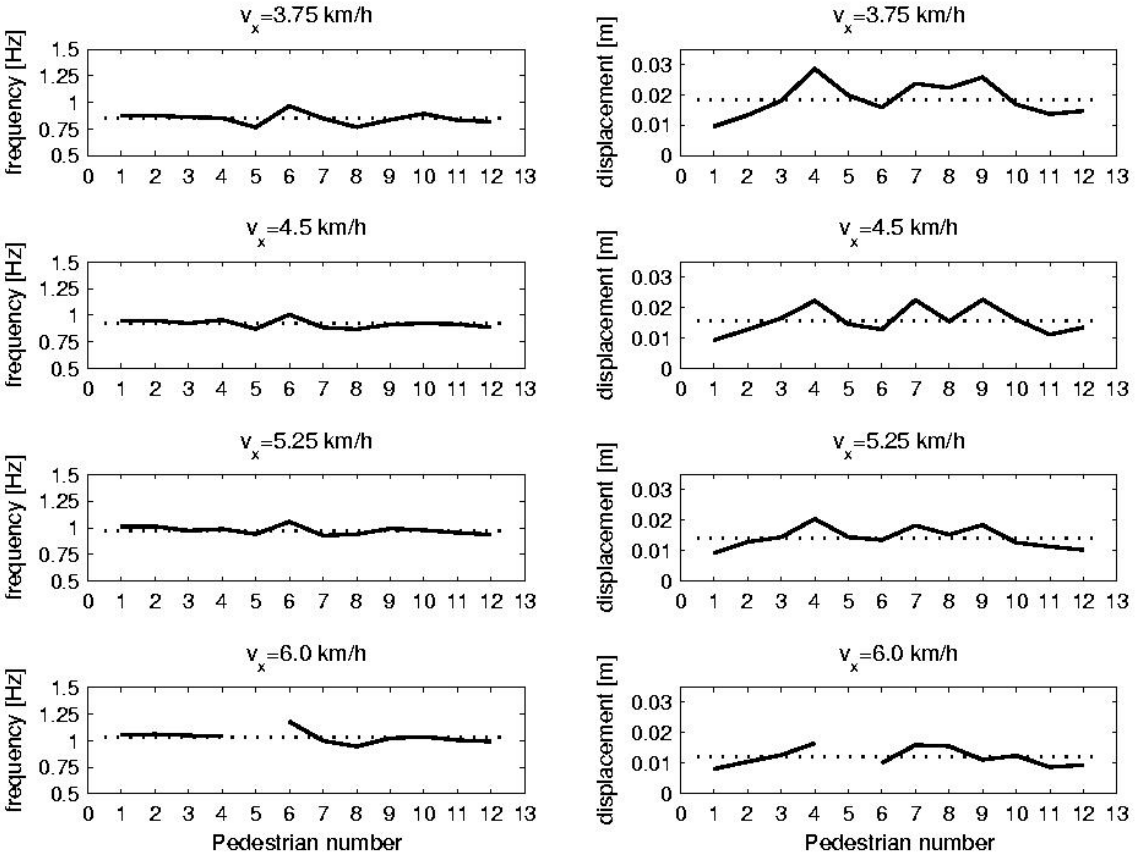

Figure 2.4: Frequencies and maximum displacement amplitudes for all pedestrians. Pedestrians are numbered according to the increasing mass order. Missing points correspond to non available experimental data.

Fig. 2.4 shows the fundamental walking frequencies and the lateral displacement amplitudes for all pedestrians. The values of the amplitudes C_1 and C_3 and of the phase differences $\Delta\phi_{1,3}$ are depicted in Fig. 2.5. Table 2.4 collects the corresponding averages.

	3.75 km/h	4.5 km/h	5.25 km/h	6.0 km/h
$f_1\,[Hz]$	0.848	0.919	0.975	1.033
$C_1\,[N]$	40.29	41.20	41.79	39.33
$C_3\,[N]$	17.37	19.11	22.06	21.41
$C_5\,[N]$	6.38	6.55	9.45	8.64
$C_7\,[N]$	3.51	2.79	5.15	5.26
$C_9\,[N]$	2.36	1.43	2.78	2.23
$\Delta\phi_{1,3}\,[rad]$	-2.91	-3.04	3.10	2.92
$\Delta\phi_{1,5}\,[rad]$	0.41	0.34	-0.08	-0.45
$\Delta\phi_{1,7}\,[rad]$	-2.62	-2.39	3.10	2.77
$\Delta\phi_{1,9}\,[rad]$	0.71	1.23	-0.02	-0.31

Table 2.4 – Average values on the set of twelve pedestrians of the walking frequency, the amplitudes and phase differences for the first five odd harmonics of the lateral force.

The displacement amplitudes of Fig. 2.4, as well as the displacement and velocity curves of Figs. 2.6 and 2.7 are computed using (2.10), (2.11) and (2.12). The displacement amplitude is about 1.8 cm, while the velocity amplitude is about 0.15 m/s. These values are very close to those measured by other authors; e.g. [34]. Moreover, observe that periodic orbits in the phase plots of Figs. 2.6e and 2.7e are characterized by a maximum velocity amplitude in the second and fourth quadrant. The phase plots are also depicted for all pedestrians and all walking speeds (Fig. 2.8): at a given speed, the orbit shape can change from one pedestrian to the other. These variations can be mainly attributed to the value of $\Delta\phi_{1,3}$, as it is explained in the next Section. One can also notice that for increasing walking speeds, the amplitude of the lateral displacement and velocity decreases: a greater walking speed is accompanied by a smaller lateral oscillation. The measurements of [34] confirm this result. The three-dimensional plots in Figs. 2.6f and 2.7f show the lateral force as a function of displacements and velocity using the harmonics up to 9th order.

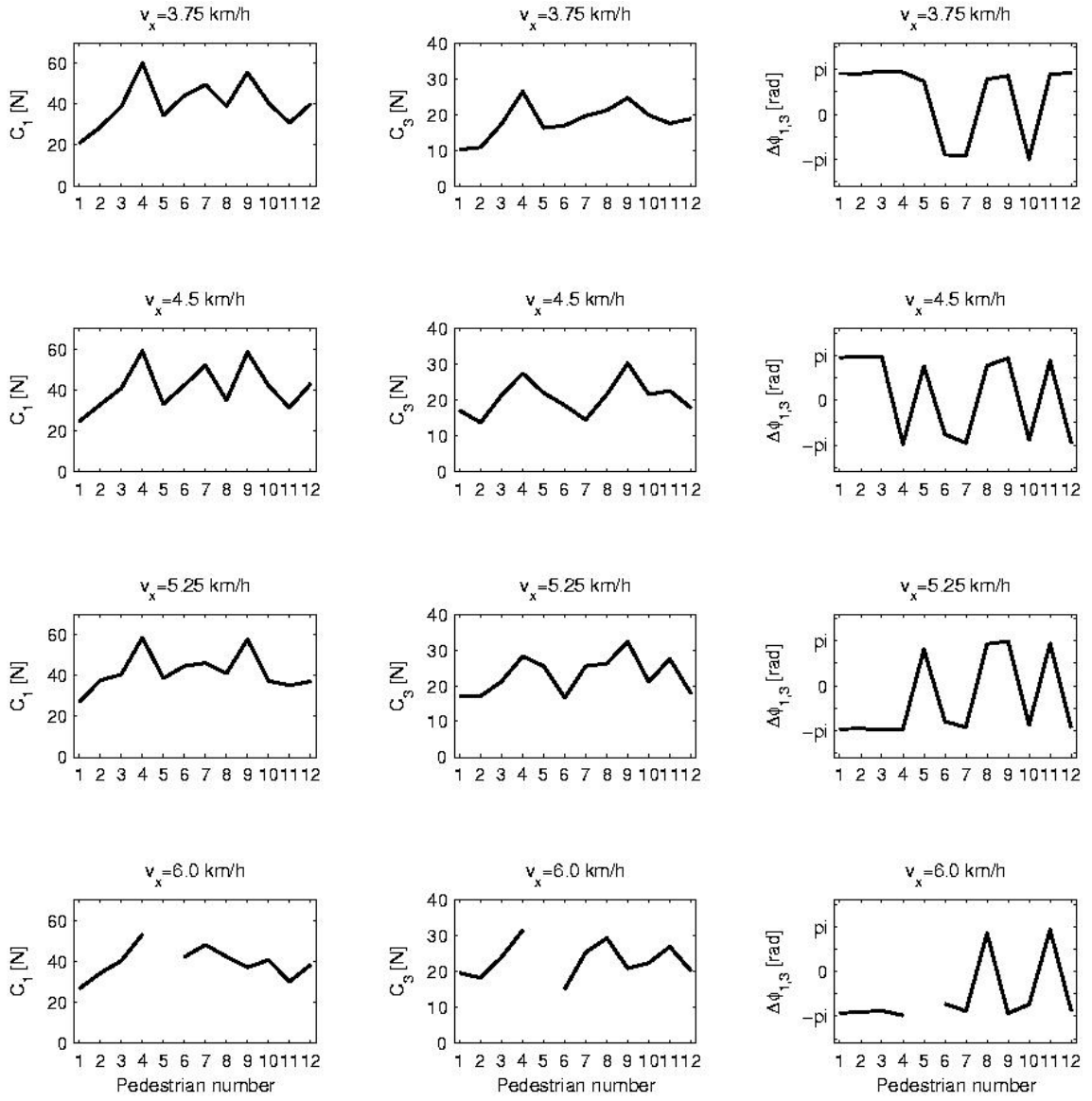

Figure 2.5: Fourier series amplitudes C_1, C_3 and phase differences $\Delta\phi_{1,3}$ of the lateral force for all pedestrians. Missing points correspond to non available experimental data.

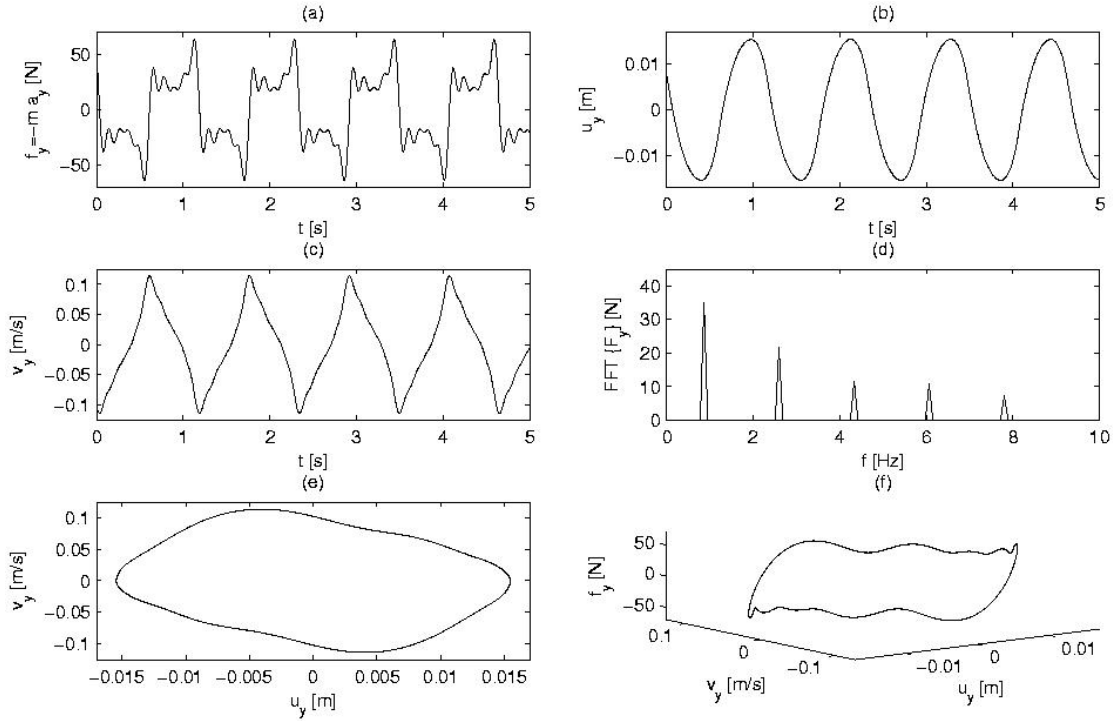

Figure 2.6: Lateral oscillation of the pedestrian "8" (walking speed 4.5 km/h). Fourier series results. (a) Time history of pedestrian-induced lateral force; (b) time history of lateral displacement and (c) velocity; (d) modulus of the FFT of the lateral force; (e) limit cycle in the phase-plane and (f) lateral force as a function of displacement and velocity.

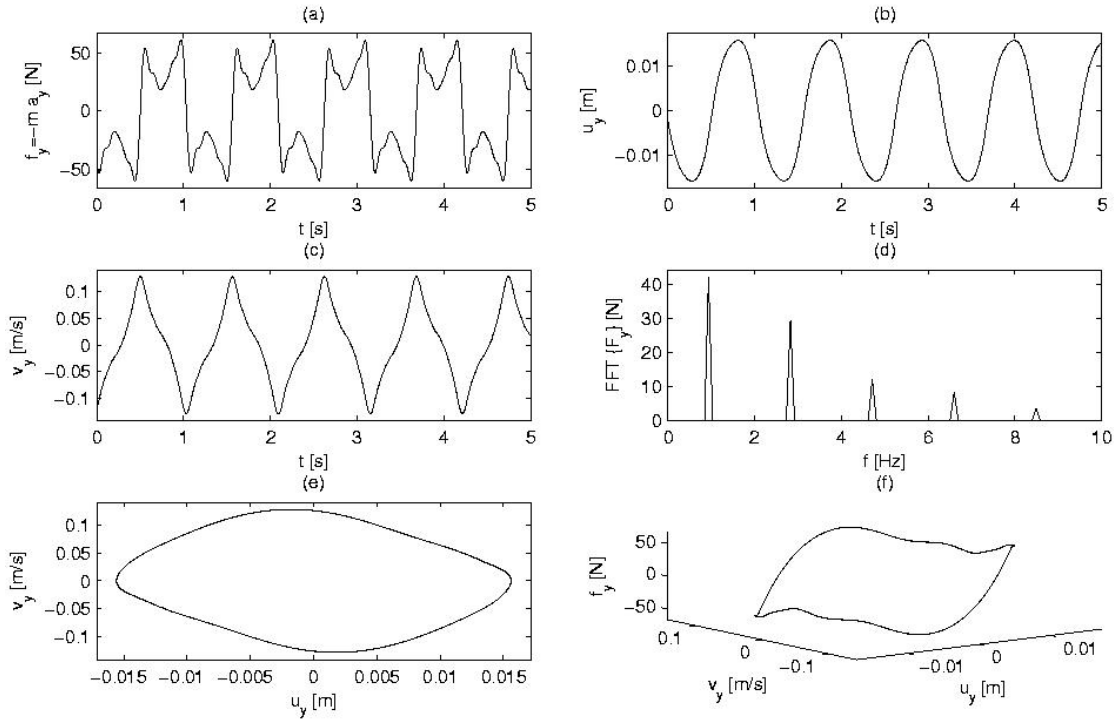

Figure 2.7: Lateral oscillation of the pedestrian "8" (walking speed 6.0 km/h). Fourier series results. (a) Time history of pedestrian-induced lateral force; (b) time history of lateral displacement and (c) velocity; (d) modulus of the FFT of the lateral force; (e) limit cycle in the phase-plane and (f) lateral force as a function of displacement and velocity.

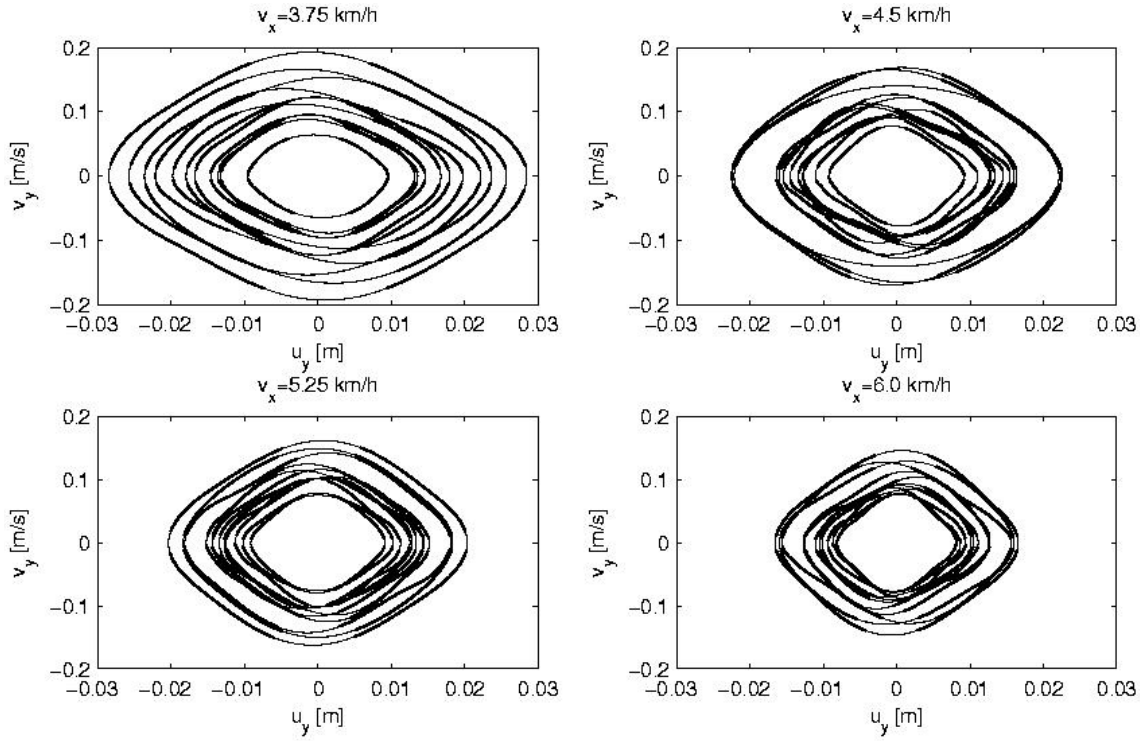

Figure 2.8: Phase plots for all pedestrians.

2.4. A modified Van Der Pol model for the lateral pedestrian force

In the first part of this Section, a modified Van der Pol (MVdP) oscillator is proposed and then analyzed by a perturbation technique. The conditions such that this oscillator is self-sustained are found. Then, an approximated expression of its periodic orbit is derived, as well as the conditions on its parameters ensuring its existence and stability. The stability analysis is made for small values of the parameter μ, related to the nonlinear part of the model restoring force (see Eq. (2.13)). As it is recalled by [23], the study of this particular case often gives an important insight into the solution also for non-small μ. Moreover, a brief discussion about the size and shape of the periodic orbit is done, as well as about the relationship between the Fourier coefficients characterizing the periodic restoring force along the orbit and the parameters of the MVdP.

Supposing that a SDoF self-sustained oscillator is an acceptable model for representing the lateral movement of the human body during walking, the

problem is then the choice of such a model. One of the simplest models is the classical Van der Pol oscillator, characterized by the restoring force expression (2.6). However, as it is proven at the end of this Section, this standard model is not general enough to provide an accurate approximation of all the experimental data. For this reason, a modification of the VdP model is proposed, defined by the following restoring force:

$$\begin{aligned}&\frac{F_{\mathrm{y}}\left(u_y,\dot{u}_y;\mathrm{p}\right)}{m}=-2\mu h\left(u_y,\dot{u}_y;\omega_0,\beta,\gamma,\delta\right)+\omega_0^2 u_y\\&h\left(u_y,\dot{u}_y;\omega_0,\beta,\gamma,\delta\right)=\omega_0\dot{u}_y\left(1-\beta u_y^2-\frac{\gamma}{\omega_0}\dot{u}_y u_y-\frac{\delta}{\omega_0^2}\dot{u}_y^2\right)\end{aligned}\tag{2.13}$$

with ω_0>0. Notice that $h\left(u_y,\dot{u}_y;\omega_0,\beta,\gamma,\delta\right)$ defines a nonlinear damping term and that $h\left(0,0;\omega_0,\beta,\gamma,\delta\right)=0$. This model has two additional parameters, γ and δ, with respect to the standard VdP model. These parameters are associated with two cubically nonlinear terms; the first one given by a displacement times a squared velocity, the second one proportional to a cubic velocity. These new terms, together with the classical one proportional to β, define the most general form of a cubic polynomial nonlinear damping.
Recalling Eq. (2.5), the dynamics equation for the case of an autonomous system with the restoring force (2.13) reads

$$\ddot{u}_y(t)-2\mu\omega_0\dot{u}_y(t)\left(1-\beta u_y^2(t)-\frac{\gamma}{\omega_0}\dot{u}_y(t)u_y(t)-\frac{\delta}{\omega_0^2}\dot{u}_y^2(t)\right)+\omega_0^2 u_y(t)=0\tag{2.14}$$

with the initial conditions $u_y(0)=u_y^0$ and $\dot{u}_y(0)=v_y^0$. If γ=δ=0 and μ>0, the standard Van der Pol oscillator is retrieved, while β=γ=0 and μ>0 leads to the Rayleigh's oscillator [23]. The periodic orbits of these two models are plotted in Fig. 2.9.

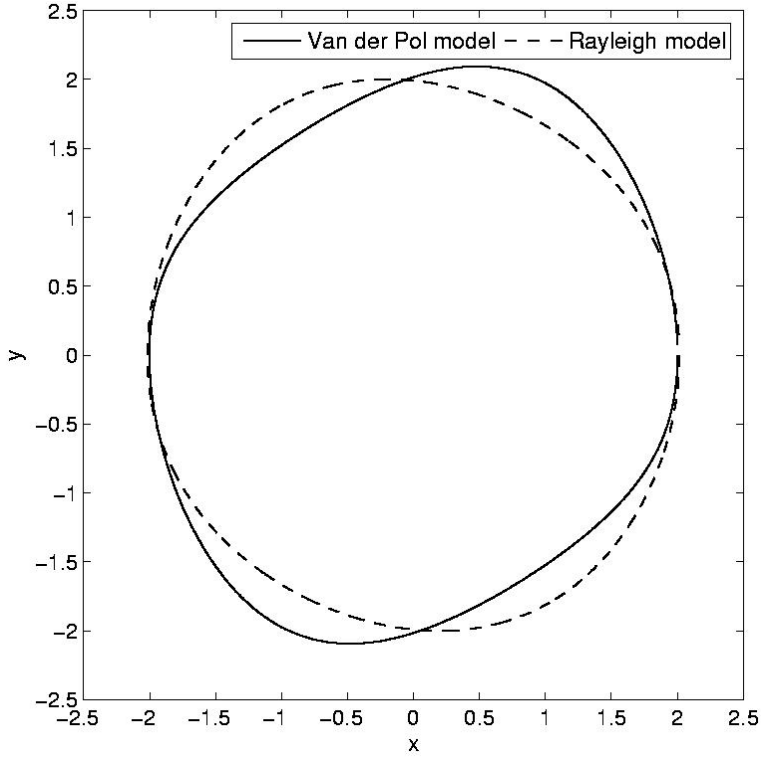

Figure 2.9: The different shapes of the limit cycles for the Van der Pol and Rayleigh's models: $x = u_y$, $y = \dot{u}_y / \omega_1$, where ω_1 is the pulsation of the autonomous oscillator. Parameter values: μ=0.15, ω_0=1 and β=1 for the Van der Pol model; μ=0.1, ω_0=1 and δ=1/3 for the Rayleigh's model.

Let us assume that (2.14) has a periodic solution $u_y = u_y(t)$ with period equal to $T = 2\pi / \rho\omega_0$, where ρ depends on the model parameters and is to be computed. Instead of solving Eq. (2.14), the new time-scale is introduced, according to a standard perturbation approach:

$$\tau = \omega_1 t \qquad \text{with} \qquad \omega_1 := \rho\omega_0 \tag{2.15}$$

where ω_1 is the (still unknown) natural circular frequency of the oscillator (2.14). Hence, one has

$$\begin{aligned} u_y(t) = \tilde{u}_y(\tau)\big|_{\tau=\rho\omega_0 t} \qquad &\Leftrightarrow \qquad \tilde{u}_y(\tau) = u_y(t)\big|_{t=\tau/\rho\omega_0} \\ \frac{du_y(t)}{dt} = \rho\omega_0 \frac{d\tilde{u}_y(\tau)}{d\tau}\Big|_{\tau=\rho\omega_0 t} \quad &\Leftrightarrow \quad \frac{d\tilde{u}_y(\tau)}{d\tau} = \frac{1}{\rho\omega_0}\frac{du_y(t)}{dt}\Big|_{t=\tau/\rho\omega_0} \end{aligned} \tag{2.16}$$

and replacing these relationships in (2.14) leads to a differential equation with periodic solutions of period 2π:

$$\begin{cases} \rho^2 \dfrac{d^2\tilde{u}_y(\tau)}{d\tau^2} - 2\mu\rho \dfrac{d\tilde{u}_y(\tau)}{d\tau}\left(1-\beta\tilde{u}_y^2(\tau)-\gamma\rho\tilde{u}_y(\tau)\dfrac{d\tilde{u}_y(\tau)}{d\tau}-\delta\rho^2\left(\dfrac{d\tilde{u}_y(\tau)}{d\tau}\right)^2\right)+\tilde{u}_y(\tau)=0 \\ \textit{Initial Conditions}: \quad \tilde{u}_y(0)=a, \qquad \dfrac{d\tilde{u}_y(0)}{d\tau}=0 \end{cases} \tag{2.17}$$

where *a* is unknown and depends on the model parameters. Notice that the initial velocity is supposed equal to zero. A solution for (2.17) can be found by a perturbation technique, in the limit of small μ (see the Appendix B for details):

$$\begin{aligned} &\rho(\mu)=1+\frac{\mu\gamma}{\beta+3\delta}+O\left(\mu^2\right) \quad \rightarrow \quad \omega_1=\omega_0\left(1+\frac{\mu\gamma}{\beta+3\delta}\right)+O\left(\mu^2\right) \\ &a(\mu)=\frac{2}{(\beta+3\delta)^{1/2}}-\mu\gamma\frac{3\beta+17\delta}{2(\beta+3\delta)^{5/2}}+O\left(\mu^2\right) \\ &\tilde{u}_y(\tau;\mu)=\left[\frac{2}{(\beta+3\delta)^{1/2}}-\mu\gamma\frac{\beta+7\delta}{(\beta+3\delta)^{5/2}}\right]\cos(\tau) \\ &-\frac{\mu}{2(\beta+3\delta)^{5/2}}\left((\beta+3\delta)\gamma\cos(3\tau)+(\beta+3\delta)(\delta-\beta)\left(3\sin(\tau)-\sin(3\tau)\right)\right)+O\left(\mu^2\right) \end{aligned} \tag{2.18}$$

This solution can be represented in the phase plane, with the coordinates $x(\tau)=\tilde{u}_y(\tau)$ and $y(\tau)=d\tilde{u}_y(\tau)/dt$. The corresponding polar coordinates read

$$\tilde{R}(\tau)=\sqrt{x(\tau)^2+y(\tau)^2}, \qquad \tilde{\theta}(\tau)=\arctan\left(x(\tau),y(\tau)\right) \tag{2.19}$$

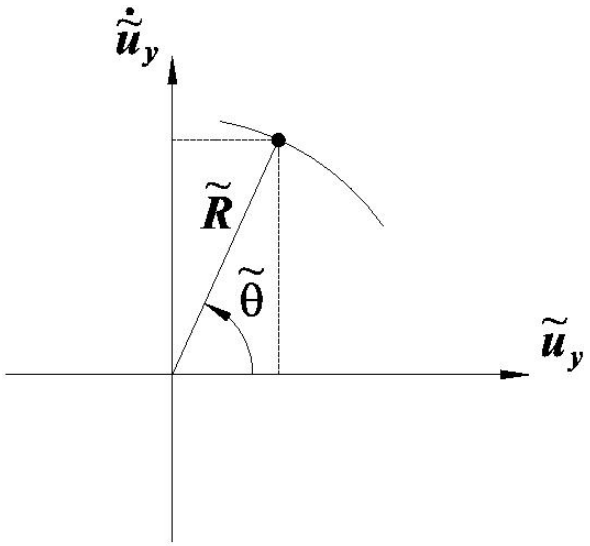

Figure 2.10: Convention for the cartesian and polar coordinates in the phase plane.

The first equation in (2.18) shows the influence of the parameter γ in the expression of the natural circular frequency ω_1: it introduces a correction of ω_0 at the first order in μ which is absent in the classical Van der Pol and Rayleigh models.

The convention on the sign of $\tilde{\theta}$ is illustrated in Fig. 2.10. Observe that the function *arctan*(*x*,*y*) used in (2.19) depends on two arguments and provides $\tilde{\theta}$-values in the interval (-π,π]. This function is implemented in all standard symbolic math software's. Conversely, the basic definition *arctan*(y/x) would lead to $\tilde{\theta} \in$(-π/2,π/2], which is not acceptable for the present analysis. From (2.19), it is possible to derive $\tilde{R}$ as a function of $\tilde{\theta}$; see Eq. (2.47) in the Appendix B. Then, the minima, maxima and points of inflexion of the radius are computed from the condition

$$\frac{d\tilde{R}\left(\tilde{\theta}\right)}{d\tilde{\theta}} = \frac{-4\mu}{\left(\beta+3\delta\right)^{3/2}} \sin\left(\tilde{\theta}\right)\left(\gamma\cos\left(3\tilde{\theta}\right)-\left(\beta-\delta\right)\sin\left(3\tilde{\theta}\right)\right)+\mathrm{O}\left(\mu^2\right)=0 \quad (2.20)$$

Neglecting the second order terms $O(\mu^2)$, Eq. (2.20) leads to $\tilde{\theta}=0$ or $\tilde{\theta}=\pi$ or $\tan\left(3\tilde{\theta}\right)=\frac{\gamma}{\beta-\delta}$, which corresponds to six solutions:

$$\tilde{\theta}_k = \arctan\left(\beta - \delta, \gamma\right) + k\frac{\pi}{3} \qquad k = 0,1,...,5 \tag{2.21}$$

These values give some information about the shape of the periodic orbit. For instance, assuming μ>0 and γ=δ=0 (classical VdP oscillator), it can be easily proven that the radius is maximum when displacements and velocities have the same sign. In detail, at the first order in μ, $\tilde{R}$ is maximum for $\tilde{\theta} = \pi/3$ and $\tilde{\theta} = -2\pi/3$. If μ>0 and γ=β=0 (Rayleigh's model), the maxima correspond to $\tilde{\theta} = -\pi/3$ and $\tilde{\theta} = 2\pi/3$; see also the example of Fig. 2.9.
Turning back to the non-normalized variables, an estimation of the displacement and velocity is obtained from (2.15), (2.16) and (2.18):

$$u_y(t) = \frac{2}{\left(\beta + 3\delta\right)^{1/2}}\cos\left(\rho\omega_0 t\right) + \mathrm{O}\left(\mu\right)$$

$$\frac{du_y(t)}{dt} = -\rho\omega_0\frac{2}{\left(\beta + 3\delta\right)^{1/2}}\sin\left(\rho\omega_0 t\right) + \mathrm{O}\left(\mu\right)$$

Let us now compute the restoring force along the periodic orbit:

$$F_y(t) = -m\frac{d^2u_y(t)}{dt^2} = -m\omega_0^2\rho^2\left[\frac{d^2\tilde{u}_y(\tau)}{d\tau^2}\right]_{\tau=\rho\omega_0 t}$$
$$= C_1\cos\left(\rho\omega_0 t - \phi_1\right) + C_3\cos\left(3\rho\omega_0 t - \phi_3\right) + ...$$

At the first order in μ, the Fourier coefficients of the first two odd harmonics read

$$\begin{aligned} C_1 &= m\omega_0^2\left(\frac{2}{\left(\beta + 3\delta\right)^{1/2}} + \mu\gamma\frac{3\beta + 5\delta}{\left(\beta + 3\delta\right)^{5/2}}\right) + \mathrm{O}\left(\mu^2\right) \\ \frac{C_3}{C_1} &= \mu\frac{9}{4}\frac{\sqrt{\left(\beta - \delta\right)^2 + \gamma^2}}{\left(\beta + 3\delta\right)^2} + \mathrm{O}\left(\mu^2\right) \end{aligned} \tag{2.22}$$

Moreover, the phase difference $\Delta\phi_{1,3}$ is equal to

$$\Delta\phi_{1,3} = \phi_3 - 3\phi_1 = \arctan(-\gamma, -\beta + \delta) - \mu \frac{3\beta^2(\beta+\delta) + \delta\left(9\delta^2 + 13\gamma^2\right) - \beta\left(15\delta^2 - 7\gamma^2\right)}{4(\beta+3\delta)\left((\beta-\delta)^2 + \gamma^2\right)} + \mathrm{O}\left(\mu^2\right) \tag{2.23}$$

The arctan function is still dependent on two arguments. Observe that at the order zero in μ, only C_1 and $\Delta\phi_{1,3}$ are non-zero. For the classical Van der Pol model, one has $C_3/C_1=9\mu/4+O(\mu^3)$ and $\Delta\phi_{1,3}=-\pi/2+3\mu/4+O(\mu^3)$. Hence, for small μ, the phase difference $\Delta\phi_{1,3}$ is equal to $-\pi/2$. When the experimental value is far from $-\pi/2$, the classical VdP model is not adequate for representing the measured lateral force. This is the case for several pedestrians of the sample analyzed here. Finally, observe that the zero-order value of $\Delta\phi_{1,3}$ in (2.23) and the angle $\tilde{\theta}_0$ in (2.21), associated with the position of stationary points of the radius $\tilde{R}$, are orthogonal. This highlights the relationship between the phase difference $\Delta\phi_{1,3}$ and the shape of the limit cycle.

2.4.1. Existence and stability of the periodic orbit

In the previous Section, a perturbation technique has been used to find an approximate expression of the periodic orbit characterizing the MVdP model. However, it is necessary to prove that this periodic orbit (or limit cycle) is stable. Therefore, a stability analysis of the model (2.14) is done in order to find the associated constraints on the values of model parameters. This analysis in performed for small values of the parameter μ, related to linear and the nonlinear damping terms of the model restoring force (see Eq. (2.13)). The standard procedure reported in [23] is applied. By definition, the total mechanical energy Π of a mechanical system is the sum of the potential and kinetic energies, indicated as K and V, respectively. Therefore, the variation of $\Pi(t)$ between two generic instants t_0 and $\bar{t}$ reads:

$$\begin{aligned}\Pi(\bar{t}) - \Pi(t_0) &:= K(\bar{t}) - K(t_0) + V(\bar{t}) - V(t_0) \\ &= \frac{1}{2}m\left(\dot{u}_y^2(\bar{t}) - \dot{u}_y^2(t_0)\right) + \frac{1}{2}m\omega_0^2\left(u_y^2(\bar{t}) - u_y^2(t_0)\right)\end{aligned} \tag{2.24}$$

In order to simplify the notation, and without loosing generality, it is supposed t_0=0. Since we are considering an autonomous system (Eqs. (2.5) and (2.13)), the difference (2.24) can be written as follows:

$$\Pi(\bar{t}) - \Pi(0) = 2\mu m \int_0^{\bar{t}} h\left(u_y(t), \dot{u}_y(t); \omega_0, \beta, \gamma, \delta\right) \dot{u}_y(t)\, dt \tag{2.25}$$

By definition, on the limit cycle of a self-sustained oscillator, the total energy returns to its original value after one period $0 \le t \le T$, i.e.

$$\Pi(T) - \Pi(0) = 2\mu m \int_0^{T} h\left(u_y(t), \dot{u}_y(t); \omega_0, \beta, \gamma, \delta\right) \dot{u}_y(t)\, dt = 0 \tag{2.26}$$

Now observe that the linearized equation, i.e. Eq. (2.14) with μ=0, has solutions of the form

$$u_y^{lin}(t) = a\cos\left(\omega_0 t + \alpha\right), \qquad \dot{u}_y^{lin}(t) = -a\omega_0 \sin\left(\omega_0 t + \alpha\right) \tag{2.27}$$

For $|\mu| \ll 1$, the limit cycle of (2.14), if it exists, is expected to be close to one of the orbits defined by a certain value of a in (2.27). Without loss of generality, one can set α=0 and a>0. Hence, on the limit cycle of the nonlinear system (2.14), for some values of a, one has $u_y(t) \cong a\cos(\omega_0 t)$ and $T \cong 2\pi/\omega_0$. Using these expressions, the variation of the total mechanical energy along one period is approximated by

$$g(a) = -2\mu m a \omega_0 \int_0^{2\pi/\omega_0} h\left(a\cos\left(\omega_0 t\right), -a\sin\left(\omega_0 t\right); \omega_0, \beta, \gamma, \delta\right) \sin\left(\omega_0 t\right) dt$$

The function $g(a)$ for the model defined by (2.14) reads

$$g(a) = 2\mu m a^2 \omega_0^2 \int_0^{2\pi/\omega_0} \sin^2\left(\omega_0 t\right) \begin{pmatrix} 1 - \beta a^2 \cos^2\left(\omega_0 t\right) + \gamma a^2 \cos\left(\omega_0 t\right)\sin\left(\omega_0 t\right) \\ -\delta a^2 \sin^2\left(\omega_0 t\right) \end{pmatrix} dt$$

$$= -\frac{\mu m a^2 \omega_0}{2} \pi \left(a^2\left(\beta + 3\delta\right) - 4\right)$$

Imposing $g(a)=0$, one obtains the constant a (see also the second equation in (2.18))

$$a = a_0 = \frac{2}{(\beta + 3\delta)^{1/2}} \tag{2.28}$$

One can see that $\beta+3\delta>0$ is needed for the existence of the solution. Moreover, if the limit cycle is *stable*, along spiral paths close and interior to the limit cycle ($a<a_0$), one has $g(a)>0$, i.e. the total energy increases, while for exterior paths $g(a)<0$. Hence, the necessary condition of stability of the limit cycle writes

$$g'(a)\Big|_{a=a_0} < 0 \quad \rightarrow \quad -\frac{8\pi\mu m\omega_0}{\sqrt{\beta + 3\delta}} < 0 \quad \rightarrow \quad \mu > 0$$

In summary, the following conditions are needed for the oscillator (2.14) to have a stable periodic orbit, i.e. it is self-sustained:

$$\mu > 0, \qquad \beta + 3\delta > 0 \tag{2.29}$$

2.4.2. Energy analysis

In this Subsection, the energy difference expression (2.25) is analyzed in more detail, with reference to the MVdP model (2.13)-(2.14). Four contributions can be distinguished, i.e.

$$\Pi(\bar{t}) - \Pi(0) := \Delta\Pi(\bar{t}) = \Delta\Pi^{(\mu)}(\bar{t}) + \Delta\Pi^{(\beta)}(\bar{t}) + \Delta\Pi^{(\gamma)}(\bar{t}) + \Delta\Pi^{(\delta)}(\bar{t})$$

where

$$\begin{aligned}
\Delta\prod^{(\mu)}\left(\bar{t}\right) &= 2\mu m\omega_0\int_0^{\bar{t}}\left(\dot{u}_y(t)\right)^2 dt \\
\Delta\prod^{(\beta)}\left(\bar{t}\right) &= -2\mu m\omega_0\beta\int_0^{\bar{t}}\left(u_y(t)\dot{u}_y(t)\right)^2 dt \\
\Delta\prod^{(\gamma)}\left(\bar{t}\right) &= -2\mu m\gamma\int_0^{\bar{t}} u_y(t)\left(\dot{u}_y(t)\right)^3 dt \\
\Delta\prod^{(\delta)}\left(\bar{t}\right) &= -\frac{2\mu m}{\omega_0}\delta\int_0^{\bar{t}}\left(\dot{u}_y(t)\right)^4 dt
\end{aligned} \tag{2.30}$$

The first term of $\Delta\prod\left(\bar{t}\right)$ is always non-negative, due to the first condition in (2.29), i.e. μ>0: it represents the energy "produced" by the oscillator, i.e. the internal energy source of the system. The second and fourth terms have a constant sign. They are always non-positive, provided that

$$\beta \geq 0 \quad and \quad \delta > 0 \qquad or \qquad \beta > 0 \quad and \quad \delta \geq 0 \tag{2.31}$$

Therefore, under one of the assumptions (2.31), the corresponding energy terms represent some dissipation phenomena. β and δ cannot be simultaneously zero due to the second inequality in (2.29). Finally, when γ≥0, the sign of the term $\Delta\prod^{(\gamma)}\left(\bar{t}\right)$ is positive when displacements and velocities have the same sign, negative otherwise. The opposite situation occurs when γ≤0. The sum of the four energy contributions (2.30) is not zero at every time $\bar{t}$. However, it is zero at the end of every cycle: the energy produced is equal to the energy dissipated after one cycle, i.e. the system is able to self-sustain its motion.

Both assumptions (2.31) are not necessary, but are sufficient to ensure the existence of the limit cycle. Stability is guaranteed when it is also supposed that μ>0. Moreover, (2.31) allows a clear energetic interpretation of the model, in the sense that it is possible to know a priori which terms represent energy dissipation and which ones represent an energy source. For these reasons, (2.31) is used for the parameters identification of the following Section.

2.5. Identification of the MVdP parameters from experimental data of the lateral pedestrian force

2.5.1. Procedure

In this Subsection, an identification procedure of the parameters of the restoring force (2.13) of the MVdP model is proposed, accounting for the parameter constraints discussed above. The identification is based on the periodic signal obtained from the experimental lateral force of a pedestrian. For the purpose of the identification, it is convenient to rewrite the restoring force (2.13) in the form:

$$\begin{aligned} &F_y = F_y\left(u_y, \dot{u}_y; \mathbf{a}\right) = a_1 u_y + a_2 \dot{u}_y + a_3 u_y^2 \dot{u}_y + a_4 u_y \dot{u}_y^2 + a_5 \dot{u}_y^3 \\ &\text{with} \qquad \mathbf{a} = \left[a_1, a_2, a_3, a_4, a_5\right]^T \end{aligned} \tag{2.32}$$

The parameters collected in the vector **a** are related to the MVdP parameters according to the following identities:

$$a_1 = m\omega_0^2, \quad a_2 = -2\mu m\omega_0, \quad a_3 = 2\mu m\omega_0\beta, \quad a_4 = 2\mu m\gamma, \quad a_5 = \frac{2\mu m}{\omega_0}\delta \tag{2.33}$$

The mass m is assumed known. Then, the optimal parameter value **a*** is computed by a constrained minimization procedure:

$$\mathbf{a}^* = \arg\left[\min_{\mathrm{a}\in S} \frac{1}{2}\sum_{i=1}^{N_{id}} \left(F_{y,per}^{(i)} - F_y\left(u_{y,per}^{(i)}, \dot{u}_{y,per}^{(i)}; \mathbf{a}\right)\right)^2\right] \tag{2.34}$$

where $F_{y,per}^{(i)} = F_{y,per}\left((i-1)\Delta t\right)$ are computed by the Fourier series (2.10) approximating the experimental walking force. Likewise, $u_{y,per}^{(i)} = u_{y,per}\left((i-1)\Delta t\right)$ and $\dot{u}_{y,per}^{(i)} = \dot{u}_{y,per}\left((i-1)\Delta t\right)$ are the periodic displacements and velocities, defined by (2.12). The time step Δt is equal to the time step of experimental data and N_{id} is the number of points used for the identification procedure, corresponding to one period. The optimization

constraints are given in (2.29), with the additional (trivial) assumption $\omega_0>0$. However, as it has been discussed in the previous Section, instead of the second inequality in (2.29), conditions (2.31) are imposed. Hence, using (2.33), the optimization constraints written on the parameters a_i are summarized as follows:

$$a_1 > 0, \quad a_2 < 0 \tag{2.35}$$

and

$$a_3 \geq 0 \quad \text{and} \quad a_5 > 0 \qquad \text{or} \qquad a_3 > 0 \quad \text{and} \quad a_5 \geq 0 \tag{2.36}$$

As a result, the definition of the set S introduced in (2.34) becomes

$$S = \left\{ \left[a_1, a_2, a_3, a_4, a_5 \right]^T \in \mathbb{R}^5 : a_1 \geq 0, \quad a_2 \leq 0, \quad a_3 \geq 0 \quad and \quad a_5 \geq 0 \right\} \tag{2.37}$$

The expressions (2.34) and (2.37) define a constrained *linear* optimization problem. After the identification of the optimal parameters, the strict inequalities in (2.35) and (2.36) are checked. In all the cases analyzed in this Chapter, the linear identification directly leads to parameters fulfilling these strict inequalities. Finally, the model parameters are deduced from the identified vector **a***:

$$\omega_0 = \sqrt{\frac{a_1^*}{m}}, \quad \mu = -\frac{a_2^*}{2a_1^*}\sqrt{\frac{a_1^*}{m}}, \quad \beta = -\frac{a_3^*}{a_2^*}, \quad \gamma = -\frac{a_4^*}{a_2^*}\sqrt{\frac{a_1^*}{m}}, \quad \delta = -\frac{1}{m}\frac{a_1^*}{a_2^*}a_5^*$$

2.5.2. Results

The parameters for the pedestrian "8" identified using the previous least square procedure are given in Table 2.5. A comparison between the periodic-experimental lateral force and the identified force reveals a very good agreement, as illustrated in Figs. 2.11 and 2.12 at two different walking speeds. Fig. 2.13 shows for the same pedestrian the time-history during a walking step

(left-and-right) of the energy terms defined in (2.30). We recall that $\Delta\prod^{(\mu)}$ has the physical meaning of energy produced to sustain the motion.

	3.75 km/h	4.5 km/h	5.25 km/h	6.0 km/h
$\omega_0\,[rad/s]$	4.00	4.28	4.39	4.57
μ	0.42	0.72	0.47	0.24
$\beta\,[m^{-2}]$	48.79	1151.05	3144.24	0
$\gamma\ [m^{-2}]$	4164.20	6949.97	11559.79	18097.17
$\delta\ [m^{-2}]$	1583.01	2655.22	1869.23	2818.99
R	1.00	0.98	0.99	0.99

Table 2.5 – MVdP model: the identified parameters associated with pedestrian "8".

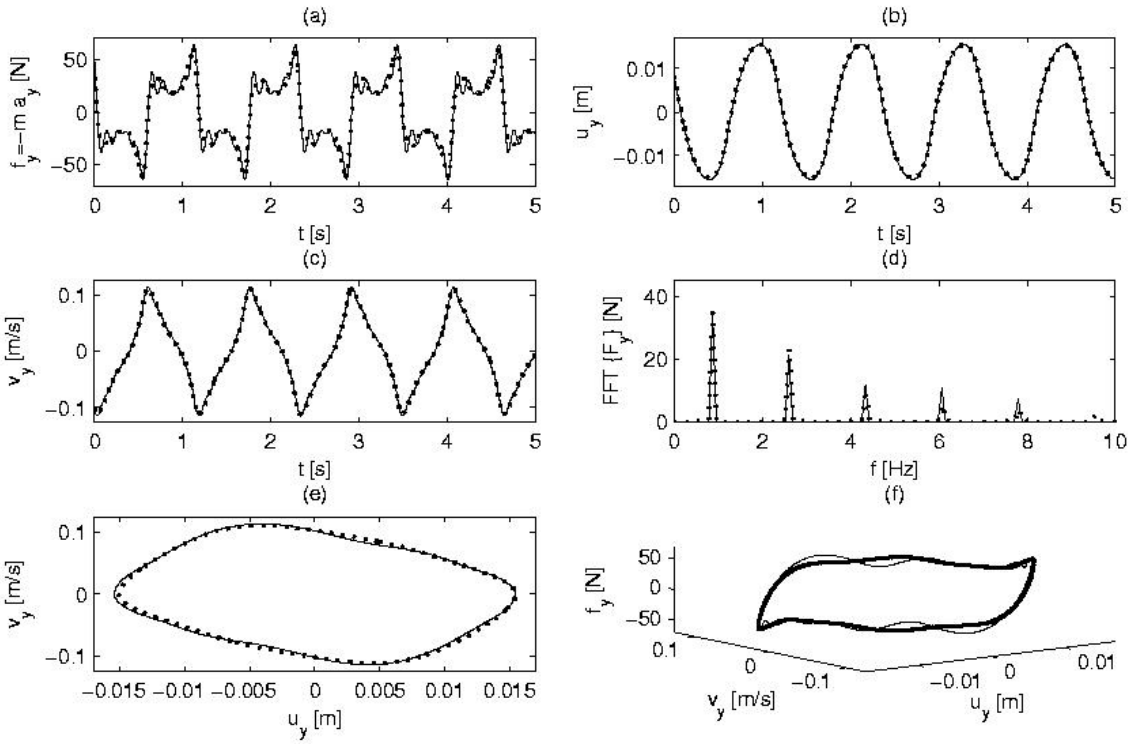

Figure 2.11: Lateral oscillation of pedestrian "8"; v_x=4.5 km/h. Identified (dotted line) vs. Fourier series (continuous line) results. (a) Time history of the lateral force; (b) time history of lateral displacement and (c) velocity; (d) modulus of the FFT of the lateral force; (e) limit cycle in the phase-plane and (f) lateral force as a function of displacements and velocities.

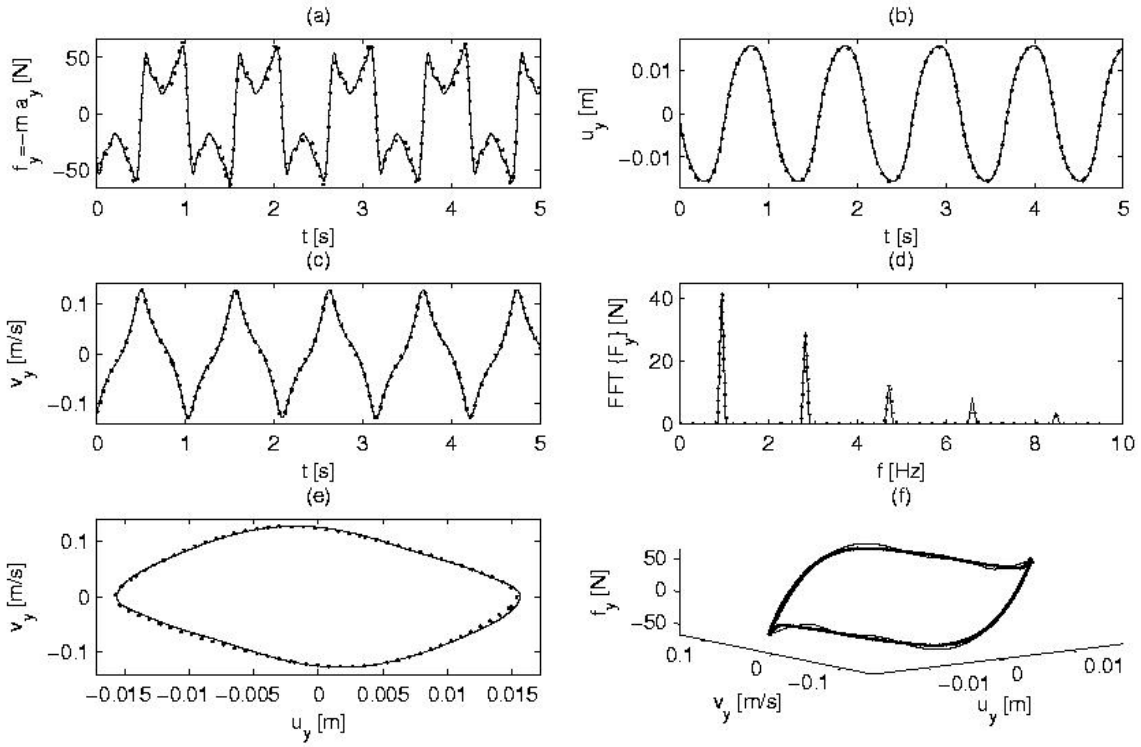

Figure 2.12: Lateral oscillation of pedestrian "8"; v_x=6.0 km/h. Identified (dotted line) vs. Fourier series (continuous line) results. (a) Time history of the lateral force; (b) time history of lateral displacement and (c) velocity; (d) modulus of the FFT of the lateral force; (e) limit cycle in the phase-plane and (f) lateral force as a function of displacements and velocities.

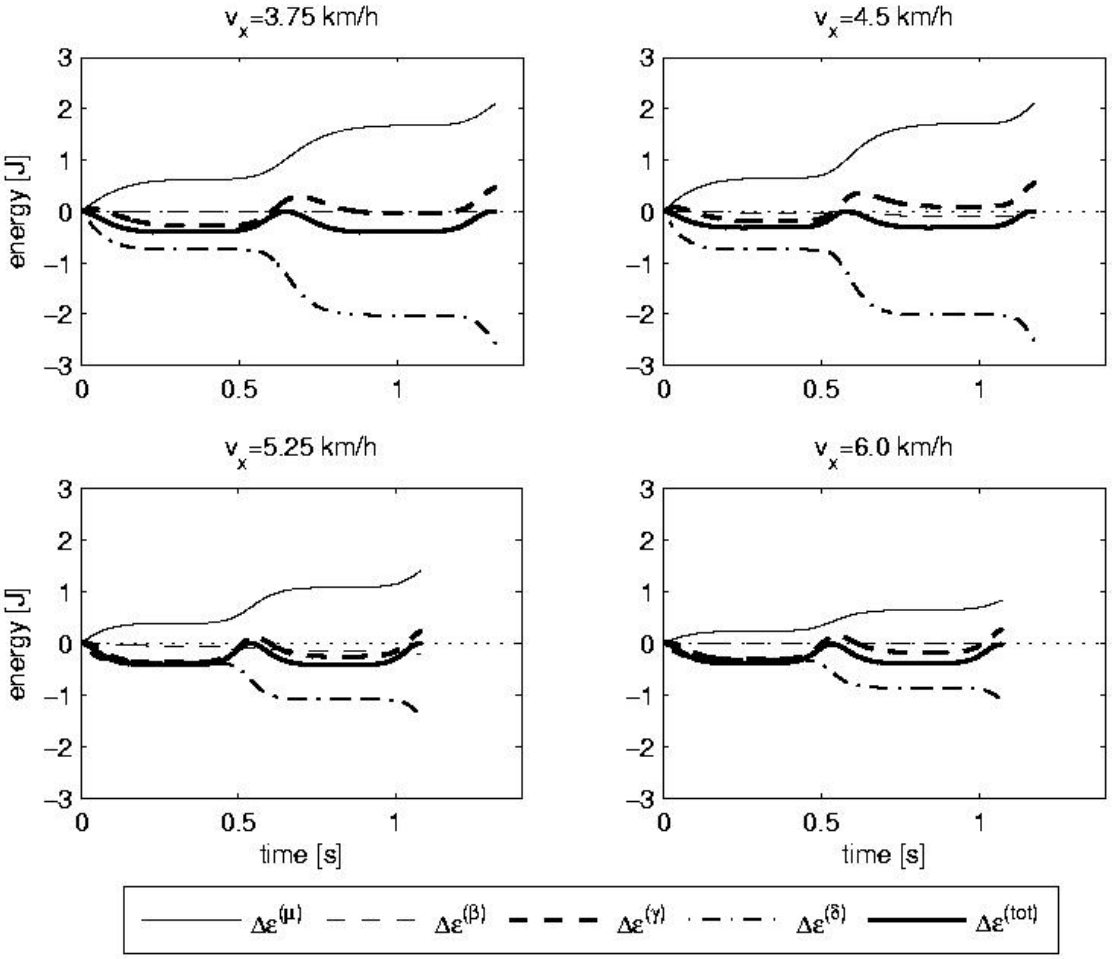

Figure 2.13: Identified MVdP model for pedestrian "8". Time-evolution during a walking step of the energy terms associated with the nonlinear damping. The continuous thin line indicates the energy produced to sustain the oscillation.

Fig. 2.14 shows that ω_0 for a given pedestrian increases when the walking speed increases. The product $\mu\gamma$ also has a quite regular behaviour, since it is directly related to the walking frequency $\omega_1=\rho\omega_0$, according to Eq. (2.18). The parameter μ varies for different walking speeds and from one pedestrian to the other, but it is almost always less than the 0.7. Accounting for the energetic interpretation that can be associated with μ and $\Delta\prod^{(\mu)}$ (Eq. (2.30)), a more regular behaviour of this parameter might be found by introducing into the identification procedure an additional constraint based on the measurement of the metabolic cost of the walk. However, this kind of measurements could be efficiently used only for a model representing the motion of the pedestrian center of gravity in the three directions, not only the lateral one, since the metabolic cost is a *global* index. This is beyond the purposes of the present

work. The third subplot of Fig. 2.14 shows that $2/(\beta+3\delta)^{1/2}$ has limited variations from one pedestrian to the others. This can be explained using (2.28), indicating the relationship between $2/(\beta+3\delta)^{1/2}$ and the lateral displacement amplitude. The experimental and identified amplitudes C_1 and C_3 as well as the phase differences $\Delta\phi_{1,3}$ are compared in Fig. 2.15 for all pedestrians and all walking speeds. The correlation coefficient R between the experimental and identified force curves gives a global measure of the quality of the identification: it is very close to one in all cases analyzed here; see Fig. 2.16.

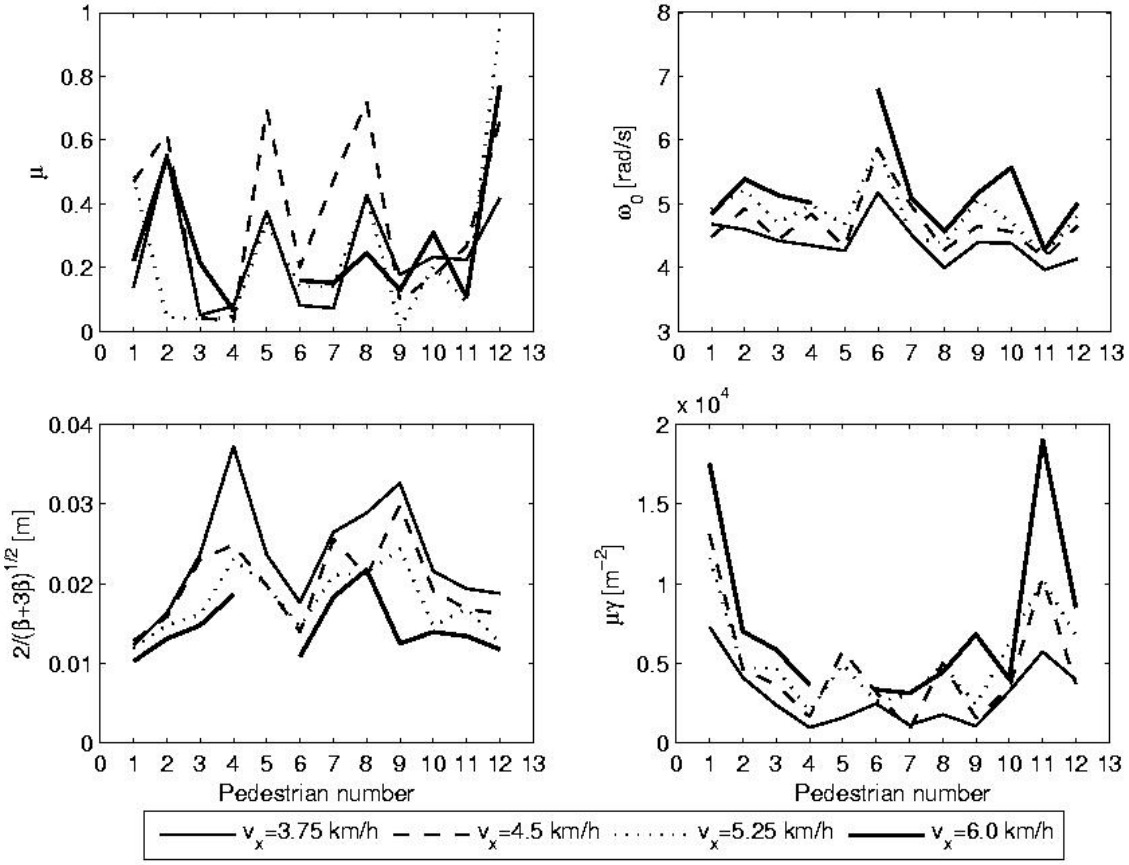

Figure 2.14: Identified parameters of the MVdP model for the twelve pedestrians. Missing points correspond to non available experimental data.

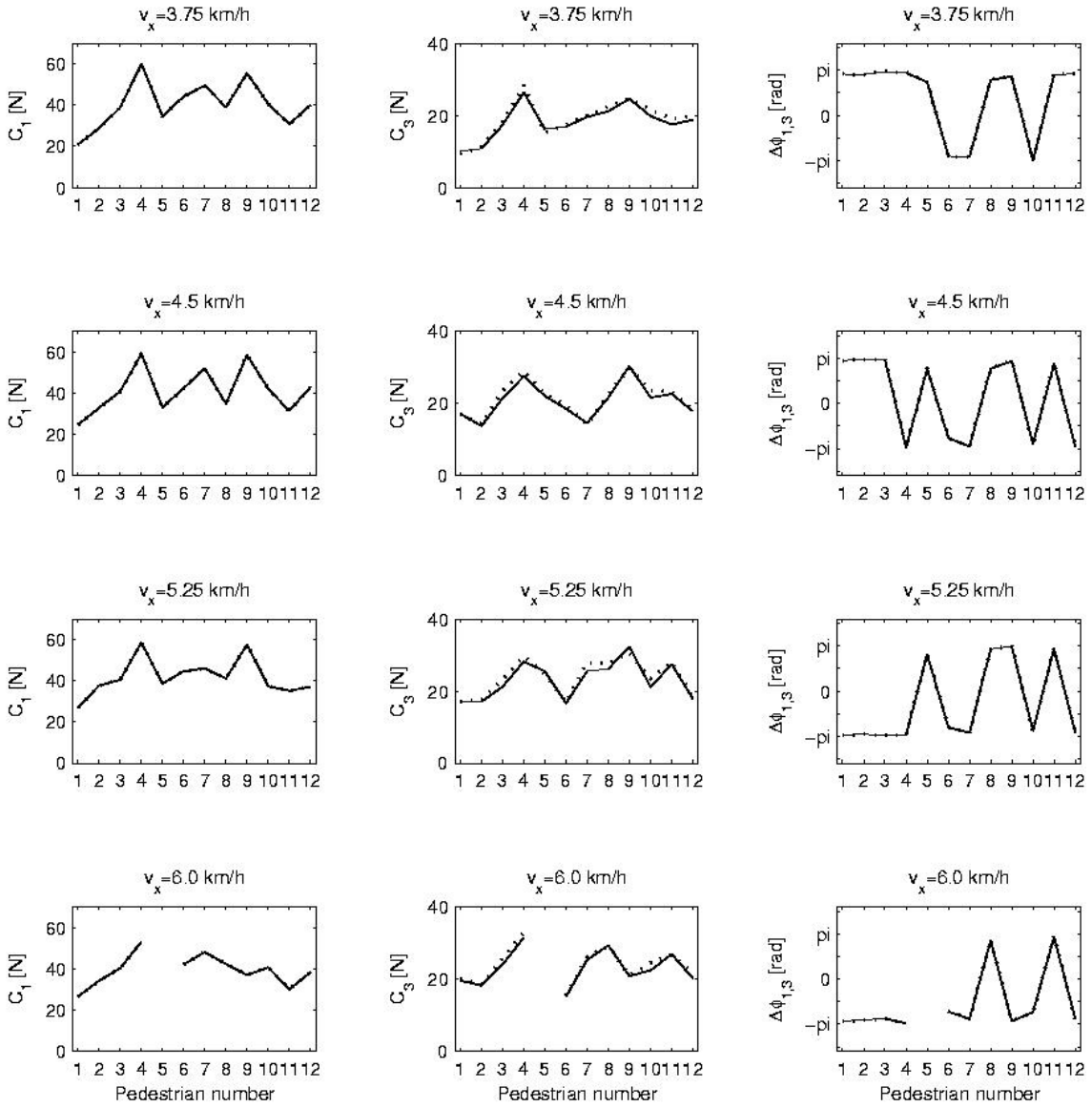

Figure 2.15: Comparison between the Fourier series computed from experimental lateral force data (continuous line) and from the force associated with the identified MVdP models (dotted line). The comparison concerns the amplitudes C_1 and C_3 and phase differences $\Delta\phi_{1,3}$.

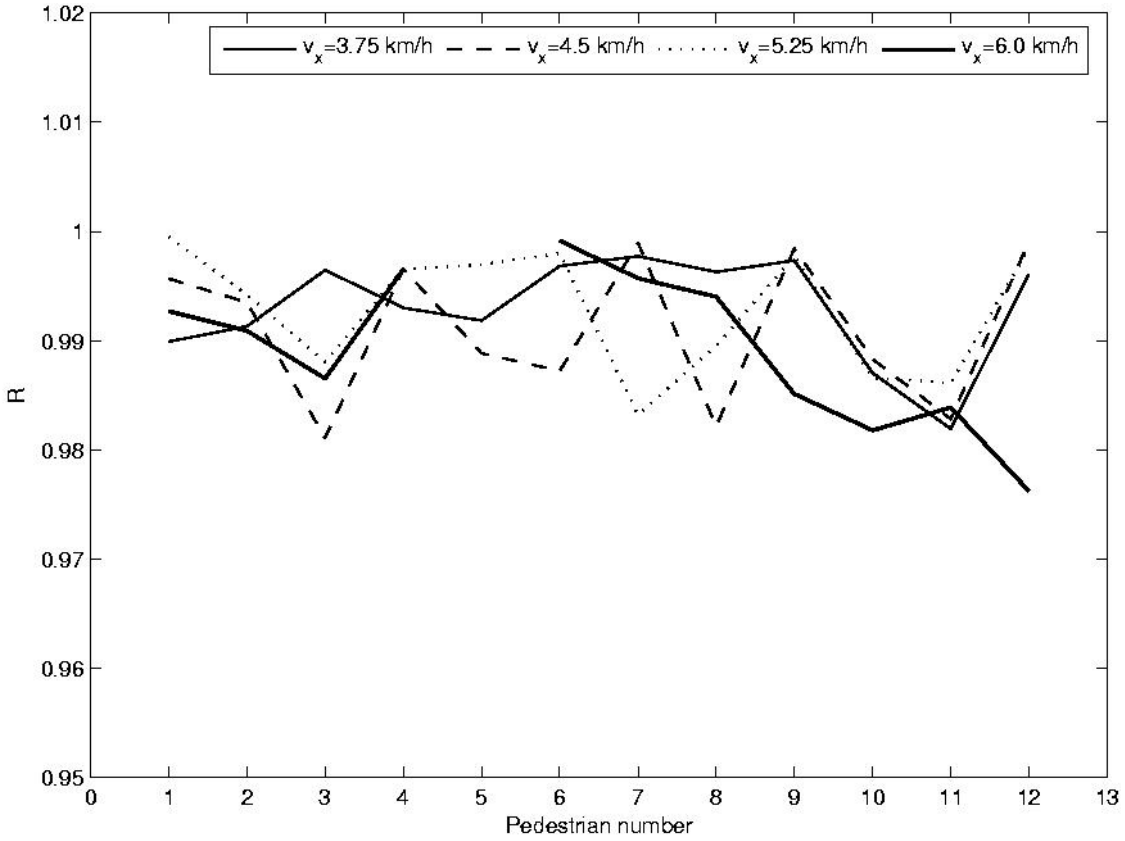

Figure 2.16: Correlation R between the lateral force computed by the Fourier series and the one associated with the identified MVdP model.

2.6. Conclusions

In this Chapter an exhaustive experimental analysis of the lateral walking force on a rigid floor has been presented. The importance of the phase differences between the Fourier harmonics in the series representing the periodic approximation of the force has been highlighted. Then, the use of a self-sustained autonomous SDoF oscillator has been proposed for modelling the lateral motion of the center of gravity of a pedestrian walking on a rigid floor: the nonlinear restoring force of this oscillator represents the lateral walking force. It has been shown by the analysis of experimental data that the modified version of the classical Van der Pol model proposed here provides a good fitting between the model behaviour and the periodic force extracted from experiments. The synchronization which may occur when a pedestrian walks on a moving floor is analyzed in the next Chapters. However, it is well-

known that forced self-sustained oscillators may have the so-called *frequency locking* effect, i.e. the synchronization between the oscillator response and the external excitation.

The application of the same approach for the vertical and longitudinal components of the walking force is also under study.

Chapter 3

A modified Van der Pol oscillator for modelling the lateral pedestrian force on a moving floor. Part I: response curves

This Chapter presents a model for the lateral oscillation of a pedestrian walking on a laterally moving floor. The basic assumption is that the lateral dynamics of a pedestrian can be modeled by a single-degree-of-freedom *self-sustained* oscillator. Using the terminology of non-linear dynamics, an autonomous self-sustained oscillator is characterized by a stable limit cycle, driven with a certain *natural* frequency. This property reproduces the intrinsic nature of the walking phenomenon: the pedestrian produces by itself the energy needed to walk, i.e. it self-sustains its motion. The previous Chapter showed that a suitable form for the restoring force of such an oscillator corresponds to a modified Van der Pol (MVdP) model and the associated parameters have been identified in the autonomous (rigid floor) case for a group of twelve pedestrians. The MVdP oscillator is analyzed here in the non-autonomous case, when the so-called *frequency entrainment* effect may occur. It means that under certain conditions, the response frequency switches from the natural value to that of the external excitation. According to the physical interpretation considered here, the entrainment corresponds to the situation where the pedestrian changes its natural walking frequency and synchronizes with the floor oscillation frequency. In this Chapter, the steady entrained response of the MVdP model subjected to a harmonic excitation is discussed in terms of *response amplitude curves*, obtained using the harmonic balance method truncated at the first harmonic. Experimental results, available in the literature, concerning pedestrians walking a shake table are compared with the

model predictions and a good agreement is obtained. The *stability* of the entrained response is analyzed in the next Chapter.

3.1. Introduction

In the non-linear dynamics literature, the so-called self-sustained oscillators are well-known and they possess some properties that seem to be well suited for a pertinent modelling of the pedestrian behavior. For this reason, in the previous Chapter has been proposed to represent the *lateral* oscillation of a pedestrian walking on a *rigid floor* by an *autonomous self-sustained* oscillator (see also [2, 5, 35]). This oscillator is named *modified Van der Pol* (MVdP) model, because it has been obtained by adding two polynomial terms of order three to the *nonlinear damping* of the classical Van der Pol model [23]. The *moving floor* case, analyzed here, corresponds to a *non-autonomous* MVdP oscillator.
In certain situations, it is useful to replace a self-sustained oscillator with a simpler dynamic model, based on the so-called phase equation [24]. Roughly speaking, the response of a self-sustained oscillator can be described in terms of amplitude and angle variable. If the amplitude is supposed constant, then the angle variable suffices to describe the oscillation. In this case, the so-called total phase, strictly related to the angle variable [24, 36], governs the system evolution by a suitable equation of phase. This idea has been used in [30] and [31] for modelling the crowd behavior: each pedestrian is represented by a phase equation. The time-derivative of the phase represents the instantaneous walking frequency. By definition, this approach neglects the amplitude variations of the pedestrian oscillations. However, several experimental tests, e.g. [27], show that the variations of the lateral oscillation amplitude of pedestrians are not negligible. In this respect, Macdonald [37] has recently suggested the use of a model for the pedestrian lateral oscillation where *only* the amplitude variations are accounted for and no frequency modulation due to the external excitation is considered. The modified Van der Pol (MVdP) model proposed here accounts for *both phase and amplitude variations* due to external excitation.

One of the most important properties of non-autonomous self-sustained oscillators is that they may have an *entrained* response [24], i.e. a response characterized by the same frequency as that of the excitation. The amplitude of

the entrained response of the MVdP model is analyzed in this Chapter following a procedure similar to that used in [23, 25] for the standard Van der Pol model an Rayleigh model. The stability analysis is discussed in the next Chapter. Differently from the standard Van der Pol model, the MVdP oscillator is *non-isochronous* [24, 38, 39].

Actually, an entrained response represents a pedestrian *synchronized* with the moving floor, even if its natural frequency is different. With a less precise terminology, it can be said that the walker *synchronizes* its frequency with that of the floor. The term synchronization should be used when two of more coupled self-sustained oscillators with different natural frequencies move at the same frequency, while the entrainment concerns an oscillator that assumes the same frequency than that of an *external agency*. Both terms will be used here indifferently, as it is usually done in the applications concerning the pedestrian-floor interaction. The particular case of a *harmonic excitation* is considered because, on one hand, it is the natural assumption required to apply the *harmonic balance method* and, on the other hand, because a floor lateral motion at constant frequency and amplitude is a simple experimental condition, easy to obtain using a shake table where pedestrians are asked to walk. This experimental situation is studied e.g. in [26]. A similar situation is obtained when pedestrians walk on a treadmill placed on a shake table (see e.g. [27, 28]): in this Chapter it is shown that the MVdP model is able to reproduce a well-known experimental result concerning pedestrians, viz. the almost linear relationship between the floor motion amplitude and the amplitude of the lateral force [9, 27].

After the Introduction, the MVdP model is presented in Section 3.2. Section 3.3 concerns the determination of the response amplitude equation for the MVdP oscillator using the harmonic balance method. Then, the response curves at constant excitation amplitude are represented in Subsection 3.3.1 using the suitable non-dimensional parameters. Section 3.4 presents a discussion about the response curves at constant excitation frequency: they are compared with some experimental results known from literature. The last Section presents some conclusions and describes the main topics treated in the next Chapter.

3.2. Models for the lateral pedestrian force

3.2.1. The Modified Van der Pol model

In the previous Chapter, the modified Van der Pol (MVdP) oscillator (2.14) has been used to represent the lateral oscillations of pedestrians during walking on a rigid floor [1, 2, 35]:

$$\frac{d^2u_y}{dt^2} - 2\mu\omega_0 \frac{du_y}{dt}\left(1 - \beta u_y^2 - \frac{\gamma}{\omega_0}\frac{du_y}{dt}u_y - \frac{\delta}{\omega_0^2}\left(\frac{du_y}{dt}\right)^2\right) + \omega_0^2 u_y = 0 \qquad (3.1)$$

where u_y is the lateral displacement of the center of mass of the pedestrian; ω_0 is the natural frequency of the underlying linear oscillator, μ, β, γ and δ are coefficients associated with the nonlinear damping term, which allows the self-sustaining mechanism responsible of perpetual periodic oscillation in the autonomous case. The oscillator (3.1) is *self-sustained*, viz. it has a stable limit cycle, when $\mu>0$ and $\beta+3\delta>0$. The parameter identification made in the previous Chapter has been performed by imposing the stronger conditions $\beta>0$ and $\delta\geq 0$ or $\beta\geq 0$ and $\delta>0$. Using this assumption, a very good fitting of experimental results in the rigid floor regime has been obtained. In the limit of small μ values, the amplitude of the limit cycle reads $u_{y,max}\simeq 2/\sqrt{(\beta+3\delta)}$, while the natural frequency is

$$\omega_1 \simeq \omega_0\left(1 + \frac{\mu\gamma}{\beta+3\delta}\right)$$

The details about this oscillator and its application to the modelling of the lateral pedestrian oscillations on a rigid floor are discussed in the previous Chapter.

The main aim of the present Chapter is to study the response of the MVdP oscillator (3.1) *under a harmonic external force*, representing a periodic floor motion, with an amplitude small enough to avoid the loss of the lateral stability of the walker. In general, the coupled system constituted by a pedestrian modelled according to Eq. (3.1) and a laterally vibrating structure

thought as a single degree-of-freedom system, can be written as follows (see also Fig. 3.1):

$$\begin{cases} \dfrac{d^2U_y}{dt^2} + 2\xi_s\omega_s \dfrac{dU_y}{dt} + \omega_s^2 U_y = \dfrac{1}{M} F_y\left(u_y, \dfrac{du_y}{dt}\right) \\ m\dfrac{d^2u_y}{dt^2} + F_y\left(u_y, \dfrac{du_y}{dt}\right) = -m\dfrac{d^2U_y}{dt^2} \end{cases} \tag{3.2}$$

where

$$F_y\left(u_y, \frac{du_y}{dt}\right) = m\left(-2\mu\omega_0 \frac{du_y}{dt}\left(1 - \beta u_y^2 - \frac{\gamma}{\omega_0}\frac{du_y}{dt}u_y - \frac{\delta}{\omega_0^2}\left(\frac{du_y}{dt}\right)^2\right) + \omega_0^2 u_y\right) \tag{3.3}$$

is the restoring force the MVdP oscillator; U_y is the horizontal displacement of the structure, M is modal mass of the structure for the considered lateral mode; ξ_s and ω_s are the modal damping ratio and circular frequency, respectively; u_y is the lateral displacement of the center of mass of the pedestrian *with respect to the structure (the floor)*; m is the pedestrian mass. Observe that Eqs. (3.2) do not take into account the mode shape effect [5]. In this Chapter, the coupled pedestrian-structure behaviour represented by Eq. (3.2) will not be considered. A simpler situation is rather analyzed, where the floor lateral motion is supposed known and harmonic with displacement amplitude A_d>0 and with frequency ω (see Fig. 3.1b)

$$U_y(t) = A_d\cos(\omega t) \quad \rightarrow \quad \frac{d^2U_y(t)}{dt^2} = -A_{acc}\cos(\omega t) \tag{3.4}$$

where A_{acc}:=$A_d\omega^2$ is the floor acceleration amplitude. Hence, the second equation in (3.2) becomes

$$\frac{d^2u_y(t)}{dt^2} - 2\mu\omega_0\frac{du_y(t)}{dt}\left(1 - \beta u_y^2(t) - \frac{\gamma}{\omega_0}\frac{du_y(t)}{dt}u_y(t) - \frac{\delta}{\omega_0^2}\left(\frac{du_y(t)}{dt}\right)^2\right) + \omega_0^2 u_y(t) = A_{acc}\cos(\omega t) \tag{3.5}$$

Eq. (3.5) defines a harmonically excited (non-autonomous) MVdP oscillator.

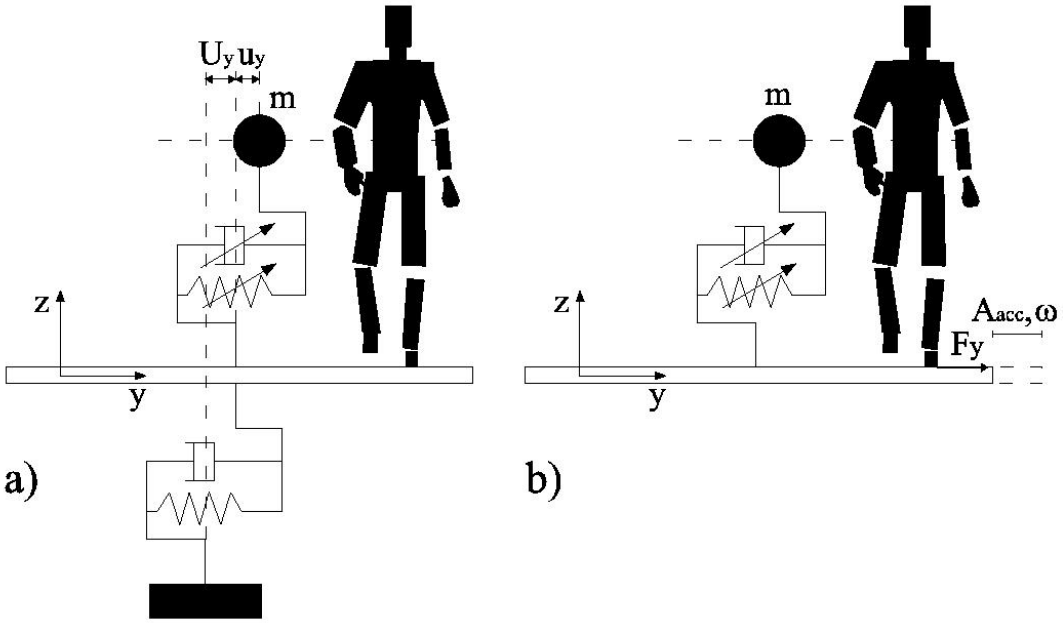

Figure 3.1: (a) Scheme of the Two-Degrees-of-Freedom system representing the coupled lateral motion of a pedestrian and the deck of a footbridge. (b) Single-degree-of-freedom oscillator representing a pedestrian on a floor undergoing a harmonic motion.

3.2.2. The model of Hof and coworkers

For comparison purposes, we briefly introduce another model for the lateral motion of pedestrians. Having in mind an inverted pendulum scheme undergoing small oscillations, Hof et al. [40] and Macdonald [37] discussed the following model:

$$\frac{d^2u_y}{dt^2}-\frac{g}{L}\left(u_y-\overline{u}\right)=-\frac{d^2U_y}{dt^2} \tag{3.6}$$

where g is the gravity acceleration, L is the distance between the contact point of a foot on the floor and the center of gravity of the pedestrian; $\overline{u}(t)$ is the instantaneous position of the center of pression of the lateral force on the floor. According to measurements made for normal walking conditions [40], the time function $\overline{u}(t)$ has a fast variation during the time intervals where both feet are simultaneously in contact with the ground and the center of pression of the force applied on the ground migrates from one foot to the other. Moreover,

during each single foot contact phase, $\overline{u}(t)$ is almost constant. In the limit case where the simultaneous contact occurs only during an infinitesimal time interval, $\overline{u}(t)$ is a piecewise constant function with jumps equal to the lateral distance between the contact points of the feet with the floor. This distance, indicated here as $2\overline{u}_{\max}$, is around equal to 10 cm during normal walking on a rigid floor [41]. A possible choice for $\overline{u}$ is proposed in [37] and [41]:

$$\overline{u}(t) = u_y(t_k) + \frac{\dot{u}_y(t_k)}{\sqrt{g/L}} \pm b_{crit} \qquad with \quad t \in (t_k, t_{k+1}) \tag{3.7}$$

where t_k=$k(2\pi/\omega_1)$ with k=0,1,2,... are the instants of discontinuity of $\overline{u}(t)$; ω_1 is the frequency of the lateral oscillations and b_{crit}≃16 mm is the so-called stability margin. The sign of the term with b_{crit} changes from left to right steps. Eq. (3.7) can be seen as a control law associated with the lateral stability strategy of a pedestrian. By using Eq. (3.6), it is possible to explicitly compute the drift of the average position of the pedestrian with respect to a target straight trajectory, since u_y and $\overline{u}$ are measured with respect to a generic reference. However, if u_y and $\overline{u}$ are measured with respect to the average trajectory supposed known, they are positive on the right (left) of the reference axis and negative in the opposite case. For a regular symmetric walking, one has $-\overline{u}_{\max} \le \overline{u} \le \overline{u}_{\max}$, where $\overline{u}_{\max}$ is the maximum lateral half-distance between the feet during walking.

By comparing (3.6) and $(3.2)_2$, one obtains the expression of the instantaneous position of the center of pression predicted by the MVdP oscillator:

$$\overline{u} = \overline{u}\left(u_y, \frac{du_y}{dt}\right) = u_y + \frac{L}{g}\left(-2\mu\omega_0 \frac{du_y}{dt}\left(1 - \beta u_y^2 - \frac{\gamma}{\omega_0}\frac{du_y}{dt}u_y - \frac{\delta}{\omega_0^2}\left(\frac{du_y}{dt}\right)^2\right) + \omega_0^2 u_y\right) \tag{3.8}$$

Eq. (3.8) shows that the MVdP oscillator postulates a position of the center of pression $\overline{u}$ which is not a piecewise constant function of time. A detailed analysis of the behaviour of the MVdP model in terms of predictions of the center of pression position is beyond the purposes of this thesis. Work is progress about this topic.

3.3. Modified Van der Pol model: harmonic balance and amplitude equation in the non-autonomous regime

In this Section, the analysis of the periodic solution of Eq. (3.5) having frequency equal to that of the excitation, is presented. Actually, the non-autonomous MVdP oscillator (3.5) is quite general: if $\beta=\gamma=0$ the Rayleigh oscillator is retrieved, while $\gamma=\delta=0$ leads to the standard Van der Pol oscillator. The non-autonomous Van der Pol and Rayleigh oscillators have been studied in textbooks (e.g. [23, 25]). A more complex analysis of the Rayleigh model is presented in [42], where an external force with *two* periodic components is considered. One also observes that the term depending on γ is analogous to the *inertia hardening* term mentioned in [43, 44, 45]. However, in the oscillator discussed by those authors, this nonlinear term is always accompanied by a second one: it is not possible to distinguish the contributions of each one, as it should be done for our purposes.
A stationary solution of the form

$$u_y(t) := R\cos(\omega t + \theta) \tag{3.9}$$

is postulated. Eq. (3.9) indicates that the oscillator/pedestrian has the same frequency as the moving floor, where R is the amplitude of the displacement measured with respect to the structure and θ is the phase difference between this displacement and $-d^2U_y/dt^2$, i.e. minus the acceleration of the floor. The research of an approximated solution of the form (3.9) corresponds to solve Eq. (3.5) by using the Harmonic Balance (HB) method with expansion limited to the first harmonic [45]. The advantages and drawbacks of this method, in particular in comparison with the multiple scales method, are discussed e.g. in [44, 46]. Instead of directly solving Eq. (3.5) with the assumption (3.9), the new time-scale

$$\tau = \omega_0 t \tag{3.10}$$

is introduced. By replacing Eq. (3.10) in Eq. (3.5), one obtains

$$\ddot{w}(\tau) - \varepsilon\dot{w}(\tau)\left(1 - \beta w(\tau)^2 - \gamma\dot{w}(\tau)w(\tau) - \delta\dot{w}(\tau)^2\right) + w(\tau) = \frac{A_{acc}}{\omega_0^2}\cos(\tilde{\omega}\tau) = A_d\tilde{\omega}^2\cos(\tilde{\omega}\tau) \tag{3.11}$$

where the dot indicates the differentiation with respect to the time-scale τ and

$$w(\tau) := u_y\left(\frac{\tau}{\omega_0}\right), \qquad \tilde{\omega} := \left(\frac{\omega}{\omega_0}\right), \qquad \varepsilon = 2\mu \tag{3.12}$$

Analogously, the periodic solution (3.9) becomes

$$w(\tau) := R\cos(\tilde{\omega}t + \theta) \tag{3.13}$$

According to HB method, the expression (3.13) is replaced into Eq. (3.11). After some trigonometric simplifications, one has:

$$\begin{aligned}
&\left(-\tilde{\omega}^2 R + R + \frac{\gamma}{4}\varepsilon\tilde{\omega}^2 R^3\right)\cos(\tilde{\omega}\tau + \theta) + \left(\varepsilon\tilde{\omega}R - \varepsilon\tilde{\omega}R^3\,\frac{1}{4}\left(\beta + 3\delta\tilde{\omega}^2\right)\right)\sin(\tilde{\omega}\tau + \theta)\\
&-\frac{1}{4}\varepsilon\tilde{\omega}R^3\left(\beta - \delta\tilde{\omega}^2\right)\sin(3\tilde{\omega}\tau + 3\theta) - \frac{1}{4}\varepsilon\tilde{\omega}R^3\gamma\tilde{\omega}\cos(3\tilde{\omega}\tau + 3\theta)\\
&= \left(A_d\tilde{\omega}^2\cos(\theta)\right)\cos(\tilde{\omega}\tau + \theta) + \left(A_d\tilde{\omega}^2\sin(\theta)\right)\sin(\tilde{\omega}\tau + \theta)
\end{aligned}$$

Neglecting third order harmonic components and equating to zero both sinus and cosinus terms, one obtains the following algebraic equations:

$$\begin{cases}
\varepsilon\tilde{\omega}\left(-\dfrac{\tilde{\omega}^2 - 1}{\varepsilon\tilde{\omega}}R + \dfrac{\gamma}{4}\tilde{\omega}R^3\right) = A_d\tilde{\omega}^2\cos(\theta)\\
\varepsilon\tilde{\omega}\left(R - R^3\,\dfrac{1}{4}\left(\beta + 3\delta\tilde{\omega}^2\right)\right) = A_d\tilde{\omega}^2\sin(\theta)
\end{cases} \tag{3.14}$$

Due to the assumptions on the sign of parameters discussed above, one has β+3δ>0. Moreover, $\tilde{\omega}$ is supposed close enough to 1, in order to have $\beta + 3\delta\tilde{\omega}^2 > 0$. Therefore, by introducing the following quantities

$$R_0 = \frac{2}{\sqrt{\beta + 3\delta\tilde{\omega}^2}}, \qquad \alpha = \frac{\gamma\tilde{\omega}}{\beta + 3\delta\tilde{\omega}^2} \tag{3.15}$$

where R_0 has the meaning of reference response amplitude and α is a normalized form of the parameter γ, three normalized variables can be defined:

$$r = \frac{R}{R_0}, \qquad \lambda = \frac{A_d \tilde{\omega}}{R_0 \varepsilon} = \frac{A_{acc}}{\omega_0^2} \frac{1}{R_0 \varepsilon \tilde{\omega}}, \qquad \nu = \frac{\tilde{\omega}^2 - 1}{\varepsilon \tilde{\omega}} \tag{3.16}$$

where r is a non-dimensional response amplitude, λ is a non-dimensional external acceleration amplitude and ν is a non-dimensional difference (detuning) between the floor frequency ω and the frequency ω_0 of the underlying linear system associated with the MVdP oscillator. By substituting Eqs. (3.15) and (3.16) into Eq. (3.14), one gets

$$\begin{cases} r\left(-\nu + \alpha r^2\right) = \lambda \cos(\theta) \\ r\left(1 - r^2\right) = \lambda \sin(\theta) \end{cases} \tag{3.17}$$

By solving these equations for $\cos(\theta)$ and $\sin(\theta)$ and then using the identity $\sin^2(\theta) + \cos^2(\theta) = 1$, one easily obtains

$$r^2\left(1 - r^2\right)^2 + r^2\left(\nu - \alpha r^2\right)^2 - \lambda^2 = 0 \tag{3.18}$$

Eq. (3.18) states that the squared normalized amplitude $z=r^2$ is a root of a polynomial of order 3, provided that ν, λ and α are fixed. Once r^2 is known, the value of θ can be determined by means of the expression

$$\tan(\theta) = \frac{1 - r^2}{-\nu + \alpha r^2} \tag{3.19}$$

obtained from (3.17). One notices that both the standard Van der Pol and Rayleigh oscillators are represented by Eqs. (3.18)-(3.19) with α=0. The additional term associated α, which is in turn related to the coefficient γ, introduces a *non-isochronous* behaviour [24]. Eq. (3.18) can also be thought as the steady-state solution of the following complex-valued equation depending on the three non-dimensional parameters ν, α and λ:

$$\frac{da}{d\zeta} = (1+i\nu)\,a - (1+i\alpha)\,|a|^2\,a + \lambda \tag{3.20}$$

where $a = re^{i\theta}$ and ζ is a generic normalized time-variable, equal to $(\varepsilon/2)\,\tau$ in the specific case considered here (see also [24]). A similar expression is analyzed in [38]:

$$\frac{da}{d\zeta} = (\xi+i\nu)\,a - (1+i\alpha)\,|a|^2\,a + 1 \tag{3.21}$$

There are still three non-dimensional parameters, but one of them is different from those used in Eq. (3.20). Another analogous expression is investigated in [39]:

$$\frac{da}{d\zeta} = (\xi \pm i)\,a - (1 \pm i\alpha)\,|a|^2\,a + \lambda \tag{3.22}$$

where the normalization is still different. The analyses of the steady solutions of (3.21) and (3.22) presented in [38] and [39], respectively, are somehow complementary, due to the different choice of the normalized parameters. Eq. (3.20) represents a third complementary viewpoint on the same equation and very few analyses of it can be found in the literature. For this reason, and without forgetting the final application to the pedestrian modelling, a detailed study of Eq. (3.18), giving the amplitude of the steady solutions of Eq. (3.20), is presented hereinafter. The stability of these solutions will be discussed in the next Chapter.

3.3.1. Response curves ν - r^2

Eq. (3.18) involves four quantities: the normalized amplitude r of the steady response of the non-autonomous self-sustained oscillator (3.5) and three non-dimensional parameters ν, λ and α. It follows that the system response may be represented in several ways, for instance in a bidimensional plot ν - r^2, with

fixed α and λ values, or by assuming constant values of α and ν and plotting r vs. λ, etc. In the next Chapter, a representation of the type λ - r will be discussed; however, instead of directly consider the non-dimensional quantities, two associated dimensional variables will be analyzed.

In this Subsection, the ν-r^2 representation is analyzed. It generalizes analogous well-known plots concerning the standard Van der Pol and Rayleigh models; see e.g. [23]. For the sake of clarity, and accounting for the novelty of the model (3.5) as well as its interest for the pedestrian behaviour modelling, a quite detailed analysis is presented, even if some of the notions discussed hereafter are known from textbooks, e.g. [23], with reference to simpler models used for other applications. In order to simplify the notation, Eq. (3.18) is rewritten by using the variable $z=r^2$:

$$p_{\nu,\alpha,\lambda}(z) := \left(1+\alpha^2\right) z^3 - 2\left(1+\nu\alpha\right) z^2 + \left(1+\nu^2\right) z - \lambda^2 = 0 \tag{3.23}$$

Due to the definition of z, only *real* and *positive* roots of $p_{\nu,\alpha,\lambda}(z)$ are admissible. Two examples of response curves ν - z plotted using Eq. (3.23) are shown in Fig. 3.2. Fig. 3.2a concerns the *isochronous* case α=0, associated with the classical models of Van der Pol and Rayleigh, while Fig. 3.2b illustrates a particular *non-isochronous* case, with α=2.

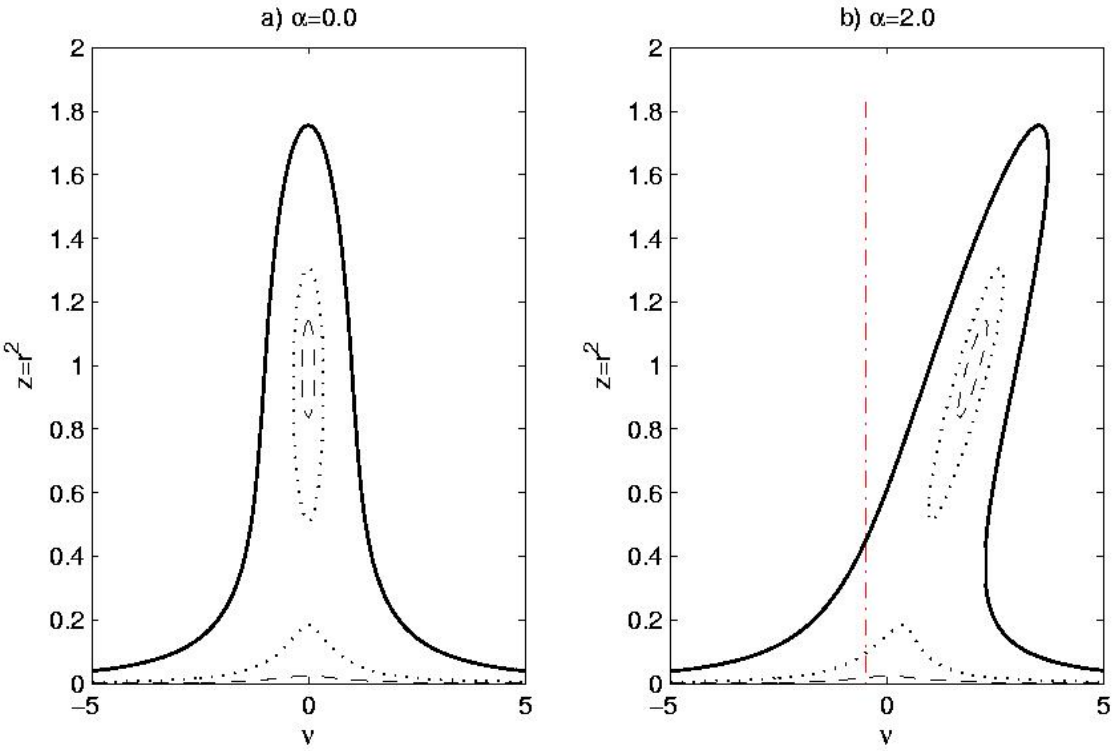

Figure 3.2: Response curves of the MVdP oscillator for the (a) isochronous case (α=0) and (b) non-isochronous case (example with α=2). The curves show the real and positive solutions of Eq. (3.18). Dotted line: λ=0.15, dashed line: λ=0.35, solid line: λ=1.0.

In both Figures, one observes that for given ν and λ values, either one or three real and positive roots of $p_{\nu,\alpha,\lambda}(z)$ may exist. More in detail, using the Descartes' sign rule, it can be proven that if the second coefficient of the polynomial (3.23) is null, i.e. if $1+\nu\alpha=0$, then $p_{\nu,\alpha,\lambda}(z)$ has one real positive root and two complex conjugate roots for any λ value. Fig. 3.2b illustrates the vertical line corresponding to $1+\nu\alpha=0$, for the case $\alpha=2$. If $1+\nu\alpha<0$, there is one real positive root for all λ, while the two other roots are either negative or complex conjugate. One can conclude that when $1+\nu\alpha\leq 0$, there is only one admissible (i.e. real and positive) root of the polynomial $p_{\nu,\alpha,\lambda}(z)$. Conversely, when

$$1+\nu\alpha > 0 \tag{3.24}$$

the situation is more difficult. The polynomial (3.23) admits either three real positive roots or one real positive and two complex conjugate roots. The transition between these two situations occurs when there is one real positive root plus another real positive root with multiplicity equal to two. This

threshold corresponds to the locus of points where the derivative of $p_{\nu,\alpha,\lambda}(z)$ is equal to zero [47]:

$$\frac{dp_{\nu,\alpha}(z)}{dz} = 3z^2\left(1+\alpha^2\right) - 4z\left(1+\nu\alpha\right) + 1 + \nu^2 = 0 \tag{3.25}$$

For a given α value, Eq. (3.25) represents a *conic* in the ν - z half-plane (z>0) independent from the external excitation parameter λ.
Let us consider the general expression of a conic, that reads

$$c_1 z^2 + c_2 z\nu + c_3 \nu^2 + c_4 z + c_5 \nu + c_6 = 0 \tag{3.26}$$

with at least one of the coefficients c_1, c_2 and c_3 different from zero. By comparing Eqs. (3.25) and (3.26), one has $c_1 = 3\left(1+\alpha^2\right)$, $c_2 = -4\alpha$, $c_3 = 1$, $c_4 = -4$, $c_5 = 0$, $c_6 = 1$. It is evident that the nature of this conic change with the value of α. Three cases may occur:

- ***(i)*** C_2^2-4C_1C_3<0 $\Leftrightarrow$ $|\alpha|<\sqrt{3}$. Eqs. (3.25)-(3.26) represent an ellipse;
- ***(ii)*** C_2^2-4C_1C_3>0 $\Leftrightarrow$ $|\alpha|>\sqrt{3}$. Eqs. (3.25)-(3.26) represent a hyperbola;
- ***(iii)*** C_2^2-4C_1C_3=0 $\Leftrightarrow$ $\alpha=\pm\sqrt{3}$. Eqs. (3.25)-(3.26) represent a parabola.

These three cases are schematically illustrated in Fig. 3.3b, c, d. In addition, Fig. 3.3a concerns the simple isochronous case α=0. The other lines plotted in the same figure are related to the nature (nodes, spirals, etc.) and stability of the equilibrium points. These topics will be discussed in the next Chapter.

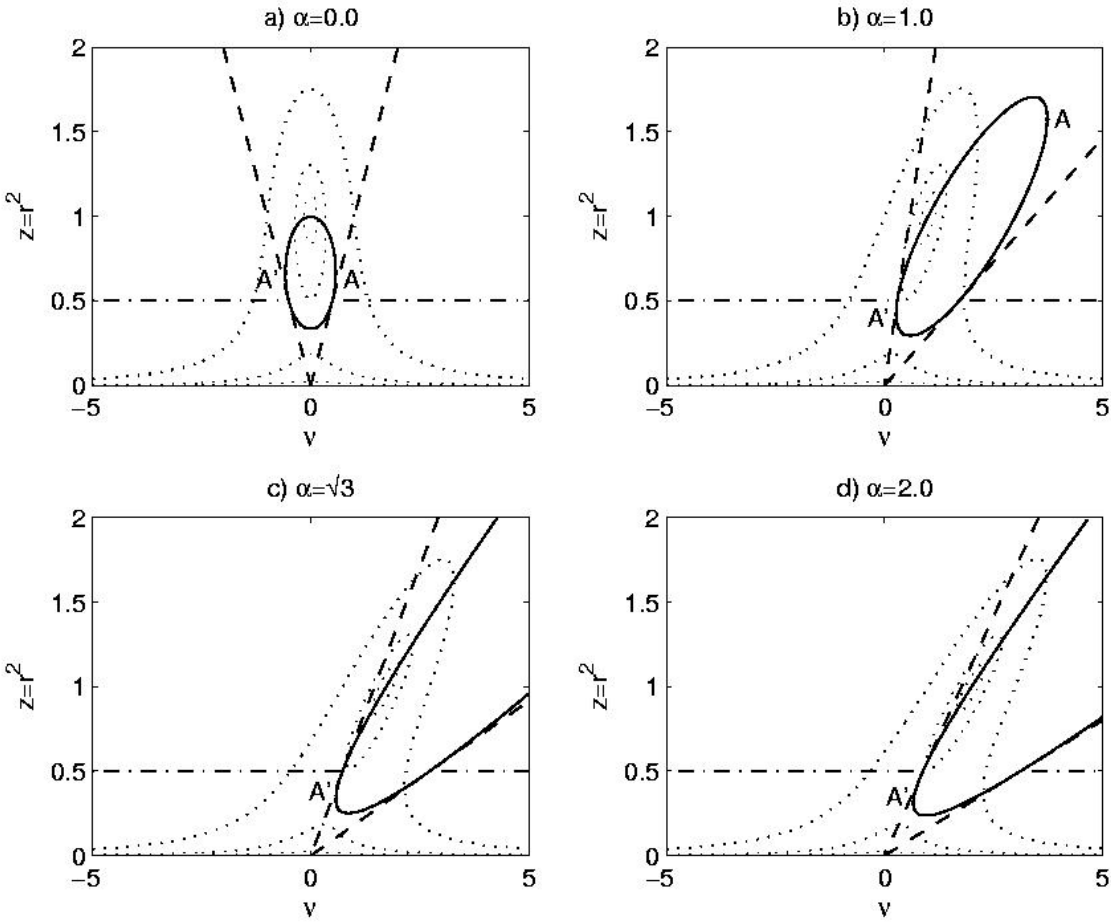

Figure 3.3: Response curves of the MVdP oscillator (dotted lines) and conics associated with the condition (3.25) (solid lines). The other straight lines are related with the stability of the response.

An illustration of the meaning of Eq. (3.25) and how it is related to the multiplicity of the roots of $p_{\nu,\alpha,\lambda}(z)$ is given in Figs. 3.4 and 3.5. The polynomial $p_{\nu,\alpha,\lambda}(z)$ is represented for $\alpha=\bar{\alpha}=1$ and $\nu=\bar{\nu}=1.4492$, and for five different values of λ, $\lambda'<\lambda_Q<\lambda''<\lambda_P<\lambda'''$, indicated in the figures. Notice that the modification of λ induces vertical translations of the curve in Fig. 3.4, but it does not affect the abscissas z_P and z_Q of the points of zero-slope, where Eq. 3.25 is fulfilled. With reference to the numerical values of the Figure, Eq. (3.25) leads to $z_P\simeq 0.42934$ and $z_Q\simeq 1.2035$. The corresponding points P and Q, belonging to the conic defined by Eq. (3.25), are indicated in Fig. 3.5.

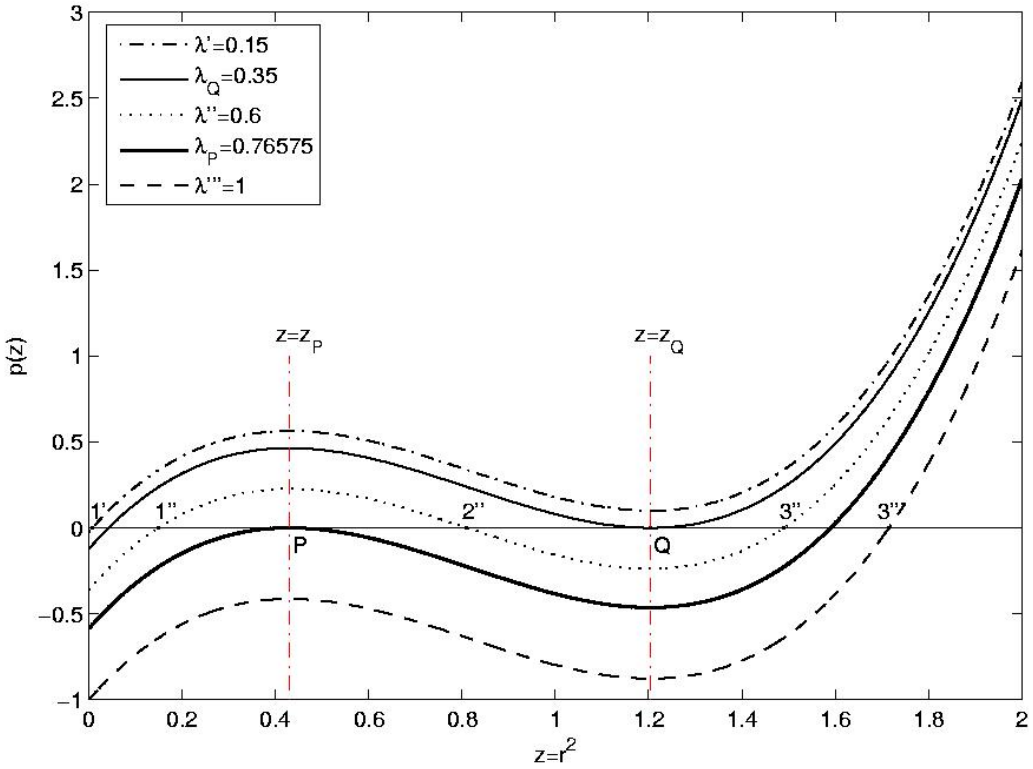

Figure 3.4: Plot of the polynomial $p(z)$, Eq. (3.23), for $\alpha = 1$, $\nu = 1.4492$ and five λ-values.

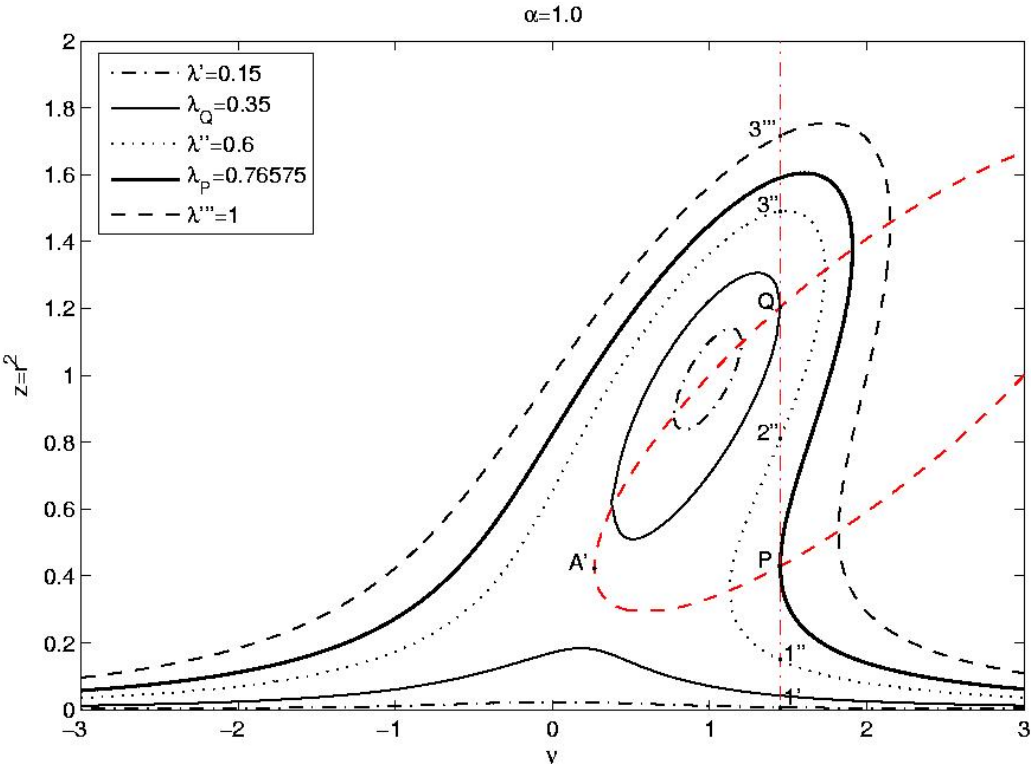

Figure 3.5 : Response curves of the MVdP oscillator (Eq. (3.18)) for $\alpha = 1$ and with five different λ-values. The vertical line corresponds to $\nu = 1.4492$, while the dashed ellipse is associated with the condition (3.25).

When $\lambda=\lambda'$, $p_{\bar{\nu},\bar{\alpha},\lambda'}(z)$ has *one* real positive root $z_{1'}<z_P$ (see Fig. 3.4). The corresponding point 1′ in Fig. 3.5, having coordinates $(\bar{\nu},z_{1'})$, is outside the region bounded by the conic (3.25). When $\lambda=\lambda''$, there are *three* real positive roots of $p_{\bar{\nu},\bar{\alpha},\lambda''}(z)$, associated with the points 1″, 2″ and 3″ indicated in Fig. 3.4. One is inside the conic, while the others are outside. In the intermediate case $\lambda=\lambda_Q$, the polynomial (3.23) has *three* real positive roots and two of them coincide and are equal to $z=z_Q$. The value $\lambda_Q\simeq 0.35$ used in Figs. 3.4-3.5 has been found by replacing the numerical value of z_Q, $\bar{\alpha}$ and $\bar{\nu}$ in Eq. (3.23). When $\lambda=\lambda'''$, $p_{\bar{\nu},\bar{\alpha},\lambda'''}(z)$ has *one* real positive root $z_{3'''}>z_Q$. When $\lambda=\lambda_P$, the situation is analogous to that of the case $\lambda=\lambda_Q$. In summary, for given α and ν values, the polynomial (3.23) has three real and distinct positive solutions when

$$\lambda_Q(\nu,\alpha)<\lambda<\lambda_P(\nu,\alpha) \tag{3.27}$$

On the boundaries of this interval two of the three real positive solutions coincide, while outside the interval there is only one real positive solution.
Looking at Figs. 3.3 and 3.5, one notices that there is one (or two) special point(s) where the tangent to the conic (3.25) is vertical, i.e. where P and Q degenerate into a single point. If the conic is an ellipse, there are two points, called A' and A. There is only one point in the other cases. The coordinates of A and/or A' can be computed by imposing that the polynomial (3.23) has three real repeated roots [47]:

$$\frac{d^2p_{\nu,\alpha}(z)}{dz^2}=6z\left(\alpha^2+1\right)-4\nu\alpha-4=0 \tag{3.28}$$

This leads to

$$z=\frac{2}{3}\frac{1+\nu\alpha}{1+\alpha^2} \tag{3.29}$$

Then, in order to impose that the points belong to the conic, Eq. (3.29) is replaced into (3.25):

$$\left(\alpha^2-3\right)\nu^2+8\alpha\nu+\left(1-3\alpha^2\right)=0 \tag{3.30}$$

The solution of Eq. (3.30) is found considering the cases (i), (ii) and (iii) defined above:

(i) $|\alpha|<\sqrt{3}$. The polynomial (3.30) has a couple of real roots

$$\nu_{A'}=\frac{\sqrt{3}\alpha-1}{\alpha+\sqrt{3}}<\nu_A=\frac{\sqrt{3}\alpha+1}{\sqrt{3}-\alpha} \tag{3.31}$$

Both values of ν in (3.31) satisfy the inequality (3.24), i.e. $1+\nu_{A'}\alpha>0$ and $1+\nu_A\alpha>0$. It means that both solutions are admissible and this is consistent with the fact that the conic is an ellipse. The coordinates $z_{A'}$ and z_A can be computed by replacing (3.31) into Eq. (3.29). Finally, the corresponding values of λ are obtained from (3.23) (see Table 3.1).

(ii) $|\alpha|>\sqrt{3}$. The polynomial (3.30) still has the couple of real roots

$$\nu_A=\frac{\sqrt{3}\alpha+1}{\sqrt{3}-\alpha}<\nu_{A'}=\frac{\sqrt{3}\alpha+1}{\sqrt{3}-\alpha} \tag{3.32}$$

However, in this case the sign of the inequality between ν_A and $\nu_{A'}$ is inverted and only one of the ν values in (3.32) fulfils (3.24), depending on the sign of α. The other one must be discarded. This is consistent with the hyperbolic shape of the conic. The final coordinates are collected in Table 3.1.

(iii) $\alpha=\pm\sqrt{3}$. Eq. (3.30) becomes of first order in the variable ν and the solution reads

$$\alpha=\sqrt{3} \quad \Rightarrow \quad \nu_{A'}=\frac{\sqrt{3}}{3},\ z_{A'}=\frac{1}{3},\ \lambda_{A'}=\frac{2}{3\sqrt{3}}$$

$$\alpha=-\sqrt{3} \quad \Rightarrow \quad \nu_{A}=-\frac{\sqrt{3}}{3},\ z_{A}=\frac{1}{3},\ \lambda_{A}=\frac{2}{3\sqrt{3}}$$

where $z_{A'}$, z_A have been calculated from (3.29) and then $\lambda_{A'}$,λ_A from (3.23). For a given value of α, only one solution exists and this means that only one limit point exists. This is consistent with the fact that the conic is a parabola (recall Fig. 3.3c). In both cases (α=±√3), the inequality (3.24) is fulfilled.

		$z=r^2$	ν	$\lambda(>0)$
$\alpha<-\sqrt{3},$	A:	$\frac{2}{3-\sqrt{3}\alpha}$	$\frac{1+\sqrt{3}\alpha}{\sqrt{3}-\alpha}$	$\sqrt{\frac{8\sqrt{3}}{9}\frac{\alpha^2+1}{\left(\sqrt{3}-\alpha\right)^3}}$
$\alpha=-\sqrt{3},$	A:	$\frac{1}{3}$	$-\frac{\sqrt{3}}{3}$	$\frac{2}{3\sqrt{3}}$
$\lvert\alpha\rvert<\sqrt{3},$	A':	$\frac{2}{3+\sqrt{3}\alpha}$	$\frac{\sqrt{3}\alpha-1}{\alpha+\sqrt{3}}$	$\sqrt{\frac{8\sqrt{3}}{9}\frac{\alpha^2+1}{\left(\alpha+\sqrt{3}\right)^3}}$
	A:	$\frac{2}{3-\sqrt{3}\alpha}$	$\frac{\sqrt{3}\alpha+1}{\sqrt{3}-\alpha}$	$\sqrt{\frac{8\sqrt{3}}{9}\frac{\alpha^2+1}{\left(\sqrt{3}-\alpha\right)^3}}$
$\alpha=\sqrt{3},$	A':	$\frac{1}{3}$	$\frac{\sqrt{3}}{3}$	$\frac{2}{3\sqrt{3}}$
$\alpha>\sqrt{3},$	A':	$\frac{2}{3+\sqrt{3}\alpha}$	$\frac{-1+\sqrt{3}\alpha}{\alpha+\sqrt{3}}$	$\sqrt{\frac{8\sqrt{3}}{9}\frac{\alpha^2+1}{\left(\alpha+\sqrt{3}\right)^3}}$

Table 3.1 : Coordinates (z; ν; λ) of the points where the conic (3.25) has vertical tangent.

The coordinates of A and A' can be also found by an alternative procedure, related to a different representation of the conic (3.25), obtained by replacing Eq. (3.25) into (3.23) and eliminating the variable z:

$$27\left(1+\alpha^2\right)^2\lambda^4+\lambda^2\left(-4+\left(60\alpha\nu-36\alpha^2-36\nu^2\right)\left(1+\nu\alpha\right)-4\alpha^3\nu^3\right)+4\left(\alpha-\nu\right)^2\left(1+\nu^2\right)^2=0 \qquad (3.33)$$

A detailed analysis of this expression is made in the next Chapter.

3.3.2. Analytical vs. numerical results

A comparison between numerical simulation results and analytical response amplitudes predicted by Eq. (3.18) or, equivalently, by Eq. (3.23) is reported in Fig. 3.6. The points associated with the numerical solution are plotted for the cases where the entrained periodic response exists, i.e. it is stable. It has been obtained by solving Eq. (3.5) by means of the solver ODE45 implemented in Matlab and then computing the amplitude of the first harmonic of the periodic response. The numerical simulations have been performed with the parameters ω_0=1 *rad*/*s*, ε=2μ=0.05, β=1 m^{-2}, δ=1 m^{-2}. The non-dimensional parameter α is constant (α=1), while three values of λ are considered (λ=0.35, λ=1.5, λ=2.5). As a result, for each fixed ν value, the remaining parameters ω, A_{acc} and γ needed for numerical integration of Eq. (3.5) are computed using (3.12) and (3.16) and the identity $A_{acc}=\omega^2 A_d$. Fig. 3.6 shows that there is a good agreement between numerical and analytical results. Actually, the good approximation obtained in this example concerns values of $z=r^2$ less than 2.5, while λ is less than 2.5 and μ is small. The accuracy of analytical predictions diminishes for higher values of these quantities and of the modulus of α.

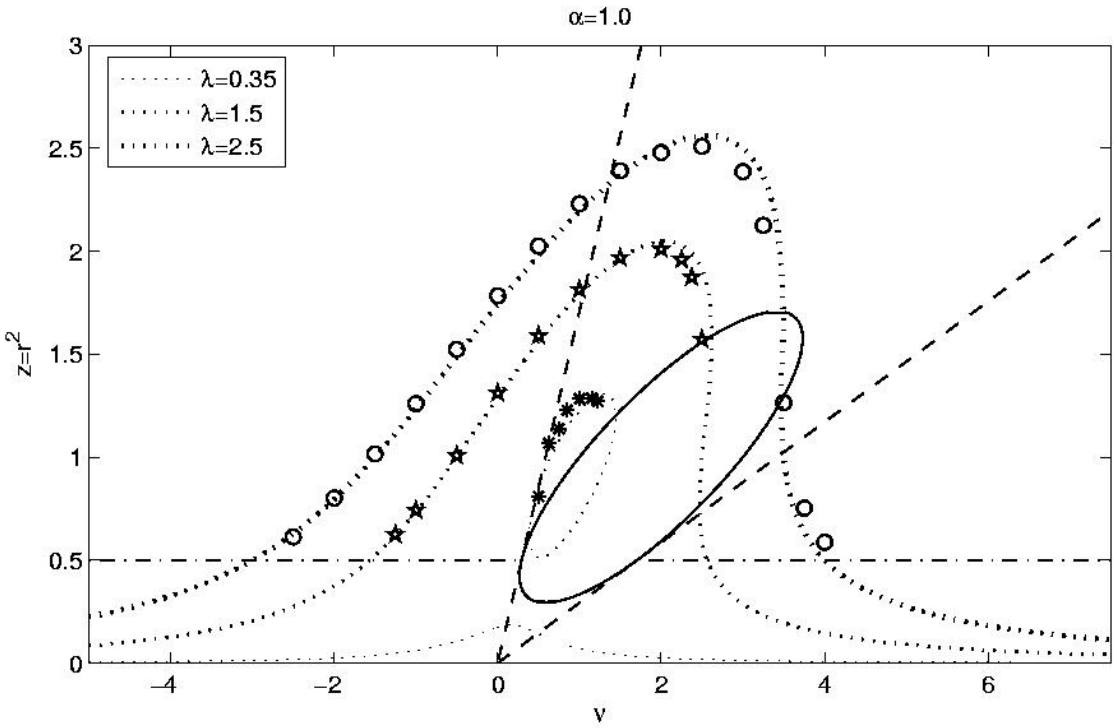

Figure 3.6 : Response curves of the MVdP oscillator (Eq.(3.18)) for α= 1. Comparison between numerical and analytical results for three different λ-values.

3.4. Force amplitude curves at constant frequency

In this Section, another interpretation of Eq. (3.18) is discussed. Instead of using non-dimensional parameters and variables, dimensional quantities are considered, pointing out their physical meaning associated with the application of the pedestrian walking on a floor with a lateral harmonic motion. The main goal is to find an explicit expression of the amplitude of the periodic lateral force $C_{1,dyn}$ applied on the floor by a walker assuming entrained conditions, as a function of the floor vibration amplitude A_d at a given constant frequency ω. Accounting for Eqs. (3.2), (3.4) and (3.9), the lateral force applied by the walker on the moving floor is given by

$$\begin{aligned} F_y(t) &= F_y\left(u_y(t), \frac{du_y(t)}{dt}\right) = m\left(-\frac{d^2U_y(t)}{dt^2} - \frac{d^2u_y(t)}{dt^2}\right) = m\left(\omega^2 A_d \cos(\omega t) - \frac{d^2u_y(t)}{dt^2}\right) \\ &= m\left(\omega^2 A_d \cos(\omega t) + R\omega^2 \cos(\omega t + \theta)\right) \end{aligned} \tag{3.34}$$

Using some well-known trigonometric identities, one has

$$\begin{aligned} F_y(t) &= m\left[\omega^2 A_d + R\omega^2 \cos(\theta)\right]\cos(\omega t) - m\left[R\omega^2 \sin(\theta)\right]\sin(\omega t) \\ &:= C_{1,dyn} \cos\left(\omega t + \phi_{1,dyn}\right) \end{aligned}$$

Hence, the squared force amplitude is given by

$$C_{1,dyn}^2 = \left(m\omega^2\right)^2 \left(\left[A_d + R\cos(\theta)\right]^2 + \left[R\sin(\theta)\right]^2\right)$$

After some algebra and using $(3.17)_1$ as well as the non-dimensional quantities ν, α and r defined by (3.15) and (3.16), one has

$$C_{1,dyn} = m\omega^2 R_0 \sqrt{\left(\frac{\varepsilon\lambda}{\omega}\omega_0\right)^2 + 2\frac{\varepsilon\omega_0}{\omega} r^2\left(-\nu + \alpha r^2\right) + r^2}$$

Recalling that λ is related to r, α and ν by Eq. (3.18), one easily obtains

$$C_{1,dyn} = m\omega^2 R_0 \sqrt{\left(r^2\left(1-r^2\right)^2 + r^2\left(\nu-\alpha r^2\right)^2\right)\left(\frac{\varepsilon\omega_0}{\omega}\right)^2 + 2\frac{\varepsilon\omega_0}{\omega}r^2\left(-\nu+\alpha r^2\right)+r^2}$$

It is now possible to define a parametric plot ($A_d(z)$, $C_{1,dyn}(z)$) with the parameter $z=r^2>0$:

$$\begin{cases} A_d(z) = R_0\varepsilon\dfrac{\omega_0}{\omega}\lambda(z) = R_0\varepsilon\dfrac{\omega_0}{\omega}\sqrt{z(1-z)^2 + z(\nu-\alpha z)^2} \\ C_{1,dyn}(z) = m\omega^2 R_0\sqrt{\left(z(1-z)^2 + z(\nu-\alpha z)^2\right)\left(\dfrac{\varepsilon\omega_0}{\omega}\right)^2 + 2\dfrac{\varepsilon\omega_0}{\omega}z(-\nu+\alpha z)+z} \end{cases} \quad (3.35)$$

Fig. 3.7 shows this parametric plot in the particular case of pedestrian "2", having natural walking frequency of 0.873 *Hz* and natural oscillation amplitude in the lateral direction of about 13.3 mm (see Fig. 2.4, case of longitudinal speed v_x=3.75 km/h). The corresponding identified model parameters read: ω_0=4.60 *rad/s*, ε=1.107, β=4785 m^{-2}, γ=7416 m^{-2}, δ=3426 m^{-2}, m=69.4 *kg*. We recall that these parameters have been identified in *rigid floor* conditions. Moreover, the frequency of the ground motion is assumed equal to $\omega=2\pi\,0.75=4.712$ *rad/s*. It can be observed that the curve has a first branch, between the origin and *P* (vertical tangent), a second branch between *P* and *Q* and the third branch for higher z values. The condition defining the points with vertical tangent is $dA_d(z)=0$, where

$$dA_d(z) = R_0\varepsilon\frac{\omega_0}{\omega}\frac{3z^2\alpha^2 + 3z^2 - 4z\alpha\nu - 4z + \nu^2 + 1}{2\sqrt{z(1-z)^2 + z(\nu-\alpha z)^2}}dz$$

It can be noticed that this condition is identical to (3.25). The stability of each branch is discussed in Chapter 4.

An interesting property of this curve is that it becomes an almost straight line for high values of z (and of A_d and $C_{1,dyn}$). A similar behaviour has been experimentally observed by several independent investigators, e.g. [9, 27]. A limit analysis for $z\to\infty$ leads to the value of the constant slope of this straight line. Let us differentiate the second equation in (3.35):

$$dC_{1,dyn}(z) = m\omega^2 R_0 \frac{\left(\frac{\varepsilon\omega_0}{\omega}\right)^2 \left((1-z)^2 - 2(1-z)z + (\nu-\alpha z)^2 - 2\alpha(\nu-\alpha z)z\right) + 2\frac{\varepsilon\omega_0}{\omega}(-\nu+\alpha z+z\alpha)+1}{2\sqrt{\left(z(1-z)^2 + z(\nu-\alpha z)^2\right)\left(\frac{\varepsilon\omega_0}{\omega}\right)^2 + 2\frac{\varepsilon\omega_0}{\omega}z(-\nu+\alpha z)+z}} dz$$

Hence, the slope at the limit $z\to\infty$ becomes:

$$\lim_{z\to+\infty} \frac{dC_{1,dyn}(z)}{dA_d(z)} = m\omega^2 \tag{3.36}$$

On one hand, this simple result offers a model-based interpretation of the experimental outcomes: for a sinusoidal lateral motion of the floor at fixed frequency ω, the amplitude $C_{1,dyn}$ of the lateral force increases proportionally to the amplitude A_d of the floor displacement and the constant of proportionality depends on the pedestrian mass and on the (constant) frequency. On the other hand, this confirms that the linear approximation of experimental data is reasonable. Notice that the limit (3.36) depends on the pedestrian mass, but does not depend on any of the other model parameters.

Finally, observe that the usual representation of experimental results is done by a plot of the so-called participation factor $C_{1,dyn}/(mg)$ as a function of A_d. In this case the limit slope becomes independent from the pedestrian mass:

$$\lim_{z\to+\infty} \frac{1}{mg}\frac{dC_{1,dyn}(z)}{dA_d(z)} = \frac{\omega^2}{g} \simeq \frac{\omega^2}{10}$$

A more detailed comparison between analytical and numerical model predictions and experimental results is given hereafter.

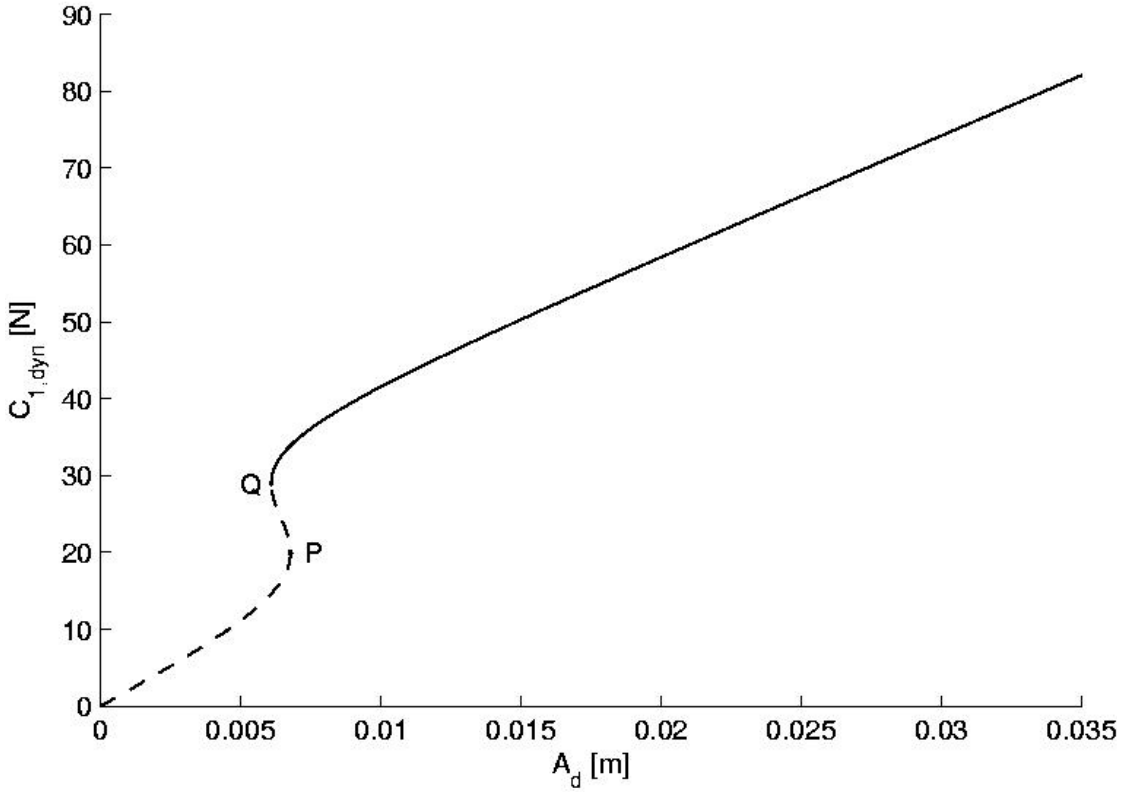

Figure 3.7: Pedestrian "2" - v_x=3.75 km/h. Parametric plot of the amplitude of the lateral pedestrian force vs. the floor oscillation amplitude. The branch PQ is unstable.

3.4.1. Analytical vs. numerical results

In this Subsection, numerical and analytical plots of the relationship A_d-$C_{1,dyn}$ are compared, in order to check the error associated with the analytical solution based on the harmonic balance method. The numerical integration of Eq. (3.5) is performed by means of the ODE45 algorithm implemented in Matlab. Then, the amplitude of the first harmonic of the entrained periodic response is computed by a standard FFT algorithm: this is the numerical counterpart of $C_{1,dyn}$ defined in Eq. $(3.35)_2$. The parameters assumed for the example of Fig. 3.8 are the same used in the previous Fig. 3.7, associated with the so-called pedestrian "2" (case of longitudinal speed v_x=3.75 km/h). The subplots (a) and (b) of Fig. 3.8 concern the case of a floor frequency of 0.75 and of 1 Hz, respectively. One observes that the error between analytical approximation and numerical results is larger when the floor frequency is

higher. The same situation can be seen in Fig. 3.9, concerning pedestrian "1" (v_x=3.75 km/h) characterized by the parameters ω_0=4.68 *rad/s*, ε=0.275, β=0, γ=52852 m^{-2}, δ=8803 m^{-2}, m=68.6 *kg* corresponding to a natural walking frequency of 0.877 *Hz* and a natural oscillation amplitude of about 9.6 *mm* [see Fig. 2.4].

The plot of numerical results begins after the point *Q*, where the synchronized solution (3.9) is stable [4]. For pedestrian "2", the onset of synchronization occurs for an amplitude of the floor motion of about 6 *mm* when the floor frequency is 0.75 *Hz* and about 1.5 *mm* when the floor frequency is 1 *Hz*. For pedestrian "1" (Fig. 3.9), the synchronization begins at a floor oscillation amplitude of about 2.5 *mm*, with a frequency of 0.75 *Hz* and at the smaller amplitude of about 1 *mm* when the frequency is 1.0 *Hz*. We recall that the natural frequency of both pedestrians is close to 0.875 *Hz*.

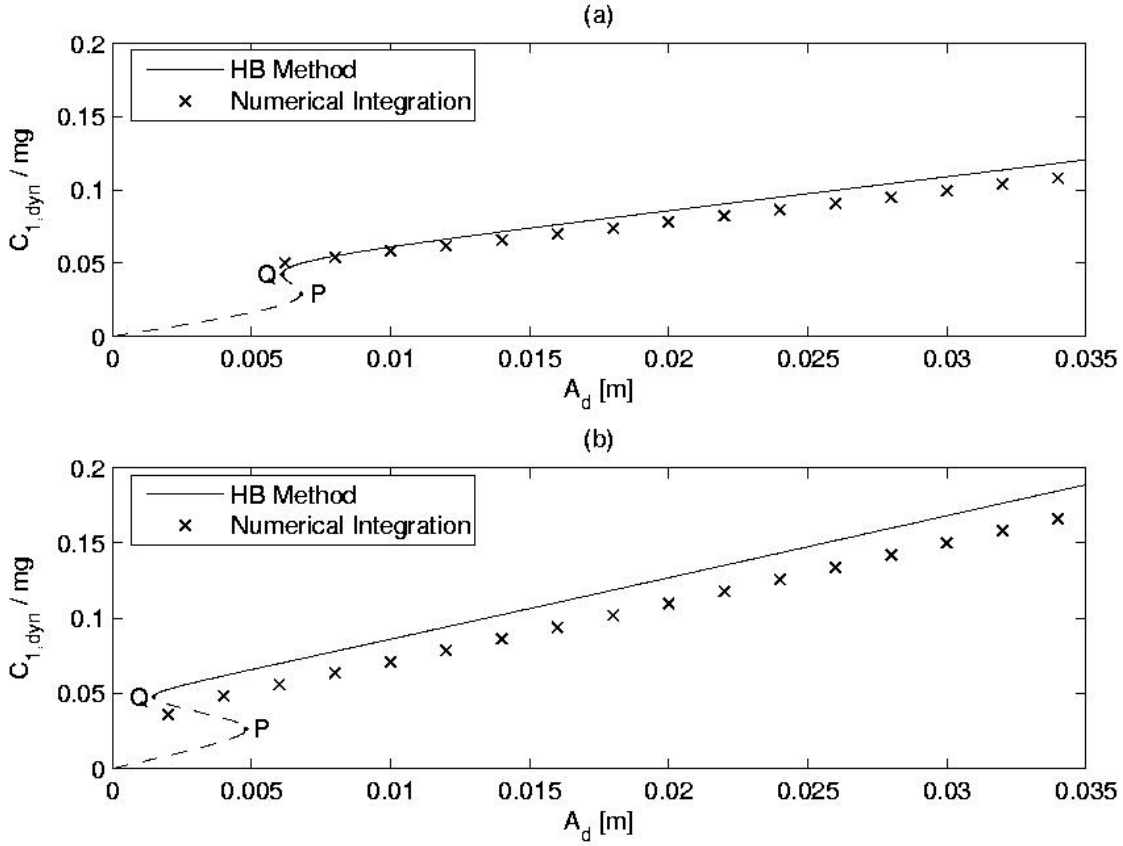

Figure 3.8: Pedestrian "2" - v_x=3.75 km/h. Dynamic Load Factor vs. floor displacement amplitude at constant floor frequency: (a) 0.75 *Hz* and (b) 1.0 *Hz*. Comparison between analytical and experimental results.

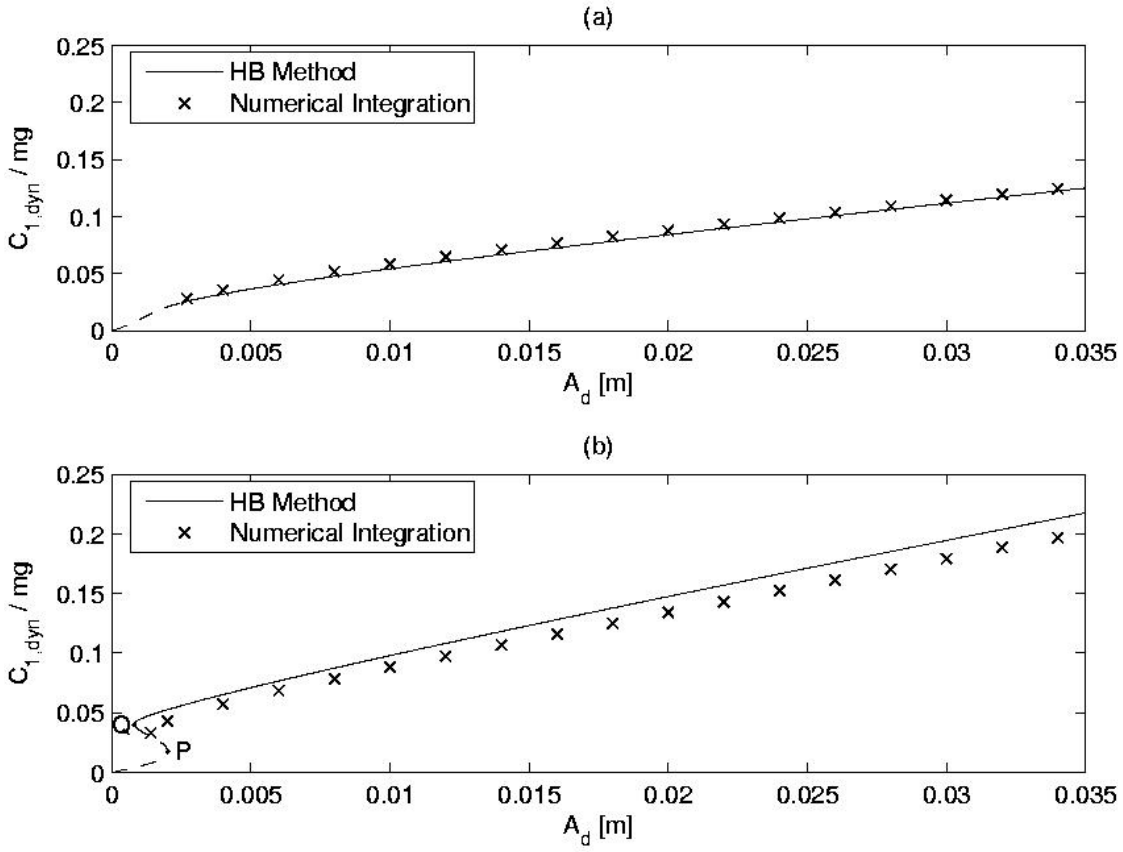

Figure 3.9: Pedestrian "1" - v_x=3.75 km/h. Dynamic Load Factor vs. floor displacement amplitude at constant floor frequency: (a) 0.75 *Hz* and (b) 1.0 *Hz*. Comparison between analytical and experimental results.

It is also possible to compare the behaviour of the models associated with pedestrians "2" and "1" at a given external frequency. At 0.75 *Hz*, the synchronization of pedestrian "1" begins before than for pedestrian "2", at an amplitude of the floor motion of 2.5 *mm* for the former and 6 *mm* for the latter (Fig. 3.8a vs. Fig. 3.9a). The same effect occurs at 1.0 *Hz*, with threshold amplitudes of 1.0 *mm* and 1.5 *mm*, respectively. This different behaviour is due to the fact that pedestrian "1" has a *natural* oscillation amplitude smaller than the pedestrian "2" (9.6 *mm* vs. 13.3 *mm*): this makes it more sensitive to the floor motion.

3.4.2. Numerical vs. experimental results

In the previous Subsection, it has been shown by some examples that the error between analytical and numerical solutions is not always small. Hence, in order to make a comparison with the experimental results available in the literature [9, 27, 28], the model behaviour is represented by the numerical simulations. Actually, this comparison is significant if the model predictions and the experiments concern the same pedestrian. Moreover, the experiment should be realized in both rigid and moving floor conditions for each individual. Unfortunately, these data are not available in the literature. For this reason, the numerical results of Fig. 3.10 have been obtained by considering models with parameters identified from measurements on pedestrians walking on a rigid floor (see Chapter 2), while the experimental points concern the moving floor regime and are taken from the articles mentioned in the legend of the Figure. Obviously, the walkers involved in these two experimental campaigns were not the same. In addition, the experimental force amplitudes normalized with the pedestrian weight, reported in the diagrams of published articles [9, 27, 28] are referred to both synchronized and non-synchronized pedestrians and it is difficult to know, for every single subject, if there was synchronization or not during the force measurement. Conversely, the stable branches obtained from the numerical simulations concern, by definition, synchronized pedestrians only. It is therefore very difficult to directly compare the experiment and the model results.

Nonetheless, even accounting for all the intrinsic limits of this comparison, it can be noticed from Fig. 3.10 that there is a rather good agreement between model predictions and experiments. The parameters used for the numerical simulations corresponds to pedestrian "2" and pedestrian "1", introduced above. As a matter of fact, the model leads to larger force amplitudes when the floor vibration frequency ω is larger (recall that the analytical solution has a limit slope proportional to ω^2). Conversely, the available experimental results show that the force amplitude is substantially independent from the floor frequency. This difference might be related to the fact that the experimental force amplitudes concern both synchronized and non-synchronized pedestrians, while model predictions only concern synchronized pedestrians.

In summary, with the available information, the modified Van der Pol oscillator (3.5) gives a proper representation of test results. In addition, it gives an insightful physical interpretation of the experimentally detected

phenomenon of the approximately linear variation of the lateral force amplitude as function of the floor oscillation amplitude. A further comparison of the model with experimental results from a larger database is in progress.

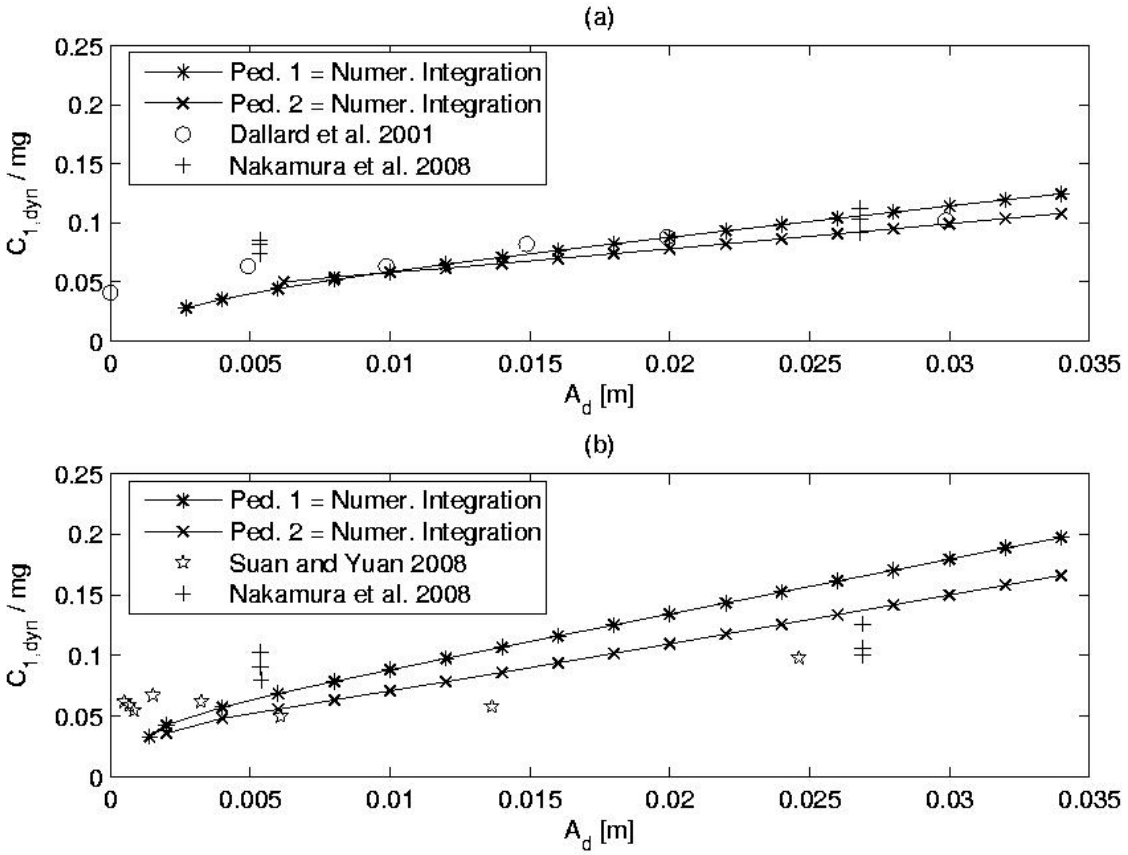

Figure 3.10: Dynamic Load Factor vs. floor displacement amplitude at constant floor frequency: (a) 0.75 *Hz* and (b) 1.0 *Hz*. Comparison between numerical results (pedestrians "1" and "2", v_x=3.75 km/h) and experimental results (from the articles cited in the legend).

3.5. Conclusions

In this Chapter, an approach where the lateral pedestrian oscillations are modelled by a suitable self-sustained oscillator is presented. This oscillator is an extension of the classical Van der Pol model. In the simplest situation of autonomous oscillations (rigid floor) this modified Van der Pol (MVdP) oscillator gives a very good representation of the experimental behaviour (see

Chapter 2). The non-autonomous case is analyzed here. Both a theoretical analysis and a comparison with experimental results concerning the pedestrian behaviour are presented. In detail, the response of the MVdP oscillator under a harmonic external force associated with the floor motion is analytically evaluated by the harmonic balance method. An approximated expression of the amplitude of the periodic entrained solution is derived and compared with numerical results. Then, the model predictions are compared with experimental results coming from the literature, and a rather good agreement is obtained. The theoretical and applied aspects concerning the stability of the solutions of the MVdP oscillator are discussed in the next Chapter.

Chapter 4

A modified Van der Pol oscillator for modelling the lateral pedestrian force on a moving floor. Part II: stability and synchronization

The modified Van der Pol (MVdP) oscillator has been proposed in Chapter 2 to model the lateral oscillations of a pedestrian walking on a *rigid floor* and it has been shown that in this case it gives a good representation of experimental results. The case of a pedestrian walking on a *floor with harmonic lateral motion* is treated in this Chapter (as in Chapter 3). The MVdP oscillator is analyzed in Chapter 3 in terms of *amplitude* of the entrained response, i.e. a response having the same frequency as that of the given periodic excitation, while the main goal of the present Chapter is the *stability analysis* of the entrained response. Some theoretical results, mainly related with the subject of the forced response of non-isochronous oscillators, are discussed. Then, these theoretical notions are applied to the pedestrian modelling problem: the conditions allowing stability of the solution are used to compute the percentages of pedestrians of a given population that can synchronize their walk with a given periodic floor motion. These model predictions are compared with experimental results concerning pedestrians walking on a shake table.

4.1. Introduction

In this Chapter, the MVdP oscillator is studied in the non-autonomous case, modelling the oscillations of a pedestrian walking on a moving floor. The curves describing the amplitude of stationary *entrained* solutions have been determined in Chapter 3 by the harmonic balance method. The *stability* of these solutions is discussed in this Chapter. According to the physical interpretation of interest here, an entrained (or synchronized) solution indicates that the pedestrian walks at the same frequency as that of the floor. We recall that the term *synchronization* should be used when two or more coupled self-sustained oscillators oscillate at the same frequency due to the reciprocal interaction, while the term *entrainment* indicates the synchronization of an oscillator with an external agency [23]. We will indifferently use both terms, even if the most pertinent is entrainment. The stability of the entrained solution indicates that the synchronized walking can actually take place and can be preserved also after some small perturbation. Vice versa, an unstable entrained solution indicates that a small perturbation induces the loss of the synchronized walking: in practice, unstable entrained solutions cannot take place.

Both theoretical and applied aspects are investigated. The stability domain is defined in terms of non-dimensional parameters and variables. These non-dimensional quantities are ”naturally” derived from the MVdP oscillator definition and are different from those used in similar analyses, like e.g. [38, 39]. Moreover, a comparison between numerical and analytically estimated stability domains is made. The differences are illustrated by some examples. Then, it is shown how these theoretical results concerning stability can be used to predict the percentages of pedestrians of a given population that may synchronize their walking frequency with that of a periodic floor motion. It is proven that the possibility of synchronization is correlated with the amplitude and frequency of the floor oscillation and with the characteristic of the single pedestrian, represented by a MVdP oscillator with identified parameters. The comparison with experimental results available in the literature [9, 27] is briefly discussed.

After the Introduction, Sections 4.2 recall the definition of the MVdP oscillator and the main relationships defining the amplitude of its stationary entrained response to a harmonic excitation. Section 4.3 concerns the stability analysis of these responses, i.e. the main theoretical goal of this Chapter. Then, the use of these notions for the application of the pedestrian-floor

synchronization is discussed in Section 4.4. The conclusions give a summary of the main results.

4.2. Summary of the proposed model

The self-sustained oscillator chosen to represent the lateral oscillations of a pedestrian is the modified Van der Pol (MVdP) model proposed in Chapter 2. If the mode shape effect is neglected [5], the coupling between this oscillator and one of the lateral modes of a structure is represented by the following system (see also Figure 3.1a):

$$\begin{cases} \dfrac{d^2U_y}{dt^2} + 2\xi_s\omega_s \dfrac{dU_y}{dt} + \omega_s^2 U_y = \dfrac{1}{M} F_y\left(u_y, \dfrac{du_y}{dt}\right) \\ m\dfrac{d^2u_y}{dt^2} + F_y\left(u_y, \dfrac{du_y}{dt}\right) = -m\dfrac{d^2U_y}{dt^2} \end{cases} \tag{4.1}$$

where

$$F_y\left(u_y, \frac{du_y}{dt}\right) = m\left(-2\mu\omega_0 \frac{du_y}{dt}\left(1 - \beta u_y^2 - \frac{\gamma}{\omega_0}\frac{du_y}{dt}u_y - \frac{\delta}{\omega_0^2}\left(\frac{du_y}{dt}\right)^2\right) + \omega_0^2 u_y\right) \tag{4.2}$$

is the restoring force the MVdP oscillator. The oscillator defined by Eqs. $(4.1)_2$ and (4.2) is self-sustained, viz. it has a stable periodic orbit, when μ>0 and β+3δ>0 [1].

Like in Chapter 3, the coupled pedestrian-structure behaviour modelled by the system (4.1) is not considered. A simpler situation is rather analyzed, where the floor lateral motion is supposed known and harmonic with displacement amplitude A_d>0 and with frequency ω:

$$U_y(t) = A_d\cos(\omega t) \quad \rightarrow \quad \frac{d^2U_y(t)}{dt^2} = -A_{acc}\cos(\omega t) \tag{4.3}$$

where A_{acc}:=$A_d\omega^2$ is the floor acceleration amplitude. Hence the second equation in (4.1) becomes

$$\frac{d^2u_y(t)}{dt^2} - 2\mu\omega_0\frac{du_y(t)}{dt}\left(1-\beta u_y^2(t)-\frac{\gamma}{\omega_0}\frac{du_y(t)}{dt}u_y(t)-\frac{\delta}{\omega_0^2}\left(\frac{du_y(t)}{dt}\right)^2\right)+\omega_0^2u_y(t)=A_{acc}\cos(\omega t) \qquad (4.4)$$

Eq. (4.4) represents a pedestrian walking on a floor undergoing lateral harmonic oscillations; see also Figure 3.1b. This condition can be easily obtained in a laboratory test, asking pedestrians to walk on a treadmill placed on a shake table [27]. The solutions of Eq. (4.4) are supposed of the form

$$u_y(t) := R\cos(\omega t+\theta) \qquad (4.5)$$

According to Eq. (4.5), $u_y(t)$ has constant amplitude and frequency and is *synchronyzed* with the external excitation frequency. A solution of this kind represents a pedestrian synchronized with the floor.
We observe that in the *autonomous case*, i.e. when A_{acc} = 0, the natural oscillations of the MVdP oscillator along its limit cycle can be represented by an expression like (4.5), where, in the limit of small μ, it holds $R \simeq 2/\sqrt{\beta+3\delta}$, θ is arbitrary and ω is equal to:

$$\omega_1 \simeq \omega_0\left(1+\frac{\mu\gamma}{\beta+3\delta}\right) \qquad (4.6)$$

4.2.1. Normalization, fixed points, amplitude equation

In Chapter 3, the fixed points of Eq. (4.4) have been derived using the harmonic balance method and an analytical expression for R and θ of Eq. (4.5) has been found. For the sake of clarity, the procedure developed in Chapter 3 is briefly recalled. First, the time-scale

$$\tau = \omega_0 t \qquad (4.7)$$

is introduced and this leads to an alternative expression of Eq. (4.4):

$$\ddot{w}(\tau)-\varepsilon\dot{w}(\tau)\left(1-\beta w(\tau)^2-\gamma\dot{w}(\tau)w(\tau)-\delta\dot{w}(\tau)^2\right)+w(\tau)=\frac{A_{acc}}{\omega_0^2}\cos(\tilde{\omega}\tau) \tag{4.8}$$

where the dot indicates the derivative with respect to τ and

$$w(\tau):=u_y\left(\frac{\tau}{\omega_0}\right),\qquad \tilde{\omega}:=\left(\frac{\omega}{\omega_0}\right),\qquad \varepsilon=2\mu \tag{4.9}$$

The periodic solution (4.5) becomes

$$w(\tau):=R\cos(\tilde{\omega}t+\theta) \tag{4.10}$$

Then, the following quantities are introduced

$$R_0=\frac{2}{\sqrt{\beta+3\delta\tilde{\omega}^2}},\qquad \alpha=\frac{\gamma\tilde{\omega}}{\beta+3\delta\tilde{\omega}^2} \tag{4.11}$$

where $\beta+3\delta>0$ and $\tilde{\omega}$ is assumed close enough to 1 to guarantee that $\beta+3\delta\tilde{\omega}^2>0$; R_0 has the meaning of reference response amplitude and α is a normalized form of the parameter γ of Eq. (4.4). Then, let us set

$$r=\frac{R}{R_0},\qquad \lambda=\frac{A_{acc}}{\omega_0^2}\frac{1}{R_0\varepsilon\tilde{\omega}},\qquad \nu=\frac{\tilde{\omega}^2-1}{\varepsilon\tilde{\omega}} \tag{4.12}$$

where r is a non-dimensional response amplitude, λ is a non-dimensional external acceleration amplitude and ν is a non-dimensional "detuning" between the external frequency ω and the frequency ω_0 of the underlying linear system associated with the MVdP oscillator. It has been proven in Chapter 3 that the harmonic balance method applied to Eq. (4.8) leads to the following expression for the non-dimensional response amplitude r at a fixed point:

$$r^2\left(1-r^2\right)^2+r^2\left(\nu-\alpha r^2\right)^2-\lambda^2=0 \tag{4.13}$$

Eq. (4.13) is an implicit relationship between r and the frequency detuning ν, with and additional dependence on the external excitation amplitude λ and on the parameter α. Moreover, Eq. (4.13) extends the analogous equation associated with the standard Van der Pol model or the Rayleigh model, corresponding to $\alpha=\gamma=0$. When the parameter α defined by Eq. (4.11) is non-zero, the MVdP oscillator (4.4) is *non-isochronous*, according to the definition given, for instance, in [24]. An expressions similar to the amplitude equation (4.13) has been discussed, among others, in [38, 39], with a different choice of the non-dimensional parameters, related to the different nature of the associated physical problem.
Let us rewrite (4.13) by using the squared amplitude $z=r^2$:

$$p_{\nu,\alpha,\lambda}(z):=\left(1+\alpha^2\right)z^3-2\left(1+\nu\alpha\right)z^2+\left(1+\nu^2\right)z-\lambda^2=0 \tag{4.14}$$

Eq. (4.14) states that the squared normalized amplitude $z=r^2$ is a root of a polynomial of order 3. Due to the definition of z, only *real* and *positive* roots of the polynomial $p_{\nu,\alpha,\lambda}(z)$ are admissible. In Chapter 3, different graphical representations of the roots z of Eq. (4.14) have been discussed. Here, we are rather interested in the *stability analysis* of these solutions having normalized amplitude r. This study is made in the next Section.

4.3. Local stability of the entrained steady response

In this Section, we analyze the *local* stability of the solution (4.10) of Eq. (4.8) by considering a small perturbation $\mathrm{v}(\tau)$, according to a procedure similar to that presented in [44]. The perturbed solution reads

$$w(\tau)=R\cos\left(\tilde{\omega}t+\theta\right)+\mathrm{v}(\tau) \tag{4.15}$$

Only the "first type" of stability is investigated [44]. This corresponds to assume that the perturbation $\mathrm{v}(\tau)$ can be approximated by a harmonic

expression with the same fundamental frequency and truncated at the same order than the assumed response (4.10):

$$\mathrm{v}(\tau) = B_{1c}(\tau)\cos(\tilde{\omega}t+\theta) + B_{1s}(\tau)\sin(\tilde{\omega}t+\theta) \tag{4.16}$$

By replacing (4.15) and (4.16) in Eq. (4.8), it is possible to derive the following relationship (see the Appendix C for the details):

$$\dot{\mathbf{B}} = \mathbf{M}\mathbf{B} \quad \text{with} \quad \mathbf{B}=\begin{bmatrix} B_{1s} \\ B_{1c} \end{bmatrix} \quad \text{and} \quad \mathbf{M}=\frac{\varepsilon}{2}\begin{bmatrix} 1-r^2 & \nu-3\alpha r^2 \\ -\nu+\alpha r^2 & 1-3r^2 \end{bmatrix} \tag{4.17}$$

By setting

$$B_{1s}(\tau) = b_{1s}e^{k\tau}, \qquad B_{1c}(\tau) = b_{1c}e^{k\tau}$$

where b_{1c} and b_{1s} are constant, the eigenproblem $(\mathbf{M}\text{-}\kappa\mathbf{I})\mathbf{b}=\mathbf{0}$ is derived. According the standard procedure [23], the stability is related to the eigenvalues $\kappa_{1,2}$ of the matrix $\mathbf{M}$, which are solutions of the characteristic equation $\kappa^2\text{-}k\,\mathrm{tr}(\mathbf{M})+\det\mathbf{M}=0$, where "*tr*" and "*det*" are the trace and determinant operators. The stability requires that the real part of the eigenvalues is negative. This means that the two following conditions must hold:

$$q = det\mathbf{M} = \frac{\varepsilon^2}{4}\left(3r^4\left(1+\alpha^2\right) - 4r^2\left(1+\nu\alpha\right) + 1 + \nu^2\right) > 0 \tag{4.18}$$

$$p = tr\mathbf{M} = \varepsilon\left(1-2r^2\right) < 0 \tag{4.19}$$

The negative determinant characterizes saddles, for all values of p. When the determinant is positive, the fixed points may be stable or unstable, according to the sign of the trace p and they are nodes or spirals, according to the sign of the discriminant

$$\Delta = p^2 - 4q = \varepsilon^2\left(\left(1-3\alpha^2\right)r^4 + 4\nu\alpha r^2 - \nu^2\right) \tag{4.20}$$

The conditions q=0, p=0 and Δ=0 define curves associated with a change of stability and/or nature of the fixed points, i.e. the steady solutions. It is

possible to represent these transition curves in the ν-r^2 plane and in the ν-λ plane. In the next two Subsections, both approaches are considered.

4.3.1. Representation in the ν-r^2 plane

Let us begin with the condition q=0. By using the definition of q given in (4.18) and setting $z=r^2$, one has:

$$B_S : q = 0 \quad \rightarrow \quad 3z^2\left(1+\alpha^2\right) - 4z\left(1+\nu\alpha\right) + 1 + \nu^2 = 0 \tag{4.21}$$

It can be easily proven that (4.21) is identical to the condition $dp_{\nu,\alpha,\lambda}(z)/dz=0$ where $p_{\nu,\alpha,\lambda}(z)$ is the polynomial given in Eq. (4.14). This condition defines the *conic* in the ν-z plane where $p_{\nu,\alpha,\lambda}(z)$ has three real positive roots and two of them are repeated. In Chapter 3, it has been shown that this conic can be an ellipse ($|\alpha|<\sqrt{3}$), a parabola ($\alpha=\pm\sqrt{3}$) or a hyperbolae ($|\alpha|>\sqrt{3}$); see also Figure 4.1. The points in the (ν-z) plane inside the conic correspond to q<0. Therefore, they are saddles. The equilibrium points outside the conic (q>0) and having the discriminant Δ>0 are nodes. For this reason, the conic is called saddle-node bifurcation B_S. Moreover, one has

$$B_H : p = 0 \quad \rightarrow \quad z = \frac{1}{2} \tag{4.22}$$

i.e. the condition $p=tr\mathbf{M}$=0 defines a horizontal line in the ν-z plane. This line intersects the conic B_S. However, since inside the conic the equilibria are saddles independently from the sign of p, the part of this line lying inside B_S does not change the nature of equilibria and it can be canceled out. Conversely, outside B_S the sign of p affects the stability of the fixed points: the two horizontal half-lines associated with (4.22) separate stable from unstable fixed points and define the so-called Hopf bifurcation B_H. The stable region (p<0) corresponds to z>1/2 (Fig. 4.1).

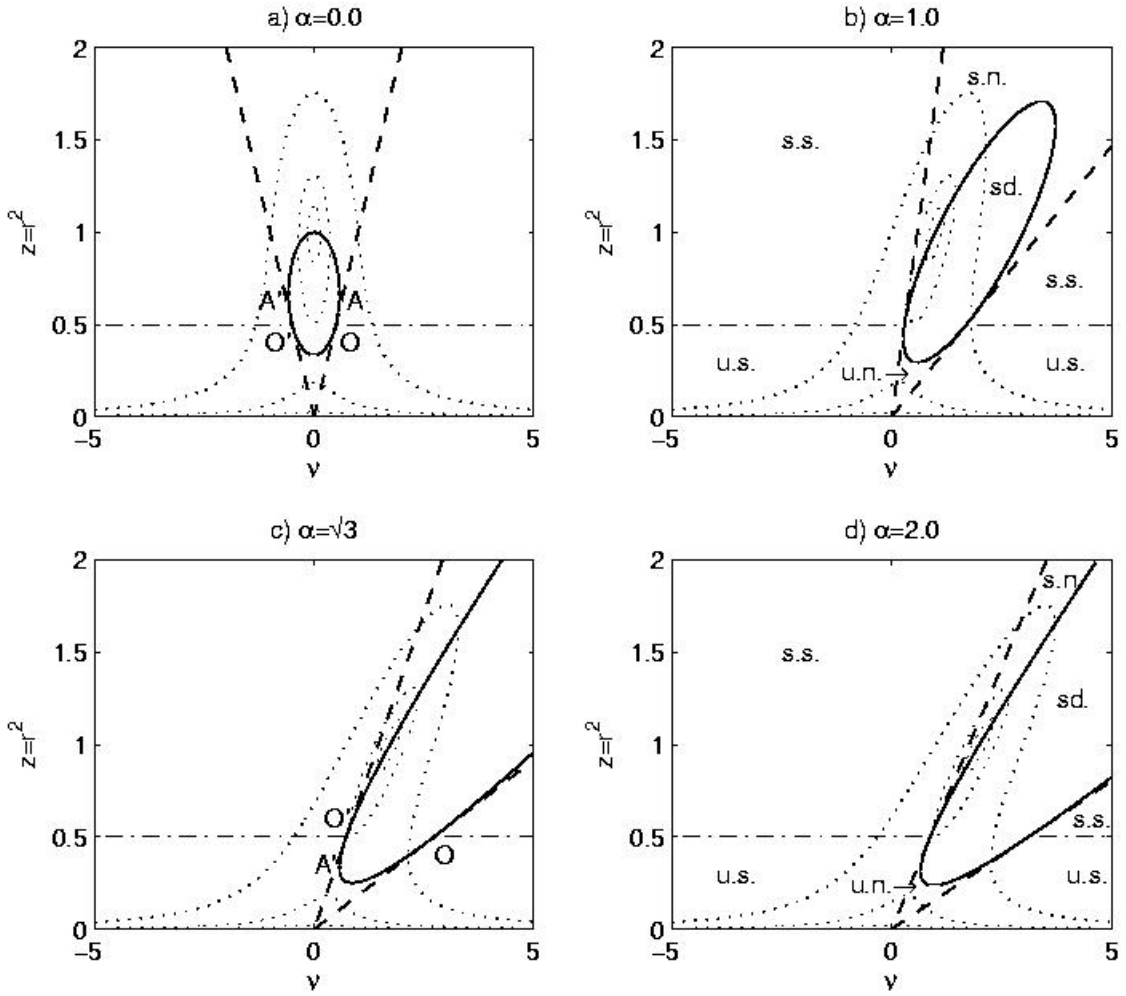

Figure 4.1: Response curves and stability regions of the MVdP oscillator. Dotted lines: response amplitude curves associated with Eq. (4.14). Continuous lines: conic associated with the saddle-node bifurcation (4.21). Dashed-dotted lines: Hopf bifurcation (4.22). Dashed lines: nodes-spirals bifurcation (4.23).

The transition between nodes and spirals is defined by the condition $\Delta=0$ (Eq. (4.20)). Four cases are distinguished, according to the α value. For each case, the transition is defined by a couple of half-lines B_N issuing from the origin of the ν-z plane (recall that $z \geq 0$):

$$(B_N):\quad \begin{cases} |\alpha|<\dfrac{1}{\sqrt{3}} \;\rightarrow\; \begin{cases} \nu=\nu_1(z)=\left(2\alpha-\sqrt{\alpha^2+1}\right)z \\ \nu=\nu_2(z)=\left(2\alpha+\sqrt{\alpha^2+1}\right)z \end{cases} \\ |\alpha|>\dfrac{1}{\sqrt{3}} \;\rightarrow\; \begin{cases} \nu=\nu_1(z)=\left(2\alpha+\sqrt{\alpha^2+1}\right)z \\ \nu=\nu_2(z)=\left(2\alpha-\sqrt{\alpha^2+1}\right)z \end{cases} \\ \alpha=\dfrac{1}{\sqrt{3}} \;\rightarrow\; \begin{cases} \nu=\nu_1=0,\forall z \\ \nu=\nu_2(z)=\dfrac{4}{\sqrt{3}}z \end{cases} \\ \alpha=-\dfrac{1}{\sqrt{3}} \;\rightarrow\; \begin{cases} \nu=\nu_1(z)=-\dfrac{4}{\sqrt{3}}z \\ \nu=\nu_2=0,\forall z \end{cases} \end{cases} \tag{4.23}$$

The condition $\Delta<0$, associated with spirals, is fulfilled for $\nu<\nu_1$ and $\nu>\nu_2$ (see Figure 4.1). The intersections between B_S, B_H and B_N define the points O and O'. By solving a system formed by Eqs. (4.21) and (4.22), one has the (ν,z) coordinates of these points; see Table 4.1. It is easy to check that B_N also passes through the same points. Then, the corresponding λ values are determined inserting (ν,z) into Eq. (4.14). Other important points are those where the tangent to the conic B_S is vertical, like the points A and A' of Fig. 4.1. Instead of studying these points in the ν-z plane, like it has been made in Chapter 3, the alternative ν-λ representation is preferred. The details are reported in the following Section.

	$z=r^2$	ν	$\lambda(>0)$
O'	$\frac{1}{2}$	$\alpha-\frac{1}{2}\sqrt{\alpha^2+1}$	$\frac{1}{2\sqrt{2}}\sqrt{1+\left(\alpha-\sqrt{\alpha^2+1}\right)^2}$
O	$\frac{1}{2}$	$\alpha+\frac{1}{2}\sqrt{\alpha^2+1}$	$\frac{1}{2\sqrt{2}}\sqrt{1+\left(\alpha+\sqrt{\alpha^2+1}\right)^2}$

Table 4.1 : Coordinates (z; ν; λ) of the points O and O', at the intersection of B_S, B_H and B_N.

4.3.2. Representation in the ν-λ plane

In this Subsection, a representation of the curves B_S, B_H and B_N in the ν-λ plane is considered. The expression of each curve is obtained by replacing the corresponding definition, i.e. (4.21), (4.22) or (4.23), into Eq. (4.14) and eliminating the variable z. By this procedure, the expression associated with B_S reads:

$$27\left(1+\alpha^2\right)^2\lambda^4+\lambda^2\left(-4+\left(60\alpha\nu-36\alpha^2-36\nu^2\right)\left(1+\nu\alpha\right)-4\alpha^3\nu^3\right)+4\left(\alpha-\nu\right)^2\left(1+\nu^2\right)^2=0 \qquad (4.24)$$

Observe that Eq. (4.24) can be rewritten under the form of the second order polynomial $a_1x^2+a_2x+a_3=0$ in the variable $x=\lambda^2$, having the coefficients

$$a_1=a_1\left(\alpha\right)=27\left(1+\alpha^2\right)^2$$

$$a_2=a_2\left(\nu,\alpha\right)=-4+\left(60\alpha\nu-36\alpha^2-36\nu^2\right)\left(1+\nu\alpha\right)-4\alpha^3\nu^3$$

$$a_3=a_3\left(\nu,\alpha\right)=4\left(\alpha-\nu\right)^2\left(1+\nu^2\right)^2$$

The two real and positive roots are indicated by $\lambda_Q^2\left(\nu,\alpha\right)$ and $\lambda_P^2\left(\nu,\alpha\right)$. Their square roots read:

$$\begin{aligned}\lambda_Q\left(\nu,\alpha\right)&=\sqrt{\frac{1}{2a_1\left(\alpha\right)}\left(-a_2\left(\nu,\alpha\right)-\sqrt{a_2^2\left(\nu,\alpha\right)-4a_1\left(\alpha\right)a_3\left(\nu,\alpha\right)}\right)}>0\\ \lambda_P\left(\nu,\alpha\right)&=\sqrt{\frac{1}{2a_1\left(\alpha\right)}\left(-a_2\left(\nu,\alpha\right)+\sqrt{a_2^2\left(\nu,\alpha\right)-4a_1\left(\alpha\right)a_3\left(\nu,\alpha\right)}\right)}>0\end{aligned} \qquad (4.25)$$

According to (4.25), for a given α one has $\lambda_Q(\nu,\alpha)<\lambda_P(\nu,\alpha)$. The plot of λ_P and λ_Q as functions of ν, for fixed α, gives the upper and bottom branches of the saddle-node bifurcation, respectively (see Figs. 4.2, 4.3, 4.4 and 4.5). The ν-values associated with the *cusps* A and A' at a given α derive from the condition $a_2^2=4a_1a_3$ (see Table 4.2). Moreover, at these points one has $\lambda_Q^2=\lambda_P^2=-a_2\left(\nu,\alpha\right)/\left(2a_1\left(\alpha\right)\right)$ and this leads to the coordinates λ of the cusps reported in the last column of Table 4.2. The corresponding amplitudes $z=r^2$

are finally derived by using Eq. (4.21). The ν - λ representation of the Hopf bifurcation B_H is obtained by replacing Eq. (4.22) into Eq. (4.14). This leads to:

$$\lambda_H(\nu,\alpha)=\sqrt{\frac{1}{8}+\frac{1}{2}\left(\nu-\frac{1}{2}\alpha\right)^2} \quad \text{with } \nu<\nu_{O'} \text{, or } \nu>\nu_O \tag{4.26}$$

Moreover, by replacing Eq. (4.23) in Eq. (4.14), one obtains the node-spiral bifurcations B_N. The explicit expressions are not reported for brevity.
In the ν-z plane, there are two common points between the Hopf bifurcation B_H and the saddle-node bifurcation B_S, viz. O and/or O' (see Fig. 4.1). In the ν-λ plane, the curves B_H and B_S are tangent at the same points (Figs. 4.2, 4.3, 4.4 and 4.5). Moreover, in this plane B_H and B_S intersect at two other points, B and B'. In order to find their coordinates, one needs to replace Eq. (4.26) into (4.24). This leads to the following equation:

$$\frac{1}{64}\left(3\alpha^2-8\alpha\nu+4\nu^2-1\right)^2\left(3\alpha^4-8\alpha^3\nu+14\alpha^2-40\alpha\nu+16\nu^2-5\right)=0 \tag{4.27}$$

The first factor is null when $\nu=\alpha\pm\frac{1}{2}\sqrt{\alpha^2+1}$, i.e. at the points O and O'. The roots of the second factor define the abscissas of B and B':

$$\nu_{B'}=\frac{1}{4}\left(\alpha\left(\alpha^2+5\right)-\left(1+\alpha^2\right)\sqrt{\alpha^2+5}\right)$$
$$\nu_B=\frac{1}{4}\left(\alpha\left(\alpha^2+5\right)+\left(1+\alpha^2\right)\sqrt{\alpha^2+5}\right)$$

The corresponding λ coordinates are easily obtained by replacing the ν-values in Eq. (4.26):

$$\lambda_{B'}=\frac{1}{2\sqrt{2}}\sqrt{1+\frac{1}{4}\left(\alpha^3+3\alpha-\left(\alpha^2+1\right)\sqrt{\alpha^2+5}\right)^2}$$
$$\lambda_B=\frac{1}{2\sqrt{2}}\sqrt{1+\frac{1}{4}\left(\alpha^3+3\alpha+\left(\alpha^2+1\right)\sqrt{\alpha^2+5}\right)^2}$$

As it is said for an analogous situation in [38], an important particular case occurs when α is such that the points A, O and B converge in a unique

bifurcation point of codimension 3. This particular α value can be computed by imposing the equality $\nu_O = \nu_A$, with the values taken from Tables 4.1 and 4.2, respectively. This leads to

$$\alpha = -\sqrt{3}/3, \quad \nu_A = \nu_O = \nu_B = 0 \quad \text{and} \quad \lambda_A = \lambda_O = \lambda_B = 1/\sqrt{6}$$

Likewise, the points O', A' and B' coincide when

$$\alpha = \sqrt{3}/3, \quad \nu_{A'} = \nu_{O'} = \nu_{B'} = 0 \quad \text{and} \quad \lambda_{A'} = \lambda_{O'} = \lambda_{B'} = 1/\sqrt{6}$$

The values $\alpha = \pm\sqrt{3}/3$ bound the so-called *small isochronicity region* [24]. The curves defining the different kinds of bifurcations have been defined.

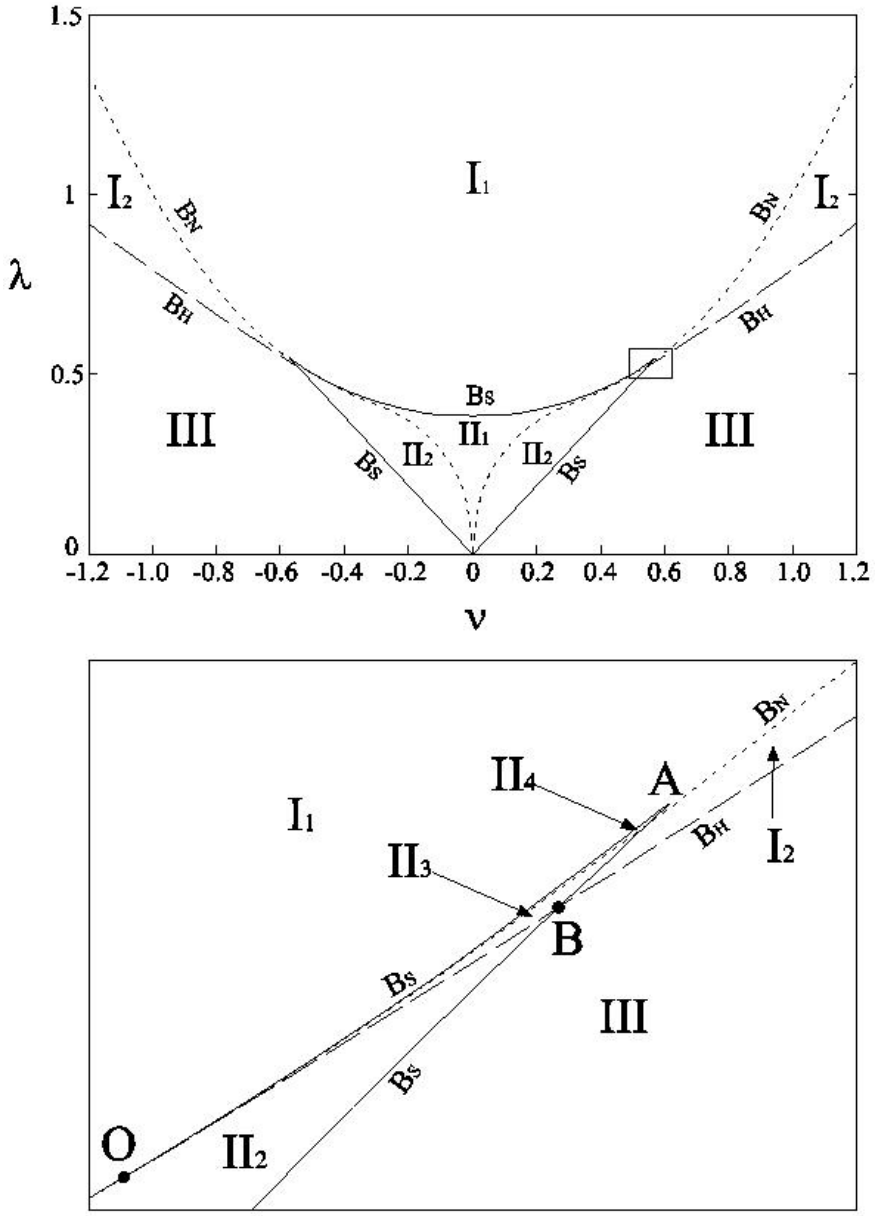

Figure 4.2: Bifurcations portraits of the MVdP oscillator in the parameter plane (ν, λ). Case α=0. Global view and detail of the zone around the right cusp *A* of the saddle-node bifurcation B_S.

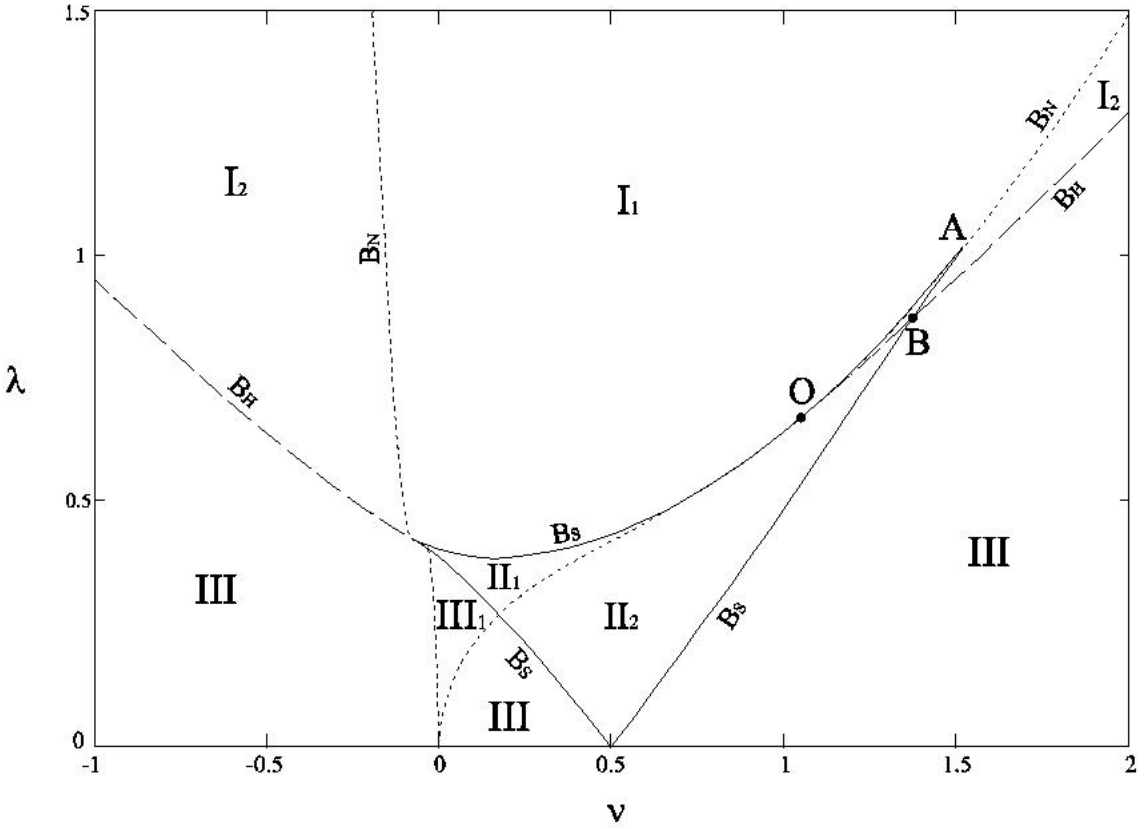

Figure 4.3: Bifurcations portraits of the MVdP oscillator in the parameter plane (ν, λ). Case α=0.5.

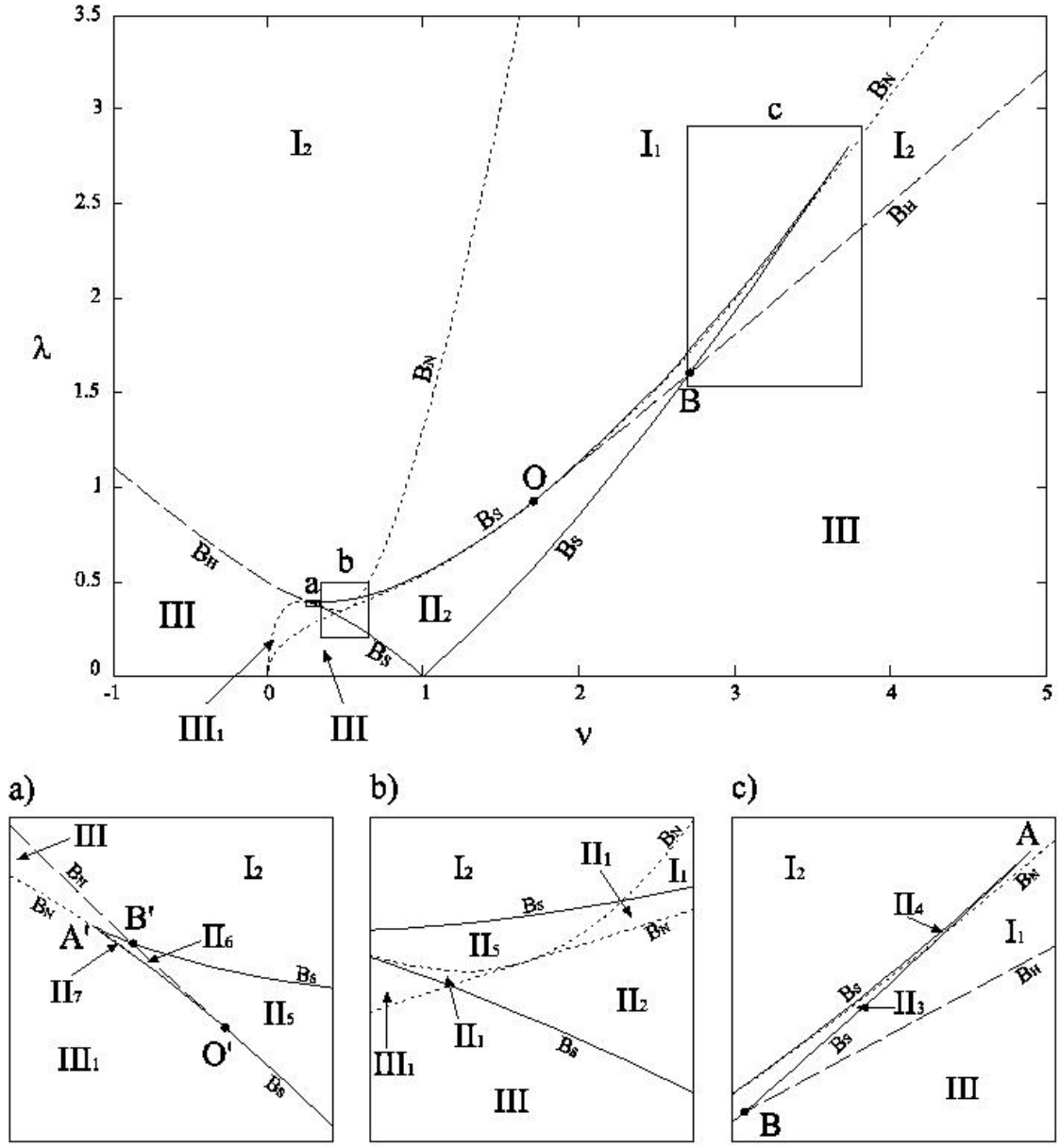

Figure 4.4: Bifurcations portraits of the MVdP oscillator in the parameter plane (ν, λ). Case α=1. Global view and (a) detail of the zone around the left cusp of B_S; (b) detail of the zone inside B_S where the branches of the node-spiral bifurcation B_N intersect; (c) detail of the zone around the right cusp of B_S.

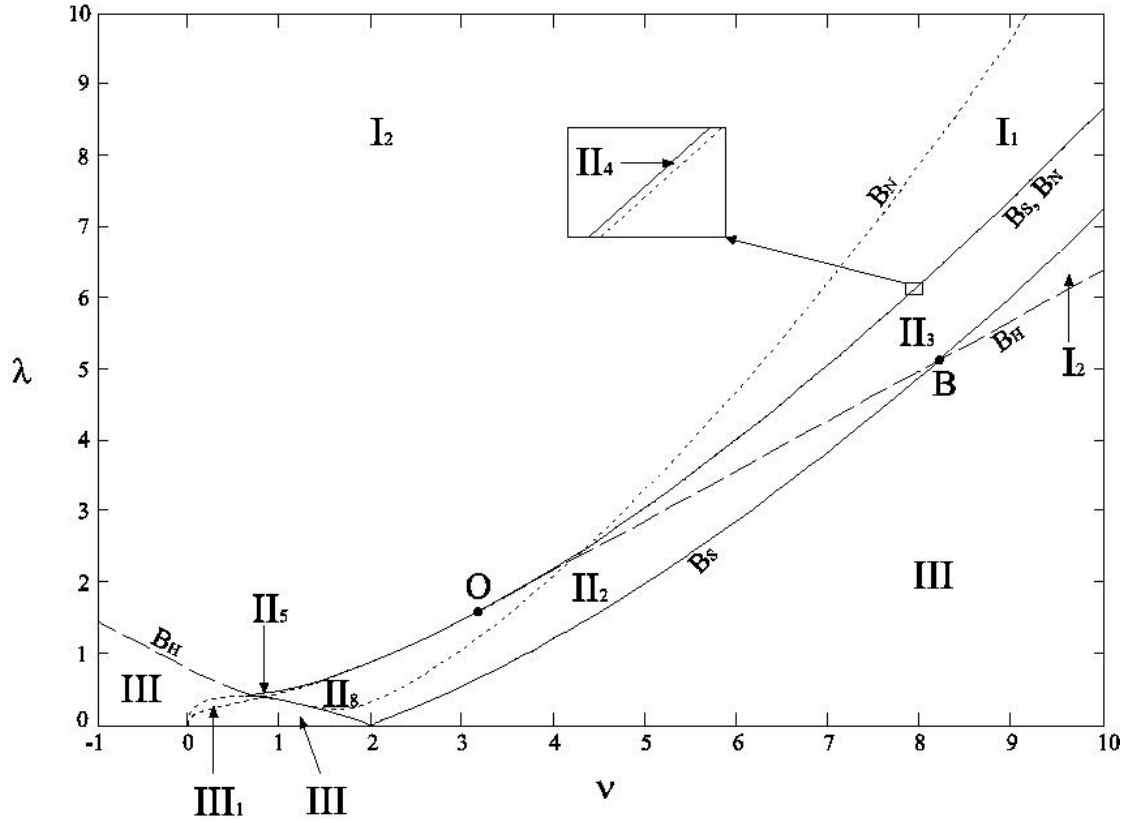

Figure 4.5: Bifurcations portraits of the MVdP oscillator in the parameter plane (ν, λ). Case α=2.

		$z=r^2$	ν	$\lambda(>0)$
$\alpha<-\sqrt{3},$	A:	$\frac{2}{3-\sqrt{3}\alpha}$	$\frac{1+\sqrt{3}\alpha}{\sqrt{3}-\alpha}$	$\sqrt{\frac{8\sqrt{3}}{9}\frac{\alpha^2+1}{\left(\sqrt{3}-\alpha\right)^3}}$
$\alpha=-\sqrt{3},$	A:	$\frac{1}{3}$	$-\frac{\sqrt{3}}{3}$	$\frac{2}{3\sqrt{3}}$
$\lvert\alpha\rvert<\sqrt{3},$	A':	$\frac{2}{3+\sqrt{3}\alpha}$	$\frac{\sqrt{3}\alpha-1}{\alpha+\sqrt{3}}$	$\sqrt{\frac{8\sqrt{3}}{9}\frac{\alpha^2+1}{\left(\alpha+\sqrt{3}\right)^3}}$
	A:	$\frac{2}{3-\sqrt{3}\alpha}$	$\frac{\sqrt{3}\alpha+1}{\sqrt{3}-\alpha}$	$\sqrt{\frac{8\sqrt{3}}{9}\frac{\alpha^2+1}{\left(\sqrt{3}-\alpha\right)^3}}$
$\alpha=\sqrt{3},$	A':	$\frac{1}{3}$	$\frac{\sqrt{3}}{3}$	$\frac{2}{3\sqrt{3}}$
$\alpha>\sqrt{3},$	A':	$\frac{2}{3+\sqrt{3}\alpha}$	$\frac{-1+\sqrt{3}\alpha}{\alpha+\sqrt{3}}$	$\sqrt{\frac{8\sqrt{3}}{9}\frac{\alpha^2+1}{\left(\alpha+\sqrt{3}\right)^3}}$

Table 4.2 : Coordinates z and (ν, λ) of the cusp points of the saddle-node bifurcation B_S.

Let us now analyze the regions of the ν-λ plane delimited by these curves. Three types of regions are distinguished:

- Type I regions: outside the saddle-node bifurcation B_S (Eq. (4.24)) and such that $\lambda>\lambda_H(\nu,\alpha)$ (Eq. (4.26)).
- Type II regions: inside the saddle-node bifurcation B_S (Eq. (4.24)).
- Type III regions: outside the saddle-node bifurcation B_S (Eq. (4.24)) and such that $0<\lambda<\lambda_H(\nu,\alpha)$ (Eq. (4.26)).

Each point (ν, λ) of the regions of type II (for given α), is associated with *three* solutions of the form (4.5)-(4.10), i.e. three values of the squared non-dimensional amplitude $z=r^2$. Conversely, each point of the regions I and III is associated with one solution. The number of sub-regions and the nature and stability of the associated solution(s) varies with the value of the parameter α. Let us analyze the following cases:

(a) $\alpha=0$ (see Figure 4.2 and Table 4.3). This situation corresponds to the standard Van der Pol and/or Rayleigh oscillators. It is the so-called *isochronous* case [24]. There are two regions of type I, where each point (ν, λ) is associated with a stable node (I_1) or a stable spiral (I_2). In both regions, the entrained solution (Eq. (4.5) or (4.10)) is stable. The region III is characterized by an unstable spiral. Therefore, the entrained solution is not stable. The transition from I_2 and III occurs via the Hopf bifurcation (4.26). In the four regions of type II, each point is associated with a saddle and two other solutions, whereof at least one is stable (Table 4.3). In summary, in the regions I and II a stable entrained solution exists, while in the region III the entrained solution is unstable. The upper bounds of the region III are the lower branch of B_S ($\lambda=\lambda_Q$) and B_H, that intersect at the point B for positive ν and at B' for negative ν.

(b) $0<|\alpha|\leq\sqrt{3}/3$. In this case, the region II is "stretched" with respect to the basic isochronous case $\alpha=0$, with a consequent loss of symmetry with respect to the λ-axis. The bifurcation diagram remains substantially unchanged, with the exception of the new region III_1, associated with

an unstable node; see the first column of Table 4.4 and, for the particular case α=0.5, Fig. 4.3.

(c) $\sqrt{3}/3<|\alpha|<\sqrt{3}$. With respect to the case (b), three new regions of type II appear (see Table 4.4 and, for the particular case α=1, Fig. 4.4). The regions II_6 and II_7 are characterized by three unstable solutions. For positive α, the left branch of the Hopf bifurcation is tangent to the lower branch λ_Q of the saddle-node bifurcation at O', while in the cases (a) and (b) it is tangent to the upper branch λ_P. The unstable domain, constituted by the regions II_6, II_7, III and III_1, is still delimited by the curves B_S ($\lambda=\lambda_Q$) and B_H, but the relevant intersection point for negative ν is O', instead of B'. An analogous situation occurs for negative α, for points O and B.

(d) $|\alpha|\geq\sqrt{3}$. In this case, the regions II_3 and II_4 become open, and the cusp A' no longer exists (see Figure 4.5, for the case α=2). The new region II_8 appears: it contains points associated with three solutions, one of which is stable (Table 4.4). The other regions are the same as in the case (c).

Region	I_1	I_2	II_1	II_2	II_3	II_4	III
P	<0	<0	<0, (-), >0	<0, (-), >0	<0, (-), <0	<0, (-), <0	>0
Q	>0	>0	>0, <0, >0	>0, <0, >0	>0, <0, >0	>0, <0, >0	>0
Δ	>0	<0	>0, >0, >0	>0, >0, <0	>0, >0, <0	>0, >0, >0	<0
	s.n.	s.s.	s.n., sd., u.n.	s.n., sd., u.s.	s.n., sd., s.s.	s.n., sd., s.n.	u.s.

Table 4.3 : Description of the fixed points in the different regions of the bifurcation diagrams. First part. (s.n.=stable node; s.s.= stable spiral; sd.= saddle; u.n.= unstable node; u.s.=unstable spiral).

Region	III_1	II_5	II_6	II_7	II_8
p	>0	<0, (-), >0	>0, (-), >0	>0, (-), >0	<0, (-), >0
q	>0	>0, <0, >0	>0, <0, >0	>0, <0, >0	>0, <0, >0
Δ	>0	<0, >0, >0	<0, >0, >0	>0, >0, >0	>0, >0, <0
	u.n.	s.s., sd., u.n.	u.s., sd., u.n.	u.n., sd., u.n.	s.s., sd., u.s.

Table 4.4 : Description of the fixed points in the different regions of the bifurcation diagrams. Second part. (s.n.=stable node; s.s.= stable spiral; sd.= saddle; u.n.= unstable node; u.s.=unstable spiral).

Collecting the conditions corresponding to the four cases, i.e. for all α, it is possible to distinguish the regions where there is at least a solution of the form (4.10) which is stable, viz. synchronization occurs, and the regions where synchronization is not possible. A summary of these conditions is given in Table 4.5. This Table defines a three-dimensional stability domain in the space (ν, λ, α). Accounting for the previous discussion, the transition between stable and unstable domains occurs either *via* the Hopf bifurcation ($\lambda=\lambda_H$) or *via* the bottom branch of the saddle-node bifurcation ($\lambda=\lambda_Q$). The graphical representation of this boundary as a surface in the space (ν, λ, α) is given in Figure 4.6, where the stability region is over the surface. Actually, the representation is made with a translated ν-axis, i.e. (ν-α, λ, α).

	$\alpha < -\sqrt{3}/3$	$\lvert\alpha\rvert \le \sqrt{3}/3$	$\alpha > \sqrt{3}/3$
$\lambda \ge \lambda_H$ when	$\nu \le \nu_{B'}$	$\nu \le \nu_{B'}$	$\nu \le \nu_{O'}$
$\lambda \ge \lambda_Q$ when	$\nu_{B'} \le \nu \le \nu_O$	$\nu_{B'} \le \nu \le \nu_B$	$\nu_{O'} \le \nu \le \nu_B$
$\lambda \ge \lambda_H$ when	$\nu \ge \nu_O$	$\nu \ge \nu_B$	$\nu \ge \nu_B$

Table 4.5 : Inequalities defining the stability domain for the entrained solutions (4.5)-(4.10) of the non-utonomous MVdP oscillator (4.4), according to the analytical approximation based on the harmonic balance method. $\lambda_Q = \lambda_Q(\alpha, \nu)$ and $\lambda_H = \lambda_H(\alpha, \nu)$ are defined by Eqs. (4.25) and (4.26), respectively.

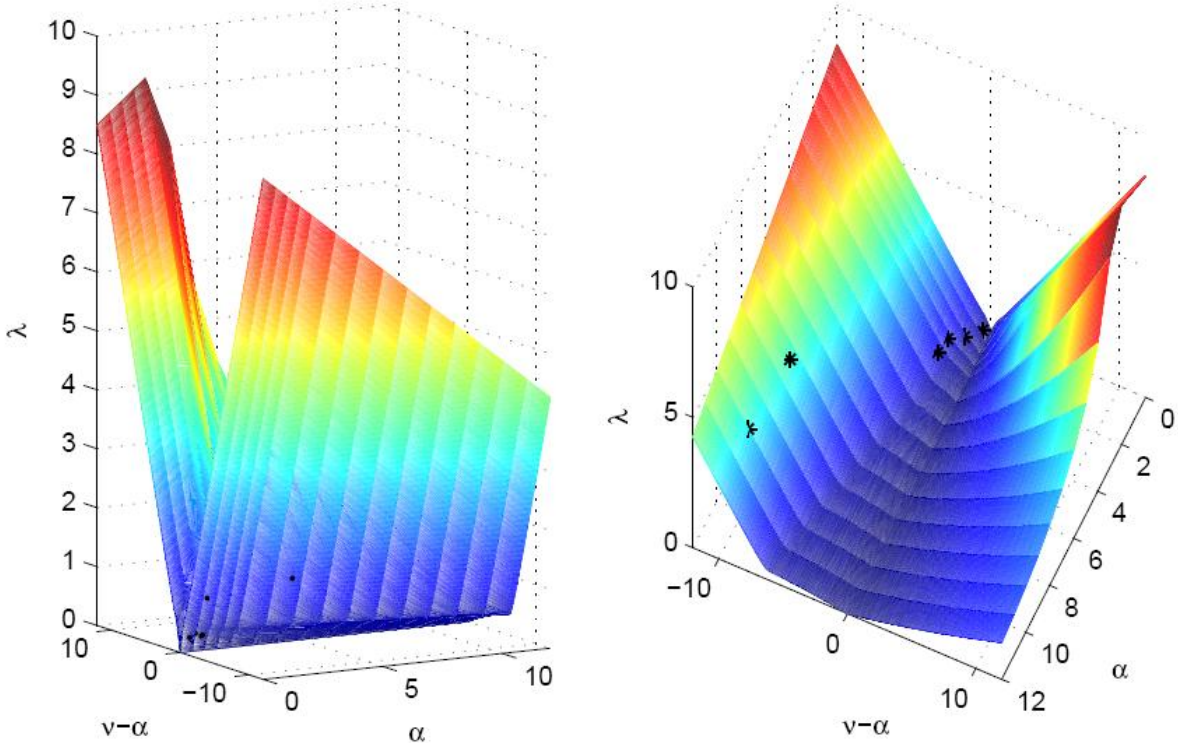

Figure 4.6: Surface representing the lower boundary of the stability domain, according to the analytical approximation defined in Table 4.5. Each point *over* the surface represents a pedestrian synchronized with the harmonically moving floor.

The domains described above are related with the *local* stability of the solution (4.5). However, it is well-known that some non-local bifurcations also exist for systems like Eq. (4.13); see e.g. [24]. The study of non-local bifurcations for the MVdP oscillator is beyond the purposes of this Chapter. One also observes that the transition between stable and unstable spirals across the Hopf bifurcation does not occur suddenly: around an unstable spiral defined by the coordinates (x_1=Rcosθ, x_2=Rsinθ), a limit cycle always raises [23]. If the spiral of coordinates (x_1, x_2) is close to the Hopf bifurcation, this limit cycle is small and does not envelope the origin of the plane (x_1, x_2): in this case the frequency of the solution u_y (Eq. (4.5)) is still that of the external force, but the amplitude is modulated, i.e. u_y is not of the form predicted by Eq. (4.5). This situation is sometimes called "nearly synchronous" regime [24]. When the spiral is far enough from the Hopf bifurcation, the limit cycle around the spiral also envelops the origin of the plane (x_1, x_2) and the frequency of the solution becomes different from that of the excitation and synchronization is

completely lost. For simplicity, these two situations are not distinguished in this Chapter and they are both considered as non-synchronized.

4.4. The use of the stability domain for predicting the pedestrian synchronization

In this Section, the theoretical notions previously discussed are used to interpret experimental results about the lateral oscillations of pedestrians walking on a moving floor. Several studies have been performed in this situation. In particular, in [9, 27] experimental results on a shake table with *harmonic* motion are discussed and some percentages of synchronized pedestrians are found. The main goal here is to show that the MVdP oscillator (4.4) gives a sound representation of experimental results of this kind.

4.4.1. Analytical viewpoint: a 3D normalized synchronization domain

Let us suppose in this Subsection that the *analytical* approximation of the synchronization domain (Table 4.5) is very close to the exact domain. If this is the case, a simple procedure can be suggested for evaluating the percentage of pedestrians that synchronize with the *harmonically* moving floor. According to the definition (4.4) of the MVdP oscillator, a pedestrian is represented by the five parameters μ, ω_0, β, γ and δ, while the harmonic floor motion is represented by two parameters, i.e. the acceleration amplitude A_{acc} and the pulsation ω. Hence, there are seven "physical" parameters. Nonetheless, it is possible to use Eqs. (4.11) and (4.12) to reduce to *three* the number of (non-dimensional) parameters necessary and sufficient to represent a pedestrian walking on a floor with a given harmonic motion:

$$\alpha = \frac{\gamma \dfrac{\omega}{\omega_0}}{\beta + 3\delta\left(\dfrac{\omega}{\omega_0}\right)^2}, \quad \nu = \frac{\left(\dfrac{\omega}{\omega_0}\right)^2 - 1}{2\mu\dfrac{\omega}{\omega_0}}, \quad \lambda = \frac{A_{acc}}{\omega_0}\frac{\sqrt{\beta + 3\delta\left(\dfrac{\omega}{\omega_0}\right)^2}}{4\mu\omega} \tag{4.28}$$

These parameters can be thought as the coordinates of a point in the 3D (ν, λ, α) space. In the same space, the synchronization domain has been defined by the conditions collected in Table 4.5 and it has been represented in Fig. 4.6, with the translation $\nu \rightarrow \nu - \alpha$. When the point is outside this domain, i.e. it is under the surface plotted in Fig. 4.6, synchronization cannot occur. Conversely, when the point is inside this domain, the synchronization of the pedestrian with the floor is possible. For instance, Fig. 4.6 shows twelve points, corresponding to twelve pedestrians (see Chapter 2, test with nominal longitudinal speed v_x=4.5 km/h) on a laterally moving floor with A_{acc}=0.15 m/s² and $f=\omega/2\pi$=0.75 *Hz*. The ratio between the number of points over the surface and the total number of points gives the synchronization percentage.

Looking at Fig. 4.6, one notices that when λ=0 the synchronization domain touches the axis $\nu - \alpha$=0 (see the Appendix D). This indicates that also for very small excitations, synchronization is possible provided that the difference $\nu - \alpha$ is close enough to zero. In terms of dimensional parameters, λ=0 entails A_{acc}=0 by means of the third identity in (4.28): it is the rigid floor condition. Moreover, it can be proven that, in terms of dimensional parameters, $\nu - \alpha$=0 corresponds to $\omega=\omega_1$ (see the Appendix D), where ω_1 is the walking frequency of the pedestrian on a rigid floor; see Eq. (4.6). Hence, synchronization is possible even for small excitation amplitudes, provided that the excitation frequency ω is very close to ω_1. Conversely, if the difference $\nu - \alpha$ is large, the synchronization occurs only when the excitation amplitude λ is large. According to this interpretation, it makes no sense to speak about an absolute threshold value of the excitation amplitude acting on a single pedestrian, without referring to the detuning $\nu - \alpha$, correlated with the frequency difference $\omega - \omega_1$. Fig. 4.6 as well as Figs. 4.3 - 4.5 show that for a given non-zero α value, the lower boundary of the stability/synchronization domain *is not an even function of* $\nu - \alpha$. Therefore, the *sign* and not only the amplitude of the frequency detuning is important. If α>0, the tendency to have synchronization is greater when the floor frequency is larger than the pedestrian natural frequency (ω-

$\omega_1>0 \Leftrightarrow \nu-\alpha>0$). This asymmetric behaviour is correlated with the term proportional to γ in the MVdP oscillator, that is in turn proportional to α. The model identification presented in Chapter 2 shows that the identified values of γ are always positive and that this parameter is essential to have a good fitting of experimental lateral forces in rigid floor regime. Concerning the test results available in the literature for the moving floor regime (e.g. [9, 27]), it is actually not easy to extract some information about the synchronization behaviour of *each single pedestrian* for different frequency detunings. The measurement results are often given under the form of percentages of synchronization, without referring to the single individual. For this reason, it is not easy to detect this asymmetric synchronization effect. Further experimental analyses might help to get a better understanding of this aspect.

4.4.2. Analytical vs. numerical synchronization domain

The analytical approximation of the stability domain presented in the previous Subsection is insightful, since it shows an essential characteristic of the synchronization behaviour: only three normalized parameters suffice, as a first approximation, to represent the seven physical parameters describing a pedestrian walking on a harmonically moving floor. However, the assumption made at the beginning of the previous Subsection is not always fulfilled. Actually, Eqs. (4.21), (4.22), (4.23) and the relationships of Table 4.5 defining the analytical approximation of the stability domain have been obtained supposing that the solution of the forced MVdP model is of the form (4.5)-(4.10), where superharmonics components of the response are neglected. Hence, this analytical representation has to be used with caution. In order to avoid an important effect of the higher harmonics, the amplitude of the force has to be small. For the same reason, the parameters μ and α related to the nonlinear damping and the frequency detuning ν should be small [23]. In addition, it should not be forgotten that this domain concerns the 1:1 synchronization only [24].

Accounting for these remarks, a comparison between analytical predictions and numerical results is presented in Figs. 4.7, 4.8 and 4.9. Three cases are considered: (a) α=0; (b) α=0.5; and (c) α=1. Each point in these figures gives the

numerical estimation of the boundary of the stability domain for a given ν value. It has been obtained doing several numerical simulations at a given value of ν and modifying the λ value. In detail, Eq. (4.4) is solved with the parameters μ=0.15, β=1, δ=1, ω_0=1; the excitation frequency ω is computed using the second identity in (4.28) for the given ν value, while γ is computed for the given α value (constant in each Figure) using the first relationship in (4.28). Finally, A_{acc} is modified according to the third identity in (4.28) in order to modify the λ value. For small λ values, the computed response is not synchronized (like in the example of Fig. 4.10a). By increasing λ, this behaviour changes at the transition across the stability domain and a solution with constant amplitude and frequency ω appears (like in the example of Fig. 4.10b). The transition value of λ, together with the given ν, defines one point. As it can be seen from Figs. 4.7, 4.8 and 4.9, the difference between analytical and numerical results is not always small, above all for the highest values of ν and α. For this reason, only the numerical results are used for the comparison of the model predictions with the experimental results (see the following Subsection).

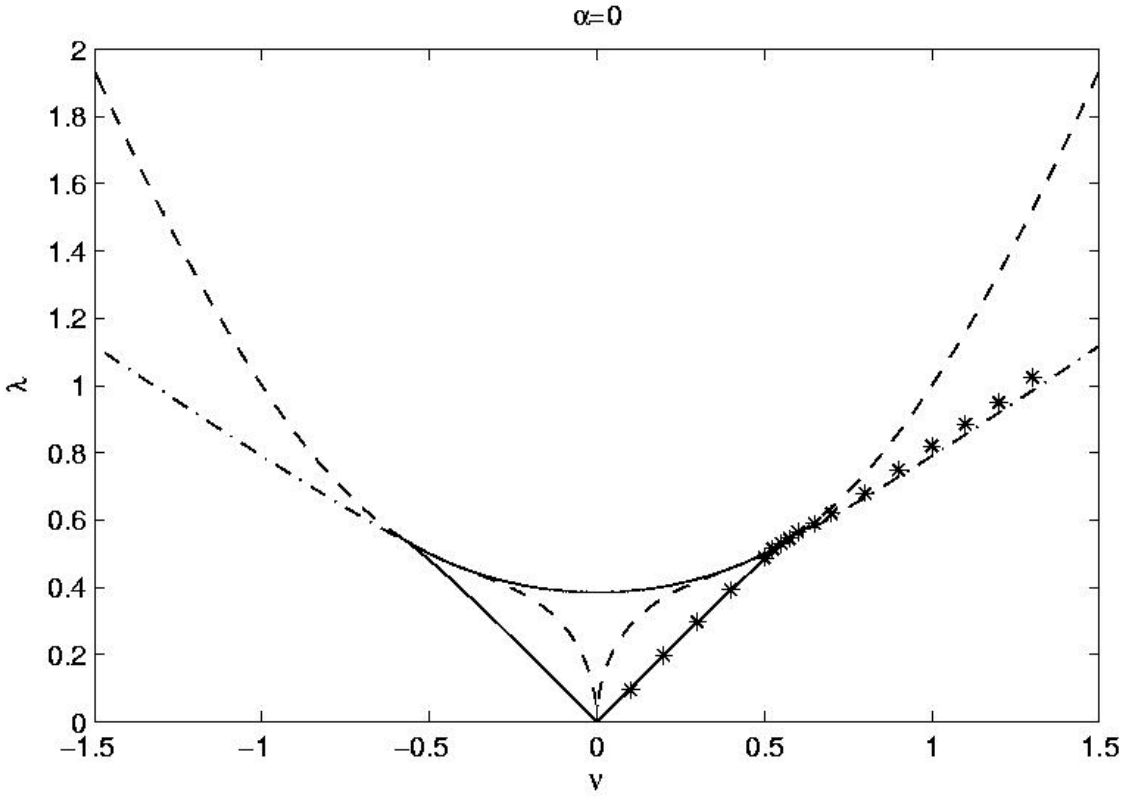

Figure 4.7: Comparison between the analytical and numerical estimations of the boundary of the stability domain of the MVdP oscillator. Case α = 0.

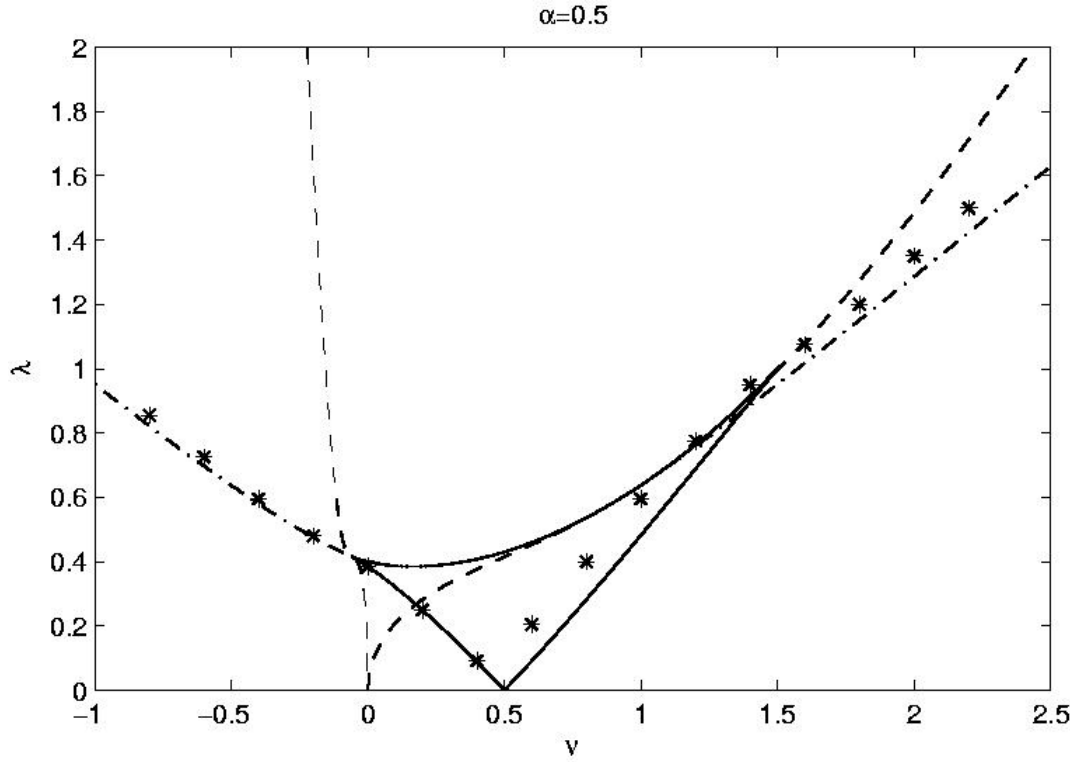

Figure 4.8: Comparison between the analytical and numerical estimations of the boundary of the stability domain of the MVdP oscillator. Case $\alpha = 0.5$.

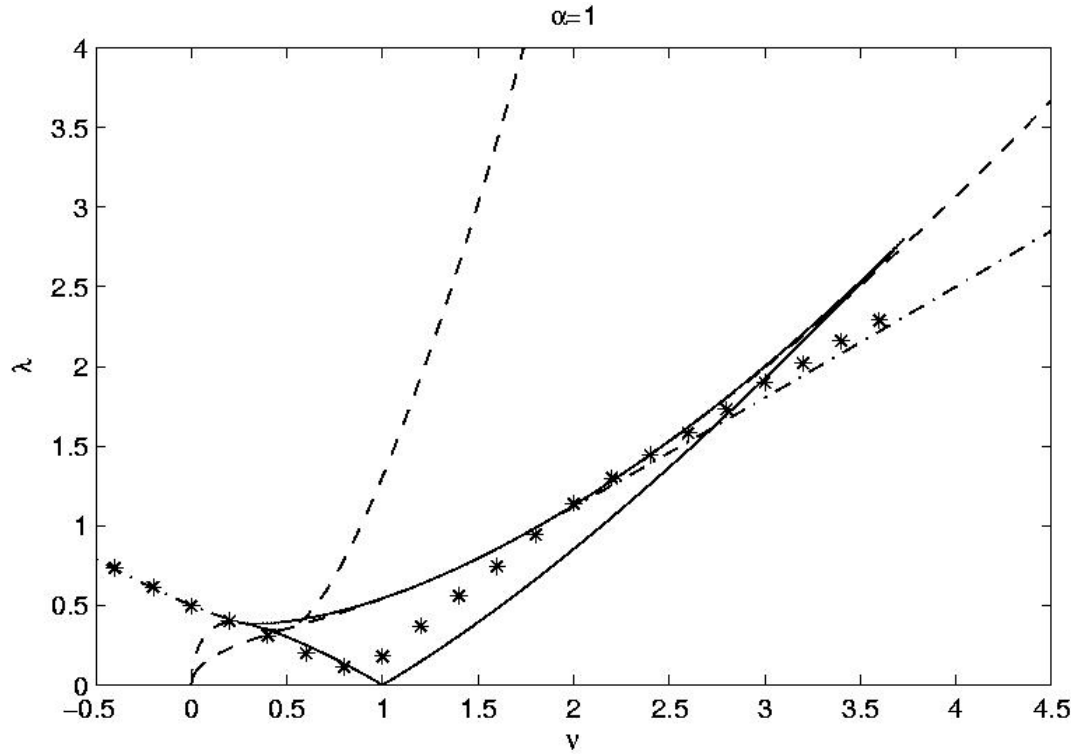

Figure 4.9: Comparison between the analytical and numerical estimations of the boundary of the stability domain of the MVdP oscillator. Case $\alpha = 1$.

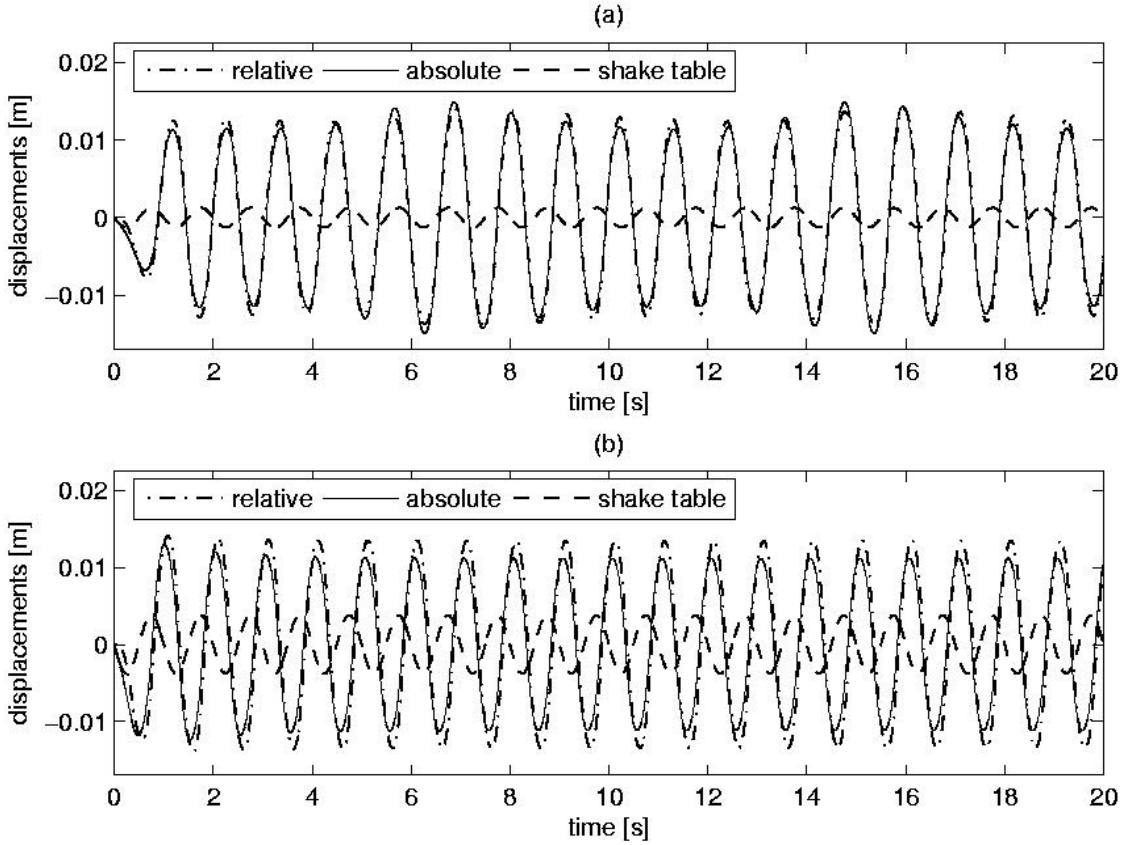

Figure 4.10: Time-evolution of the displacements of the center of mass of pedestrian "2" (v_x = 3.75 km/h) in the case of (a) *non-entrained* oscillation (A_{acc}=0.05 m/s^2, $\omega/(2\pi)$=1 Hz) and (b) *entrained* oscillation (A_{acc}=0.15 m/s^2, $\omega/(2\pi)$=1 Hz). u_y : relative displacement; $U_y + u_y$: absolute displacement; U_y : shake table displacement.

4.4.3. Percentages of synchronization for a group of pedestrians

We consider here two populations of twelve pedestrians, represented by two groups of twelve MVdP oscillators. The parameters defining these pedestrians have been identified from *rigid floor* walking tests [see Chapter 2]. Actually, the pedestrians of the first population were asked to walk on a treadmill with a nominal speed v_x=3.75 km/h . Each pedestrian has a natural walking frequency corresponding to this longitudinal speed. The average of the natural frequencies of this group is 0.848 Hz with a standard deviation of 0.055 Hz. The same pedestrians were also asked to walk at the nominal speed v_x=4.5 km/h. The average frequency in this case is 0.923 Hz with a standard deviation of 0.053 Hz.

For each oscillator/pedestrian a numerical simulation is made with an periodic excitation corresponding to a floor motion with given acceleration amplitude A_{acc} and frequency ω. The response is computed considering zero initial conditions: if a steady response with constant amplitude and frequency equal to ω is reached after a transient (see Fig. 4.10b), then the oscillator/pedestrian is considered synchronized with the floor. It is non-synchronized in the opposite case (see Fig. 4.10a). The plots of Fig. 4.10 concern the pedestrian "2" (case of longitudinal speed v_x=3.75 km/h), having natural walking frequency of 0.873 Hz. The corresponding model parameters (identified in *rigid floor* conditions) read: ω_0=4.60 rad/s, ε=1.107, β=4785 m^{-2}, γ=7416 m^{-2}, δ=3426 m^{-2}, m=69.4 kg.

Table 4.6 concerns the first population and shows the percentages of synchronized pedestrians for several amplitudes and frequencies of the floor motion. Table 4.7 concerns the second population, characterized by a slightly higher averaged frequency. It can be seen that the highest percentages of synchronization occur for the highest floor acceleration amplitudes and for floor frequencies close to the average value of the population. This dependence of the synchronization percentages on the floor motion amplitude and frequency is analogous to that obtained from the tests discussed in [9] and [27], realized with different populations of pedestrians walking on a shake table with harmonic lateral motion.

f [Hz] / Acc [m/s^2]	0.5	0.75	1.0	1.25
0.05	0/12	5/12	1/12	0/12
0.15	0/12	12/12	7/12	0/12
0.30	9/12	12/12	12/12	3/12

Table 4.6 : Percentages of synchronized pedestrians in a population of twelve people. The average of the natural walking frequencies of all pedestrians is $\overline{f}_1$ = 0.848 Hz with a standard deviation of 0.055 Hz.

f [*Hz*] / Acc [m/s^2]	0.5	0.75	1.0	1.25
0.05	0/12	0/12	5/12	0/12
0.15	0/12	10/12	11/12	0/12
0.30	9/12	12/12	12/12	7/12

Table 4.7 : Percentages of synchronized pedestrians in a population of twelve people. The average of the natural walking frequencies of all pedestrians is $\overline{f}_1$ = 0.923 *Hz* with a standard deviation of 0.053 *Hz*.

4.5. Conclusions

In this Chapter, the modified Van der Pol (MVdP) oscillator defined in Chapter 2 is studied in the non-autonomous regime. The analysis mainly concerns the local stability of steady entrained solutions, i.e. the periodic solutions having the same frequency as the imposed harmonic excitation. These results supplement those of the Chapter 3, where the amplitude of the entrained solutions was computed without evaluating the stability. The stability domain of the MVdP oscillator found by an analytical procedure is compared with numerical simulations results. Then, these theoretical notions are used to estimate the percentage of pedestrians synchronized with a floor undergoing a given periodic motion. The proposed procedure provides an effective way of interpreting the results of synchronization percentages obtained by tests where pedestrians walk on a shake table undergoing harmonic oscillations.

Chapter 5

Conclusions

In this thesis, an exhaustive experimental analysis of the lateral walking force on a rigid floor has been presented. The importance of the phase differences between the Fourier harmonics in the series representing the periodic approximation of the force has been highlighted. Then, the use of a self-sustained autonomous SDoF oscillator has been proposed for modelling the lateral motion of the center of gravity of a pedestrian walking on a rigid floor: the nonlinear restoring force of this oscillator represents the lateral walking force. It has been proven from the analysis of experimental data that a modified version of the classical Van der Pol model provides a very good fitting between the model behaviour and the periodic force extracted from experiments.

When the floor is moving (non-autonomous MVdP oscillator), both a theoretical analysis and a comparison with experimental results concerning the pedestrian behaviour are presented. In detail, the response of the modified Van der Pol (MVdP) oscillator under a harmonic external force associated with the floor motion is analytically evaluated by the harmonic balance method. An approximated expression of the amplitude of the periodic entrained solution is derived and compared with numerical results. Then, the model predictions are compared with experimental results coming from the literature, and a good agreement is obtained.

Once the behaviour of the single pedestrian/oscillator in known, a set of several non-autonomous MVdP oscillators can be considered in order to represent the total lateral force of a crowd on a moving floor. These analyses will be addressed in future work.

Chapter 6

Appendix

A. Fourier series coefficients

By definition, a periodic signal $F_y(t)$ can be written as follows:

$$F_{y,per}(t) = \frac{A_0}{2} + \sum_{k=1}^{\infty} A_k \cos\left(k2\pi f_1 t\right) + B_k \sin\left(k2\pi f_1 t\right)$$

with the coefficients

$$A_k = \frac{2}{T}\int_0^T F_y(t)\cos\left(k2\pi f_1 t\right)dt \qquad k \geq 0$$

$$B_k = \frac{2}{T}\int_0^T F_y(t)\sin\left(k2\pi f_1 t\right)dt \qquad k \geq 1$$

Equivalently, one can write

$$F_{y,per}(t) = \frac{C_0}{2} + \sum_{k=1}^{\infty} C_k \cos\left(k2\pi f_1 t - \phi_k\right)$$

where

$$\begin{aligned} C_0 &= A_0 \\ C_k &= \sqrt{A_k^2 + B_k^2} \qquad k \geq 1 \\ \phi_k &= \arctan\left(A_k, B_k\right) \qquad k \geq 1 \end{aligned} \tag{2.38}$$

Observe that the function arctan(x,y) provides ϕ_k-values in the interval (-π, π] (or equivalently, in the interval [0, 2π)), because it takes into account the sign

of both arguments x and y. Moreover, ϕ_k is zero on the positive x-axis and increases in the counter-clockwise direction.

B. Perturbation analysis of the MVdP model

According to a standard perturbation method, one assumes $|\mu| \ll 1$ and the solution of (2.14) is supposed of the form

$$\begin{aligned} &\tilde{u}_y(\tau) = \tilde{u}_y(\tau;\mu) = \tilde{u}_{y,0}(\tau) + 2\mu\ \tilde{u}_{y,1}(\tau) + O\left(\mu^2\right) \\ &\rho = \rho(\mu) = 1 + 2\mu\ \rho_1 + O\left(\mu^2\right) \end{aligned} \tag{2.39}$$

with the initial conditions

$$\begin{aligned} &\tilde{u}_y(0;\mu) = a(\mu), \qquad \frac{d\tilde{u}_y(0;\mu)}{d\tau} = 0 \\ &a = a(\mu) = a_0 + 2\mu\ a_1 + \mathrm{O}\left(\mu^2\right) \end{aligned} \tag{2.40}$$

Replacing these expressions in (2.17) and then writing out the equations up to the first order of μ, one obtains

$$\mathrm{O}(1): \begin{cases} \dfrac{d^2\tilde{u}_{y,0}(\tau)}{d\tau^2} + \tilde{u}_{y,0}(\tau) = 0 \\ \tilde{u}_{y,0}(0) = a_0, \qquad \dfrac{d\tilde{u}_{y,0}(0)}{d\tau} = 0 \end{cases} \tag{2.41}$$

$$\mathrm{O}(\mu): \begin{cases} \dfrac{d^2\tilde{u}_{y,1}(\tau)}{d\tau^2} + \tilde{u}_{y,1}(\tau) \\ = \dfrac{d\tilde{u}_{y,0}(\tau)}{d\tau}\left(1 - \beta\left(\tilde{u}_{y,0}(\tau)\right)^2 - \gamma\tilde{u}_{y,0}(\tau)\dfrac{d\tilde{u}_{y,0}(\tau)}{d\tau} - \delta\left(\dfrac{d\tilde{u}_{y,0}(\tau)}{d\tau}\right)^2\right) - 2\rho_1\dfrac{d^2\tilde{u}_{y,0}(\tau)}{d\tau^2} \\ \tilde{u}_{y,1}(0) = a_1, \qquad \dfrac{d\tilde{u}_{y,1}(0)}{d\tau} = 0 \end{cases}$$

The solution of the first equation reads

$$\tilde{u}_{y,0}(\tau) = a_0 \cos(\tau) \tag{2.42}$$

where a_0 is unknown. This expression can be substituted in the second equation of (2.41). Then, the r.h.s. terms proportional to cos(τ) and to sin(τ) are imposed to be zero, in order to remove the so-called "secular terms". These two conditions lead to the computation of a_0 and ρ_1:

$$a_0 = \frac{2}{(\beta+3\delta)^{1/2}}, \qquad \rho_1 = \frac{1}{\beta+3\delta}\frac{\gamma}{2} \tag{2.43}$$

Observe that the condition $\beta+3\delta>0$ must be satisfied for the existence of this solution. Moreover, ρ_1 is zero when $\gamma=0$, i.e. for both the Van der Pol and Rayleigh's models. It is now possible to compute the solution of the first order equation $\tilde{u}_{y,1}(\tau)$. An analogous procedure leads to a_1, ρ_2 and $\tilde{u}_{y,2}(\tau)$ and higher order terms. In summary, up to the first order term, one has

$$\begin{aligned}
&\rho(\mu) = 1 + \frac{\mu\gamma}{\beta+3\delta} + \mathrm{O}\left(\mu^2\right) \\
&a(\mu) = \frac{2}{(\beta+3\delta)^{1/2}} - \mu\gamma\frac{3\beta+17\delta}{2(\beta+3\delta)^{5/2}} + \mathrm{O}\left(\mu^2\right) \\
&\tilde{u}_y(\tau;\mu) = \left[\frac{2}{(\beta+3\delta)^{1/2}} - \mu\gamma\frac{\beta+7\delta}{(\beta+3\delta)^{5/2}}\right]\cos(\tau) \\
&-\frac{\mu}{2(\beta+3\delta)^{5/2}}\left((\beta+3\delta)\gamma\cos(3\tau) + (\beta+3\delta)(\delta-\beta)\left(3\sin(\tau)-\sin(3\tau)\right)\right) + \mathrm{O}\left(\mu^2\right)
\end{aligned} \tag{2.44}$$

The last expression can be derived with respect to τ, in order to get the normalized velocity $\frac{d\tilde{u}_y(\tau;\mu)}{d\tau}$. In the phase plane, the polar coordinates can be computed by setting

$$\begin{aligned}
&\tilde{R}(\tau;\mu) = \sqrt{\tilde{u}_y(\tau;\mu)^2 + \left(\frac{d\tilde{u}_y(\tau;\mu)}{d\tau}\right)^2}, \\
&\tilde{\theta}(\tau;\mu) = \arctan\left(\tilde{u}_y(\tau;\mu), \frac{d\tilde{u}_y(\tau;\mu)}{d\tau}\right)
\end{aligned} \tag{2.45}$$

The convention on the sign of $\tilde{\theta}$ is illustrated in Fig. 2.10. At the first order,

$$\begin{aligned}
&\tilde{R}(\tau;\mu) = \frac{2}{\sqrt{\beta+3\delta}} - \mu\gamma\frac{\beta+7\delta}{(\beta+3\delta)^{5/2}} \\
&+\mu\frac{1}{2(\beta+3\delta)^{5/2}}\left[\gamma(\beta+3\delta)\left(\cos(4\tau)-2\cos(2\tau)\right)+\left(\beta^2+2\beta\delta-3\delta^2\right)\left(\sin(4\tau)-2\sin(2\tau)\right)\right]+\mathrm{O}\left(\mu^2\right) \\
&\tilde{\theta}(\tau;\mu) = -\tau+\frac{\mu}{4}\frac{1}{\beta+3\delta}\left[(\beta-\delta)\left(3-2\cos(2\tau)-\cos(4\tau)\right)+\gamma\left(2\sin(2\tau)+\sin(4\tau)\right)\right]+\mathrm{O}\left(\mu^2\right)
\end{aligned} \tag{2.46}$$

From (2.46), one has that $\tilde{\theta} = -\tau$ at the zero order. Hence, the radius can be written as function of the angle $\tilde{\theta}$:

$$\tilde{R}\left(\tilde{\theta};\mu\right) = \frac{2}{\sqrt{\beta+3\delta}} - \frac{\mu}{2(\beta+3\delta)^{5/2}}\begin{pmatrix}2\gamma(\beta+7\delta)+\gamma(\beta+3\delta)\left(2\cos\left(2\tilde{\theta}\right)-\cos\left(4\tilde{\theta}\right)\right)\\+\left(\beta^2+2\beta\delta-3\delta^2\right)\left(\sin\left(4\tilde{\theta}\right)-2\sin\left(2\tilde{\theta}\right)\right)\end{pmatrix}+\mathrm{O}\left(\mu^2\right) \tag{2.47}$$

C. *Perturbation of the steady solution*

It has been shown in Chapter 3 that by replacing the periodic solution (4.10) in Eq. (4.8), one obtains the following equilibrium equations:

$$\begin{cases}
\varepsilon\tilde{\omega}\left(-\dfrac{\tilde{\omega}^2-1}{\varepsilon\tilde{\omega}}R+\dfrac{\gamma}{4}\tilde{\omega}R^3\right) = A_d\tilde{\omega}^2\cos(\theta) = \dfrac{A_{acc}}{\omega_0^2}\cos(\theta) \\
\varepsilon\tilde{\omega}\left(R-R^3\dfrac{1}{4}\left(\beta+3\delta\tilde{\omega}^2\right)\right) = A_d\tilde{\omega}^2\sin(\theta) = \dfrac{A_{acc}}{\omega_0^2}\sin(\theta)
\end{cases} \tag{4.29}$$

Moreover, by inserting the expression (4.15) of the perturbed solution into the equation (4.8), one obtains

$$
\begin{aligned}
&\ddot{\mathrm{v}}(\tau)+\mathrm{v}(\tau)\\
&-\varepsilon\dot{\mathrm{v}}(\tau)\begin{pmatrix}
1-\beta\left(R^2\left(\frac{1}{2}+\frac{1}{2}\cos(2\tilde{\omega}\tau+2\theta)\right)+\mathrm{v}^2(\tau)+2\mathrm{v}(\tau)R\cos(\tilde{\omega}\tau+\theta)\right)\\
-\gamma\left(-R^2\tilde{\omega}\frac{1}{2}\sin(2\tilde{\omega}\tau+2\theta)-R\tilde{\omega}\sin(\tilde{\omega}\tau+\theta)\mathrm{v}(\tau)\right)\\
-\gamma\left(R\cos(\tilde{\omega}\tau+\theta)\dot{\mathrm{v}}(\tau)+\mathrm{v}(\tau)\dot{\mathrm{v}}(\tau)\right)\\
-\delta\left(R^2\tilde{\omega}^2\left(\frac{1}{2}-\frac{1}{2}\cos(2\tilde{\omega}\tau+2\theta)\right)+\dot{\mathrm{v}}(\tau)^2-2\dot{\mathrm{v}}(\tau)R\tilde{\omega}\sin(\tilde{\omega}\tau+\theta)\right)
\end{pmatrix}\\
&+\varepsilon R\tilde{\omega}\begin{pmatrix}
-\beta\left(2R\frac{1}{2}\sin(2\tilde{\omega}\tau+2\theta)\mathrm{v}(\tau)+\sin(\tilde{\omega}\tau+\theta)\mathrm{v}(\tau)^2\right)\\
-\gamma\left(-R\tilde{\omega}\left(\frac{1}{2}-\frac{1}{2}\cos(2\tilde{\omega}\tau+2\theta)\right)\mathrm{v}(\tau)+R\frac{1}{2}\sin(2\tilde{\omega}\tau+2\theta)\dot{\mathrm{v}}(\tau)\right)\\
-\gamma\left(\sin(\tilde{\omega}\tau+\theta)\dot{\mathrm{v}}(\tau)\mathrm{v}(\tau)\right)\\
-\delta\left(-2R\tilde{\omega}\left(\frac{1}{2}-\frac{1}{2}\cos(2\tilde{\omega}\tau+2\theta)\right)\dot{\mathrm{v}}(\tau)+\sin(\tilde{\omega}\tau+\theta)\dot{\mathrm{v}}(\tau)^2\right)
\end{pmatrix}\\
&=0
\end{aligned}
\tag{4.30}
$$

The external excitation term related to A_{acc} does not appear in Eq. (4.30), since it cancels out together with the terms fulfilling the equilibrium equations (4.29). The third order harmonics have also been neglected, according to the harmonic balance method and to the assumption (4.16). The *linearization* of (4.30) leads to

$$
\begin{aligned}
&\ddot{\mathrm{v}}(\tau)+\mathrm{v}(\tau)\left(1-\varepsilon\beta R^2\tilde{\omega}\sin(2\tilde{\omega}\tau+2\theta)+\gamma\varepsilon R^2\tilde{\omega}^2\left(\frac{1}{2}-\frac{1}{2}\cos(2\tilde{\omega}\tau+2\theta)\right)\right)\\
&-\varepsilon\dot{\mathrm{v}}(\tau)\left(1-\beta R^2\left(\frac{1}{2}+\frac{1}{2}\cos(2\tilde{\omega}\tau+2\theta)\right)+\gamma R^2\tilde{\omega}\sin(2\tilde{\omega}\tau+2\theta)\right)\\
&-\varepsilon\dot{\mathrm{v}}(\tau)\left(-3\delta R^2\tilde{\omega}^2\left(\frac{1}{2}-\frac{1}{2}\cos(2\tilde{\omega}\tau+2\theta)\right)\right)\\
&=0
\end{aligned}
\tag{4.31}
$$

We recall the definition (4.16) and make a Van der Pol transformation between the variables $(\mathrm{v},\dot{\mathrm{v}})$ and (B_{1c}, B_{1s}):

$$
\begin{cases}
\mathrm{v}(\tau)=B_{1c}\cos(\tilde{\omega}\tau+\theta)+B_{1s}\sin(\tilde{\omega}\tau+\theta)\\
\dot{\mathrm{v}}(\tau)=-B_{1c}\tilde{\omega}\sin(\tilde{\omega}\tau+\theta)+\tilde{\omega}B_{1s}\cos(\tilde{\omega}\tau+\theta)
\end{cases}
\tag{4.32}
$$

with the compatibility condition

$$\dot{B}_{1s}\sin\left(\tilde{\omega}\tau+\theta\right)=-\dot{B}_{1c}\cos\left(\tilde{\omega}\tau+\theta\right) \tag{4.33}$$

This identity is obtained imposing that the velocity defined in $(4.32)_2$ is equal to the velocity computed by differentiating Eq. $(4.32)_1$. The acceleration, obtained by differentiating $(4.32)_2$, reads:

$$\ddot{\mathrm{v}}(\tau)=-B_{1s}\tilde{\omega}^2\sin\left(\tilde{\omega}\tau+\theta\right)-B_{1c}\tilde{\omega}^2\cos\left(\tilde{\omega}\tau+\theta\right)+\dot{B}_{1s}\tilde{\omega}\cos\left(\tilde{\omega}\tau+\theta\right)-\dot{B}_{1c}\tilde{\omega}\sin\left(\tilde{\omega}\tau+\theta\right) \tag{4.34}$$

By replacing (4.32) and (4.34) in Eq. (4.31) and after some trigonometric development, one has

$$\begin{aligned}
&-B_{1s}\tilde{\omega}^2\sin\left(\tilde{\omega}\tau+\theta\right)-B_{1c}\tilde{\omega}^2\cos\left(\tilde{\omega}\tau+\theta\right)+\dot{B}_{1s}\tilde{\omega}\cos\left(\tilde{\omega}\tau+\theta\right)-\dot{B}_{1c}\tilde{\omega}\sin\left(\tilde{\omega}\tau+\theta\right)\\
&+B_{1s}\left(\sin\left(\tilde{\omega}\tau+\theta\right)-\varepsilon\beta R^2\tilde{\omega}\frac{1}{2}\cos\left(\tilde{\omega}\tau+\theta\right)+\gamma\varepsilon R^2\tilde{\omega}^2\left(\frac{1}{2}\sin\left(\tilde{\omega}\tau+\theta\right)+\frac{1}{4}\sin\left(\tilde{\omega}\tau+\theta\right)\right)\right)\\
&+B_{1c}\left(\cos\left(\tilde{\omega}\tau+\theta\right)-\varepsilon\beta R^2\tilde{\omega}\frac{1}{2}\sin\left(\tilde{\omega}\tau+\theta\right)+\gamma\varepsilon R^2\tilde{\omega}^2\frac{1}{4}\cos\left(\tilde{\omega}\tau+\theta\right)\right)\\
&-\varepsilon\tilde{\omega}B_{1s}\left(\cos\left(\tilde{\omega}\tau+\theta\right)-\beta R^2\frac{3}{4}\cos\left(\tilde{\omega}\tau+\theta\right)+\gamma R^2\tilde{\omega}\frac{1}{2}\sin\left(\tilde{\omega}\tau+\theta\right)-\frac{3}{4}\delta R^2\tilde{\omega}^2\cos\left(\tilde{\omega}\tau+\theta\right)\right)\\
&+\varepsilon B_{1c}\tilde{\omega}\left(\sin\left(\tilde{\omega}\tau+\theta\right)-\beta R^2\frac{1}{4}\sin\left(\tilde{\omega}\tau+\theta\right)+\gamma R^2\tilde{\omega}\frac{1}{2}\cos\left(\tilde{\omega}\tau+\theta\right)-\frac{9}{4}\delta R^2\tilde{\omega}^2\sin\left(\tilde{\omega}\tau+\theta\right)\right)\\
&=0
\end{aligned}$$

where the third harmonic components have been neglected like in the previous expressions. This equation and the compatibility condition (4.33) constitute a system of two first order equations which can be rewritten, after some developments, as follows:

$$\begin{cases}
-2\tilde{\omega}\dot{B}_{1s}=B_{1s}\left(\varepsilon\tilde{\omega}\beta R^2\frac{1}{4}-\varepsilon\tilde{\omega}+\varepsilon\tilde{\omega}\delta R^2\tilde{\omega}^2\frac{3}{4}\right)+B_{1c}\left(-\left(\tilde{\omega}^2-1\right)+\gamma\varepsilon R^2\tilde{\omega}^2\frac{3}{4}\right)\\
2\tilde{\omega}\dot{B}_{1c}=B_{1s}\left(-\left(\tilde{\omega}^2-1\right)+\gamma\varepsilon R^2\tilde{\omega}^2\frac{1}{4}\right)+B_{1c}\left(\varepsilon\tilde{\omega}-\varepsilon\tilde{\omega}\beta R^2\frac{3}{4}-\frac{9}{4}\varepsilon\tilde{\omega}\delta R^2\tilde{\omega}^2\right)
\end{cases}$$

The even superharmonics have been neglected. By using the normalized parameters and variables defined by (4.11) and (4.12), one obtains the equivalent system:

$$\begin{cases}
2\dot{B}_{1s}=\varepsilon\left(1-r^2\right)B_{1s}+\varepsilon\left(\nu-3\alpha r^2\right)B_{1c}\\
2\dot{B}_{1c}=\varepsilon\left(-\nu+\alpha r^2\right)B_{1s}+\varepsilon\left(1-3r^2\right)B_{1c}
\end{cases} \tag{4.35}$$

The corresponding matrix form is given in (4.17).
Observe that the perturbation v(τ) given in Eq. (4.16) could be defined in an alternative way:

$$u_y(t) := R_1 \cos(\tilde{\omega}\tau + \theta_1) \tag{4.36}$$

with

$$R_1 = R + \eta, \qquad \theta_1 = \theta + \xi$$

where η and ξ are small perturbations of the response amplitude and phase, respectively. Hence, Eq. (4.36) becomes

$$\begin{aligned} u_y(t) &= (R+\eta)\cos(\tilde{\omega}\tau + \theta + \xi) \\ &= (R+\eta)\big(\cos(\tilde{\omega}\tau+\theta)\cos(\xi) - \sin(\tilde{\omega}\tau+\theta)\sin(\xi)\big) \\ &= (R+\eta)\big(\cos(\tilde{\omega}\tau+\theta) - \sin(\tilde{\omega}\tau+\theta)\xi\big) \end{aligned}$$

The assumption that ξ is small has been used to develop in Taylor series cos(ξ) and sin(ξ). Finally,

$$\mathrm{v}(\tau) = \eta\cos(\tilde{\omega}\tau+\theta) - R\xi\sin(\tilde{\omega}\tau+\theta) \tag{4.37}$$

By comparing (4.16) and (4.37), it can be concluded that

$$B_{1c} = \eta \quad \text{and} \quad B_{1s} = -R\xi \tag{4.37}$$

By replacing Eq. (4.38) in Eq. (4.35), one has

$$\begin{bmatrix} \dot{\xi} \\ \dot{\eta}_r \end{bmatrix} = \frac{\varepsilon}{2}\begin{bmatrix} 1-r^2 & \dfrac{3\alpha r^2 - \nu}{r} \\ \nu r - \alpha r^3 & 1-3r^2 \end{bmatrix}\begin{bmatrix} \xi \\ \eta_r \end{bmatrix}$$

The trace and determinant of the matrix are identical to those of **M** defined in (4.17).

D. The condition $\nu=\alpha$

According to the conditions listed in Table 4.5, only the boundary B_S ($\lambda=\lambda_Q(\nu,\alpha)$) of the stability domain can fulfil the condition $\lambda=0$. Hence, using Eq. (4.25) and setting $\lambda_Q(\nu,\alpha)=0$, one obtains $\nu=\alpha$. The physical meaning of the condition $\nu=\alpha$ can be explained by rewriting it in terms of non-normalized variables. For the sake of simplicity, this is done in the case where the parameter μ associated with the nonlinear terms of the MVdP oscillator representing a pedestrian (Eq. (4.4)) is very small and assuming that ω is very close to the frequency ω_0 of the underlying linear system:

$$\tilde{\omega}=\frac{\omega}{\omega_0}=1+s \qquad \text{with} \quad s=\mathrm{O}(\mu)\ll 1 \tag{4.39}$$

In this case, the definition of ν given in Eq. (4.12) leads to:

$$s=\nu\mu \tag{4.40}$$

Under the same assumptions, the parameter α defined in Eq. (4.11) becomes $\alpha=\gamma/(\beta+3\delta)$. By using this expression of α and the identity $\nu=\alpha$, Eq. (4.40) entails

$$s=\alpha\mu=\frac{\mu\gamma}{\beta+3\delta} \tag{4.41}$$

It follows from Eq. (4.39)

$$\omega=\omega_0\left(1+\frac{\mu\gamma}{\beta+3\delta}\right):=\omega_1 \tag{4.42}$$

i.e. the non-normalized counterpart of the condition $\nu=\alpha$ is $\omega=\omega_1$, where ω_1 is the *natural* frequency of the autonomous MVdP oscillator (see Chapter 2). The approximated expression (4.42) the natural frequency ω_1 can be found by means of a suitable perturbation technique applied on the MVdP in the autonomous case (see Chapter 2). Due to the assumptions $\omega_0>0$, $\mu>0$ and using Eqs. (4.39)-(4.42), it can be also proven that $\nu-\alpha>0$ implies $\omega>\omega_1$ and vice versa.

References

[1] S. Erlicher, A. Trovato, P. Argoul, *Modeling the lateral pedestrian force on a rigid floor by a self-sustained oscillator.* Mechanical Systems and Signal Processing, in Press.

[2] A. Trovato, S. Erlicher, P.Argoul. *A modified Van der Pol oscillator for modelling the lateral force of a pedestrian during walking*, Proceeding of the Conference Vibrations, Chocs Bruit, Lyon, France, 2008.

[3] S. Erlicher, A. Trovato, P. Argoul, *A modified Van der Pol oscillator for modelling the lateral pedestrian force on a moving floor. Part I: Response curves*, submitted to the Journal of Sound and Vibration.

[4] A. Trovato, S. Erlicher, *A modified Van der Pol oscillator for modelling the lateral pedestrian force on a moving floor. Part II: stability and synchronization*. Submitted to the Journal of Sound and Vibration.

[5] S. Erlicher, *Modèles non linéaires et leur identification dans le genie civil et sismique*. Mémoire d'Habilitation, Université Paris-Est Marne-la-Vallée, France, 2009 (in French).

[6] P. Charles, *Passerelles piétonnes – Évaluation du comportement vibratoire sous l'action des piétons*. Technical Report SETRA, Bagneux, France, 2006 (in French).

[7] E. Caetano, Á. Cunha, C. Moutinho, F. Magalhães, *Lessons from the practical implementation of a passive control system at a new Coimbra footbridge,* in: Footbridge 2008, Third International Conference, Porto, Portugal, 2008.

[8] Y. Fujino, B.M. Pacheco, S. Nakamura, P. Warnitchai, *Synchronization of human walking observed during lateral vibration of a congested pedestrian bridge*, Earthquake Engineering and Structural Dynamics 22 (1993) 741-758.

[9] P. Dallard, A.J. Fitzpatrick, A. Flint, S. Le Bourvas, A. Low, R.M. Ridsdill, M. Willford, *The London Millennium Footbridge*, The Structural

Engineer 79 (22) (2001) 17-33.

[10] P. Dallard, T. Fitzpatrick, A. Flint, A. Low, R.R. Smith, M. Willford, M. Roche, *London Millennium Bridge: Pedestrian-Induced Lateral Vibration*, Journal of Bridge Engineering 6 (6) (2001) 412-417.

[11] R. Ricciardelli, A.D. Pizzimenti, *Experimental evaluation of the dynamic lateral loading of footbridges by walking pedestrians*, in: Proceedings of Eurodyn 2005 Conference, Paris, France, 2005, pp. 435-440.

[12] F. Danbon, G. Grillaud, *Dynamic behaviour of a steel footbridge: characterization and modelling of the dynamic loading induced by a moving crowd on the Solferino footbridge in Paris*, in: Proceedings of Footbridge 2005- 2nd International Conference, Venice, Italy, 2005, CDRom.

[13] J. Bodgi, S. Erlicher, P. Argoul, *Lateral vibration of footbridges under crowd-loading: continuous crowd modelling approach*, Key Engineering Materials 347 (2007) 685-690.

[14] J. Bodgi, S. Erlicher, P. Argoul, *Lateral vibration of footbridges under crowd-loading: on the modelling of the crowd-synchronization effects*, in: Proceedings of Evaces'07, Porto, Portugal, 2007, CDrom.

[15] S. Nakamura, T. Kawasaki, *Lateral vibration of footbridges by synchronous walking*, Journal of Constructional Steel Research 62 (2006) 1148-1160.

[16] S. Živanovic, A. Pavic, A. Flint, P. Reynolds, *Vibration serviceability of footbridges under human induced excitation*: a literature review, Journal of Sound and Vibration 279 (2005) 1-74.

[17] J.H. Rainer, G. Pernica, D.E. Allen, *Dynamic loading and response of footbridges*, Canadian Journal of Civil Engineering 15 (1988) 66-71.

[18] J.M.W. Brownjohn, A. Pavic, P. Omenzetter, *A spectral density approach for modelling continuous vertical forces on pedestrian structures due to walking*, Canadian Journal of Civil Engineering 31 (1) (2004) 65-77.

[19] R. Ricciardelli, A.D. Pizzimenti, *Lateral Walking-Induced Forces on Footbridges*, Journal of Bridge Engineering 12 (6) (2007) 677-688.

[20] H. Bachmann, W. Amman, *Vibrations in structures induced by man and machine*, IABSE structural engineering documents N3E, 1-176, Zurich, Switzerland, 1987.

[21] M.S. Garcia, *Stability, scaling and chaos in passive-dynamic gait models*,

Ph.D. Thesis, Cornell University, 1999.

[22] J. Park, *Synthesis of natural arm swing motion in human bipedal walking*, Journal of Biomechanics 41 (2008) 1417-1426.

[23] D.W. Jordan, P. Smith, *Nonlinear Ordinary Differential Equations*, fourth ed., Oxford University Press, Oxford, 2007.

[24] A. Pikowski, M. Rosenblum, J. Kurths, *Synchronization. A universal concept in nonlinear sciences*, First Ed., Cambridge University Press, Cambridge, UK, 2001.

[25] J. Guckenheimer, P. Holmes, *Nonlinear Oscillations, Dynamical Systems, and Bifurcation of Vector Fields*, Springer-Verlag, New York, 1983.

[26] E.C. Butz, *Beitrag zur Berechnung fußgängerinduzierter Brückenschwingungen*. RWTH Aachen, PhD Thesis, 2006, Shaker Verlag, ISBN 3-8322-5699-7 (in German).

[27] S. Nakamura, T. Kawasaki, H. Katsuura, K. Yokoyama, *Experimental studies on lateral forces induced by pedestrians*. Journal of Constructional Steel Research 64 (2008) 247-252.

[28] L. Sun, X. Yuan, *Study on pedestrian-induced vibration of footbridge*, in: Footbridge 2008, Third International Conference, Porto, Portugal, 2008.

[29] D.E. Newland, *Pedestrian excitation of bridges - recent results*, in: Proceedings of the Tenth International Congress on Sound and Vibration, Stockholm, Sweden, 2003.

[30] S.H. Strogatz, D.M. Abrams, A. McRobie, B. Eckhardt, E. Ott, *Crowd synchrony on the Millennium Bridge*, Nature 438 (2005) 43-44.

[31] B. Eckhardt, E. Ott, S.H. Strogatz, D.M. Abrams, A. McRobie, *Modeling walker synchronization on the Millennium Bridge*, Physical Review E 75 (2007) 021110.

[32] A. Belli, P. Bui, A. Berger, A. Geyssant, J.R. Lacour, *A treadmill ergometer for three-dimensional ground reaction forces measurement during walking*, Journal of Biomechanics 34 (2001) 105-112.

[33] A. Trovato, *Modelling the motion of the center of gravity of a pedestrian during walking*, Internal Report UR Navier, ENPC-LAMI, Champs-sur-Marne, France, 2008.

[34] J.D. Ortega, C.T. Farley, *Minimizing center of mass vertical movement*

increases metabolic cost in walking, Journal of Applied Physiology 99 (2005) 2099-2107.

[35] A. Trovato, S. Erlicher, P.Argoul. *Modelling the lateral pedestrian force on rigid and moving floors by a self-sustained oscillator*, Proceeding of the COMPDYN 2009 Conference, Island of Rhodes, Greece, June 2009.

[36] Y. Kuramoto, *Chemical Oscillations, Waves, and Turbulence*, Dover Publications, Mineola, New York, 1984.

[37] J.H.G. Macdonald, *Lateral excitation of bridges by balancing pedestrians*, Proceedings of the Royal Society A, doi:10.1098/rspa.2008.0367.

[38] P. Glendinning, M. Proctor, *Travelling waves with spatially resonant forcing: bifurcations of a modified Landau equation*. International Journal of Bifurcation and Chaos 3 (6) (1993) 1447 - 1455.

[39] G.V. Levina, A.A. Nepomnyaschiy, *Analysis of an Amplitude Equation for Autovibrational Flow Regimes at Resonance External Forces*. Zeitschrift für angewandte Mathematik und Mechanik, Wiley-VCH, Berlin, 66 (6) (1986) 241-246.

[40] A.L. Hof, M.G.J. Gazendam, W.E. Sinke. *The condition for dynamic stability*, Journal of Biomechanics 38 (2005) 1–8.

[41] A.L. Hof, R.M. van Bockel, T. Schoppen, K. Postema. *Control of lateral balance in walking: experimental findings in normal subjects and above-knee amputees*, Gait & Posture 25 (2007) 250–258.

[42] J.C. Chedjou, L.K. Kana, I. Moussa, K. Kyamakya, A. Laurent, *Dynamics of a Quasiperiodically Forced Rayleigh Oscillator*. Journal of Dynamic Systems, Measurement and Control 3 (128) (2006) 600-607.

[43] M.N Hamdan, N.H. Shabaneh, *On the large amplitude free vibrations of a restrained uniform beam carrying an intermediate lumped mass*. Journal of Sound and Vibration 199 (5) (1997) 711-736.

[44] A.A. Al-Qaisia, M.N. Hamdan, *On the steady state response of oscillators with static and inertia non-linearities*. Journal of Sound and Vibration 223 (1) (1999) 49-71.

[45] A.A. Al-Qaisia, M.N. Hamdan, *Bifurcations and Chaos of an immersed cantilever beam in a fluid and carrying an intermediate mass*. Journal of Sound and Vibration 253 (4) (2002) 859-888.

[46] A. Hassan, T.D. Burton, *Extraneous solutions predicted by the harmonic balance method*. Journal of Sound and Vibration 182 (1995) 523-538.

[47] R.H. Rand, *Lecture Notes on Nonlinear Vibrations*, version 52, Dept. Theoretical & Applied Mechanics, Cornell University, Ithaca NY 14853, 2005.

RINGRAZIAMENTI:

Giunto al termine di questo lavoro desidero ringraziare ed esprimere la mia riconoscenza nei confronti di tutte le persone che mi sono state vicine e hanno permesso e incoraggiato la realizzazione e la stesura di questa tesi. I miei più sentiti ringraziamenti vanno:

All'Ing. Silvano Erlicher per la continua disponibilità e pazienza che mi ha dedicato durante l'intera esperienza parigina, per gli incoraggiamenti, i consigli e per aver stimolato con suggerimenti ed osservazioni la mia curiosità intellettuale. Rimarrà in me il piacevole ricordo trascorso durante questo periodo di ricerca.

Al Prof. Domenico Bruno, che nella figura di tutor mi ha permesso di vivere la straordinaria esperienza di ricerca all'estero, offrendomi piena fiducia in ogni passo di questo percorso.

Al Prof. Pierre Argoul per la grande cortesia e disponibilità.

Al Prof. Luciano Ombres, per la fiducia fin da subito dimostratami, per avermi seguito e aiutato ad intraprendere, ogni volta, le scelte più appropriate e per tutto il suo supporto morale.

Un ringraziamento va, inoltre, a mio padre Antonio, a mia madre Palmerina, a mia sorella Angela, a mio fratello Franco e al mio amore Giusy. A loro dedico questo lavoro di tesi: senza il loro aiuto non avrei mai potuto raggiungere questa meta. Sono davvero grato per tutto il sostengo e l'aiuto scaturito dal loro cuore.

Ringrazio Davide, Salvatore e Philippe insostituibili amici.

Ringrazio tutto il gruppo di ricerca del dottorato in Ingegneria dei Materiali e delle Strutture che mi è stato vicino in questi anni, offrendomi preziosi suggerimenti ed opportunità di crescita culturale.